Radboud Repository

Radboud University Nijmegen

PDF hosted at the Radboud Repository of the Radboud University Nijmegen

The following full text is a publisher's version.

For additional information about this publication click this link.
http://hdl.handle.net/2066/27418

Please be advised that this information was generated on 2017-12-05 and may be subject to change.

GaN grown on sapphire by MOCVD

- Material for HEMT structures -

Andrzej Paweł Grzegorczyk

GaN grown on sapphire by MOCVD

- Material for HEMT structures -

een wetenschappelijke proeve op het gebied van
de Natuurwetenschappen, Wiskunde en Informatica

Proefschrift

ter verkrijging van de graad van doctor
aan de Radboud Universiteit Nijmegen
op gezag van de Rector Magnificus prof. dr. C.W.P.M Blom
volgens besluit van het College van Decanen
in het openbaar te verdedigen op woensdag 5 April, 2006
des namiddags om 1:30 uur precies

door

Andrzej Paweł Grzegorczyk

geboren op 21 januari 1976
te Warschau, Polen

Promotor: Prof. Dr. P.K. Larsen
Co-promotor: Dr. P.R. Hageman

Manuscriptcommissie:
Prof. Dr. E. Vlieg

Prof. Dr. Ing. L.M.F. Kaufmann
(Technical University Eindhoven)

Dr. A.v. Geelen
(Philips Semiconductors Nijmegen)

The work described in this thesis was financially supported by the Dutch Technology Foundation (STW).

Preface

Proudly I present to you my doctoral thesis which is the result of my research at the Radboud University Nijmegen. Disregarding the technical problems that continuously occurred during my PhD studies, proving that Murphy’s Law ”anything that can go wrong, will” is true, it was a great pleasure to conduct research in the department of Experimental Solid State Physics 3. I have learnt a lot during these past few years. The completion of this work would certainly not have been possible without the help of several people. To begin with, I am much indebted to my mentors Prof. Poul Larsen and Dr. Paul Hageman for supervising my research project and their confidence in me. They both gave me academic and practical support and patiently provided critical reviews of the numerous drafts of this thesis. Moreover, I would like to thank Jan Weyher who always showed great interest in my research. His academic expertise has been a great help and his comments were always clear and correct. Furthermore, I am grateful to Wil Corbeek, Harry van der Linden, and Erik Haverkamp - the professionals who provided technical support and were always ready to struggle with the stubborn machines. It was a great joy to work with them. A word of thanks to my colleagues: Corina van Dam, Gerard Bauhuis, Joop van Deelen, Lukasz Macht, Maarten Voncken, Mariusz Rudzinski, Peter Mulder (in alphabetic order) for many inspiring discussions about physics and a friendly atmosphere. We shared a nice time together. And also, I would like to thank my wife Ola, for all support and for being my best friend.

Contents

1 Introduction 1

1.1 Short history of GaN research 2

1.2 Introduction to HEMTs 3

Bibliography 8

2 Basic properties of III-V nitrides 11

2.1 Crystal structure of III-V nitrides 11

2.2 Mechanical, optical, and thermal properties of GaN 13

2.3 Sapphire as a substrate for GaN epitaxy 14

2.4 Piezoelectric and spontaneous polarization in III-V nitrides. GaN/AlGaN based HEMT structure 16

Bibliography 22

3 Characterization techniques 25

3.1 Hall measurement 25

3.2 Depletion capacitance-voltage measurements 27

3.3 In-situ reflectance measurements 32

3.4 Grazing X-ray reflectometry 36

3.5 X-ray diffraction 39

3.6 Scanning electron microscopy 41

3.7 Atomic force microscopy 42

Bibliography 43

4 **Growth of GaN epilayers on Si(111) substrates using multiple buffer layers** **47**
4.1 Introduction 48
4.2 Experimental details 48
4.3 Results and discussion 49
4.4 Conclusions 52
4.5 Acknowledgements 52
Bibliography 53

5 **Structural properties of maskless epitaxial lateral overgrown MOCVD GaN layers on Si (111) substrates** **55**
5.1 Introduction 56
5.2 Experimental details 56
5.3 Results and discussion 57
5.4 Conclusions 60
5.5 Acknowledgements 60
Bibliography 60

6 **Influence of the nucleation layer morphology and epilayer structure on the resistivity of GaN films grown on c-plane sapphire by MOCVD** **63**
6.1 Introduction 64
6.2 Experimental details 65
6.3 Results and discussion 67
6.4 Conclusions 72
Bibliography 72

7 **Resistivity control of unintentionally doped GaN films** **75**
7.1 Introduction 75
7.2 Experimental details 76
7.3 Results and discussion 77
7.4 Conclusions 79
Bibliography 79

8 Influence of sapphire annealing in trimethylgallium atmosphere on GaN epitaxy by MOCVD 83
8.1 Introduction 84
8.2 Experimental details 85
8.3 Results and discussion 87
8.4 Conclusions 92
Bibliography 95

9 Influence of sapphire annealing in trimethylaluminum atmosphere on GaN epitaxy by MOCVD 97
9.1 Introduction 98
9.2 Experimental details 99
9.3 Results and discussion 101
9.4 Conclusions 107
9.5 Acknowledgements 108
Bibliography 110

10 GaN/AlGaN based HEMTs - development of the product 113
10.1 How good are we? 113
10.2 Suggestions for future research 118
Bibliography 119

Summary 121

Samenvatting 125

Publication list 129

Curriculum Vitae 130

Abbreviations and Acronyms

ϵ	represents the strain
e_{ij}	represents the piezoelectric constants
2DEG	two dimensional electron gas
2DHG	two dimensional holes gas
AFM	atomic force microscopy
ATS	aluminum treatment step
BL	buffer layer
C-V	capacitance-voltage (measurements)
CW	continuous-wave
ECR	electron cyclotron resonance
ELO	epitaxial lateral overgrowth
FEG	field emission gun
GTS	gallium treatment step
HEMT	high electron mobility transistor
HFET	heterostructure field effect transistor
HJFET	heterojunction field effect transistor
HT	high temperature
HVPE	hydride vapor phase epitaxy

ICP	inductively coupled plasma
IL	intermediate layer
k	extinction coefficient - it define, how much light is absorbed in the material
LD	laser diodes
LED	light emitting diodes
LEO	lateral epitaxial overgrowth
LT	low temperature
MBE	molecular beam epitaxy
ML	main layer
MOCVD	metal-organic chemical vapor deposition
n	refractive index defined as the ratio of the speed of light in vacuum to the speed of light in the material
NH_3	ammonia
NL	nucleation layer (in literature described also as buffer layer)
PE	pendeo epitaxy
PEC	photo-electrochemical
PL	photoluminescence
PP	piezoelectric polarization
RIE	reactive ion etching
RMS	root-mean square
SAG	selective area growth
SEM	scanning electron microscope
SP	spontaneous polarization
TEM	transmission electron microscope
TMA	trimethylaluminum

TMG	trimethylgallium
XRD	X-ray diffraction
XRR	grazing incidence X-ray reflectometry

Chapter 1

Introduction

In the history of the world there are some big technological inventions like electricity, nuclear power or computers that changed people's lives completely. There are also smaller inventions like telephone or radio that just improved the quality of everyday life. Semiconductors, among them Gallium Nitride, seem to belong to this second group of discoveries. Due to its advantageous physical and chemical properties, GaN is a very promising material for high power, high frequency electronic and opto-electronic devices. The many potential applications of this prospective material make it very challenging from a scientific point of view. To explain why it is so, I would like to point out a few facts from the history of semiconductors.

Germanium, the first material ever used for constructing a transistor, was discovered by Clemens Winkler in 1886. However, the first transistor was not born before 1947 when John Bardeen and Walter Brattain, two scientists working with William Shockley at Bell Telephone Laboratories, observed that electrical signals measured on the contacts on a crystal of germanium had an output power larger than the input. Thus, it took scientists 61 years from the discovery of the material to the first presentation of the transistor. For comparison, the first GaN material was synthesized in 1932 [1] and the first publication presenting a High Electron Mobility Transistor (HEMT) was published in 1992 [2]. Despite of the well developed theory of semiconductors, modern technologies and computer, scientists did not manage to present the first GaN based HEMT structure until 60 years after the discovery of this material! It means that the small number of pioneers of modern electronics needed almost the same time to make Ge based transistors, as needed the army of scientists specialized in semiconductor physics to make the first GaN based HEMT. This fact perfectly illustrates how huge the knowledge gap was which had to be filled in, to develop GaN based devices. However, for scientists this knowledge was valuable enough to spend a few decades gathering it, and in the meantime make huge efforts in studying the whole group of III-V compounds.

From an economical point of view, the physical properties of GaN, such as its wide bandgap, chemical and thermal stability, and the high electron mobility, stimulated the development of blue lasers, diodes, and high power, high temperature transistors. On the other hand, the extreme growth conditions needed for GaN [3, 4], and the lack of lattice and thermally matched substrates provide a scientific challenge to develop this material. Among the group of III-V compounds GaN is the material deposited on the widest range of substrates [5], for instance: Si, GaAs, Al_2O_3, SiC, $LiGaO_2$, $(Mn,Zn)Fe_2O_4$, and $Ca_8La_2(PO_4)6O_2$ to name only a few. Lack of properly matched substrates for GaN epitaxy implies a large dislocation density in the epilayers. Because of the diminishing effect on the device performance, a reduction of the dislocation density was, and still is, the key issue in the GaN material development. For this purpose, scientists developed fascinating techniques [6] such as selective area growth (SAG) , lateral epitaxial overgrowth (LEO), and pendeo- (from Latin: to hang or be suspended) epitaxy (PE). Moreover, there is a long list of publications dealing with different types of nucleation layer and substrate pretreatment steps used for the reduction of the lattice mismatch [4, 7, 8]: AlN nucleation layer (NL) , GaN NL, AlGaN layer, Si_3N_4 treatment, nitridation of substrates, and many others. All these efforts were done just to reduce the number of defects in GaN epilayers; however, the dislocation density in the epitaxially grown GaN material still remains high (10^5-10^9 cm^{-2}). It should be stressed that even with this high density of dislocations the production of the working Light Emitting Diodes (LED) , lasers, and transistors is still possible. In the next part of this thesis I will demonstrate that by making use of these (electrically active) dislocations the GaN resistivity can be controlled over a few orders of magnitude. As will be explained in the next chapter, this is necessary for a decent HEMT performance. Probably GaN is the only one material where defects can have a constructive impact on the device performance. In order to provide a good theoretical framework for my GaN growth research some additional facts from the history of this material will be presented in the next part.

1.1 Short history of GaN research

The history of GaN begins in 1932 when Johnson et al. [1] synthesized GaN by passing ammonia over hot gallium. By applying this synthesis it was possible to produce small needles and platelets of GaN. In 1969 Maruska and Tietjen [9] realized epitaxial growth of GaN using the hydride vapor phase epitaxy (HVPE) technique and were able to deposit large scale GaN layers on sapphire substrates. As source of gallium they used GaCl, which was in situ synthesized by passing HCl over liquid gallium at 800-900 °C. Crystals prepared by this method had an inherent electron density exceeding $10^{19}\,\mathrm{cm}^{-3}$ with a mobility of about $150\,\mathrm{cm}^2\mathrm{V}^{-1}\mathrm{s}^{-1}$ at room temperature. Physical data for non-polycrystalline GaN material became available for the scientific community after extracting them from these crystals.

In 1971 Manasevit et al. [10] succeeded in growing nitrides of gallium and aluminum using metalorganic compounds as a source of Ga and Al. This was the premiere of the application of metal-organic chemical vapor deposition (MOCVD) technique to III-V nitrides. Up to now, MOCVD remains the most popular growth method for GaN. Because the majority of data presented in this thesis were gained from MOCVD-grown samples, the details of this important technique will be presented thoroughly in the coming chapters.

In the history of GaN development it is easy to pin-point a few of the most significant publications that should be particularly mentioned because they inspired the scientific community and boosted the current GaN research. At first, in 1986, Amano et al. [4] introduced a brand new method of improving the GaN layer grown on sapphire using a low temperature (LT) AlN NL followed by the high temperature main layer growth. This method is now commonly known as the two-step growth method. Five years later Nakamura et al. [7] and Wickenden [11] developed independently a similar method based on a GaN low temperature NL. They demonstrated that by applying the two-step growth method enables deposition of high quality GaN with a well defined polarity (Ga or N), a defect density of about $10^{9}\,\mathrm{cm}^{-2}$, and a mirror-like surface morphology (for Ga polar material), which can be employed in all kind of devices. This idea is still the basis for most of the publications concerning GaN growth on sapphire by MOCVD and Molecular Beam Epitaxy (MBE). In 1988 Amano et al. [12, 13] presented p-type conductivity in GaN layers from Mg donors which were activated by electron beam irradiation. Before this publication, p-type GaN was thought to be the main factor limiting device development. Thanks to these results the first p-n GaN LED was fabricated one year later. Finally, in 1994, Nakamura et al. [14] demonstrated bright light emitting diodes ready for commercialization.

1.2 Introduction to HEMTs

The High Electron Mobility Transistor (HEMT) is also known as Heterostructure Field Effect Transistor (HFET) or Heterojunction Field Effect Transistor (HJFET) - all these names refer to a whole group of devices based on a two dimensional electron gas. The HEMT was originally described by Mimura, who wrote a patent for a HEMT based on a GaAs/AlGaAs structure in 1979. Two decades later his revealing idea was adapted to the III-V nitrides, and since then is the subject of a large, world

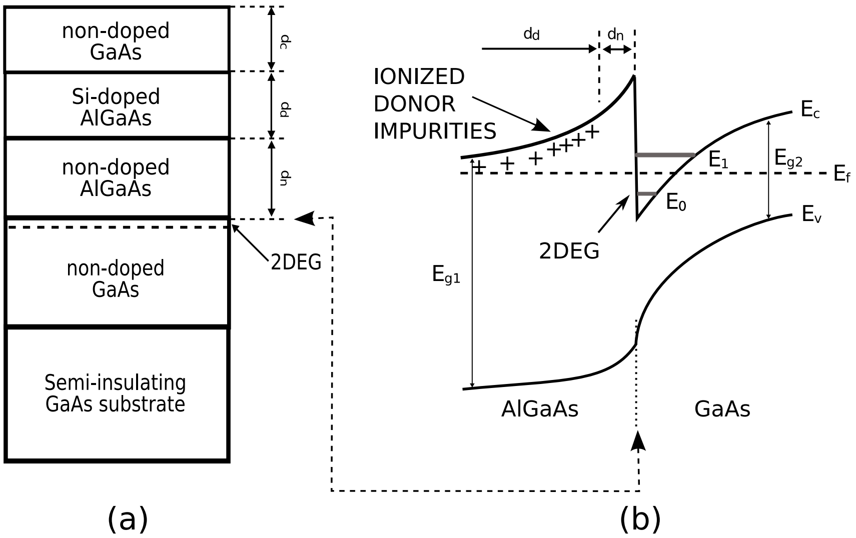
non-doped GaAs
Si-doped AlGaAs
non-doped AlGaAs
non-doped GaAs
Semi-insulating GaAs substrate
dc
dd
dn
2DEG
(a)
dd
dn
IONIZED DONOR IMPURITIES
Ec
Eg2
Ef
Ev
E1
E0
2DEG
Eg1
AlGaAs
GaAs
(b)

Figure 1.1: Schematic drawing (a) and a band diagram (b) of the GaAs/AlGaAs HEMT structure [18, 19].

wide research activity.

This thesis focuses on growth and basic characterization of AlGaN/GaN based HEMT structures. Therefore it will be useful to present some details of the GaAs/AlGaAs based HEMT properties first, in order to clarify the similarities and differences between these two materials.

The main part of a HEMT device is the GaAs/AlGaAs heterojunction (Figure 1.1) [15–17]. As a result of the differences in work function and bandgap, electrons diffuse from the n-doped AlGaAs to the non-doped GaAs and, as a result, a triangular quantum well is formed at the GaAs/AlGaAs interface. The motion of the electrons confined in this well is quantized in the plane parallel to the GaAs/AlGaAs interface, forming sub-bands of energy E_0, E_1, etc. Since these systems aim to minimize the total energy, depending on the density of the electrons, first the E_0 energy band level is filled completely and thereupon the next level. To explain comprehensively how this idea is realized in a structure, the layer structure will be described in detail. At the beginning of the epitaxy process, high-quality non-doped GaAs material is usually deposited to reduce the number of defects (continuing from the substrate) and to improve GaAs/AlGaAs interface smoothness. The thickness of this layer is between 1 and 4 μm [20], the dislocation density is reduced to about 100 cm^{-2} and the sheet resistance exceeds 100 Ω cm . The typical ionized acceptor level (grown by MBE) is N_A $<10^{15}$ cm^{-3}. In order to increase the two dimensional electron gas (2DEG) mobility, a non-doped AlGaAs layer (commonly referred to as a “spacer”) is deposited. The typical thickness of this layer (d_n) is between 1-100 nm, depending on the desired electron density and mobility. This layer aims to separate the ionized donors from the electrons to reduce Coulomb interaction between the electrons in the quantum well and the ionized donors. These ionized donors are present in the Si-doped AlGaAs layer where the typical donor concentration is estimated to be about N_D $>10^{18}$ cm^{-3}, being a source of electrons for the 2DEG. The thickness of this layer is about d_d=80 nm. The positive charge of the ionized donors, present in the Si-doped AlGaN layer, is compensated by electrons gathered in the triangular potential well. The last part is a top GaAs layer which is deposited in order to reduce oxidation of the AlGaAs surface and to improve the formation of the electrical contacts. It is worth to stress that the 2DEG density for this kind of HEMT structure is about n_s=6.9×10^{11} cm^{-2} and the electrons mobility exceeds μ=7000 cm^{2}V^{-1}s^{-1} at 300 K [16, 17].

The first results regarding a 2DEG in a GaN/AlGaN structure were presented by Khan et al. [2] in 1992. They measured a room temperature electron mobility of 834 cm^{2}V^{-1}s^{-1}, which was much higher than the value for the individual GaN and AlGaN layers with comparable thickness. For comparison, the highest value for the mobility of a similar structure exceeds 2500 cm^{2}V^{-1}s^{-1} [21]. One year later, the same group of scientists [19] showed the first working HEMT transistor based on a GaN/AlGaN structure. The measured value for the 2DEG density and mobility were 1.15×10^{13} cm^{-2} and 563 cm^{2}V^{-1}s^{-1}, respectively. Since that demonstration, an increased research activity in the field of HEMT structures based on the group III nitrides is observed. From Figure 1.2 is apparent that the number of scientific publications related to HEMTs based on GaN rapidly increases every year, what suggests a high scientific activity regarding this part of GaN research.

GaN is the key semiconductor material for future technologies and the new generation of electronic devices. Due to the outstanding material properties, III-V nitrides have the potential to fulfill the commercial and military needs for optical storage application, UV photodetectors, and devices operating at extremely hostile environments and elevated temperatures (up to 500 °C).

The previous generation of semiconductor materials, including silicon, arsenides and phosphides, are not able to meet the growing high-power, high frequency and high temperature requirements for the new electronic applications. It is therefore expected that the GaN based transistors fill (partly) the market for the high power and high frequency devices in the next few years (Figure 1.3). The GaN research and development is strongly influenced by the market demand, and it is foreseen to

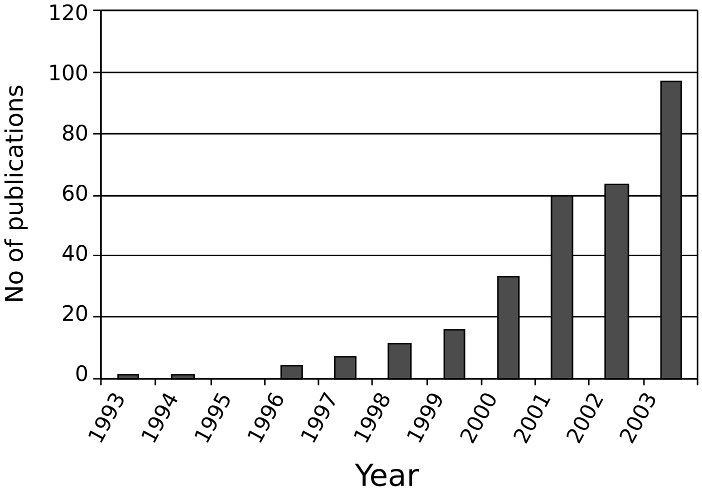

Figure 1.2: The number of publications concerning HEMT (and HFET) structures based on GaN material, according to the data acquired from the Web of Science (ISI) database.

conquer a strong position in the field of the electronic industry in the near future.

The most important aim of this study was to make a contribution to the understanding and development of MOCVD growth technique for GaN, with a particular interests in HEMT structures. First, the theoretical framework is presented in Chapter 2. Subsequently, a short review of the techniques used for the characterization of the samples studied is provided (Chapter 3). The main part of this thesis is presented in the following chapters and deals in general with the growth and characterization of a GaN layers with different properties. Due to the fact that the density of dislocations in GaN epilayers often exceeds $10^9\,\mathrm{cm}^{-2}$, the reduction of these defects has been chosen as the first object of this study. The results are presented in Chapter 4 and Chapter 5.

In order to grow high quality HEMT structures it is necessary to solve the problem of the low resistivity of an GaN buffer layers. Generally, the resistivity of semiconductors can be controlled by compensation of the majority carriers. In case of GaN it can be done by Fe, Mg, or Zn doping. There is also another method based on changing the growth condition. For the purpose of this study, this last method is preferred for two reasons: first, the ”classical” doping complicates the deposition process and through this it becomes less reproducible. The second reason was more scientific - in literature there was no clear explanation of what are the main factors, except for intentional doping, defining the resistivity of GaN epilayers. Chapter 6 and 7 describe a new method of GaN resistivity control by using different carrier gases during nucleation layer deposition. The presented method allows to obtain

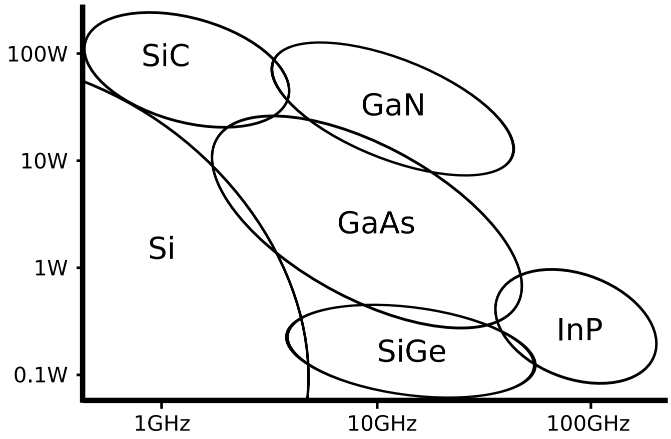

Figure 1.3: Foreseen capabilities of RF power solid-state technologies for a single device in a medium term.

GaN material with electrical resistivity exceeding $10^{11}\,\Omega\,\mathrm{cm}$. The method itself is very simple, so its implementation to another MOCVD systems should be also relatively easy.

Besides the resistivity control it is necessary to optimize the GaN/AlGaN interface in order to obtain good starting material for HEMTs applications. For this purpose, a lot of knowledge has been used adopted from classical III-V materials in growth of which our department has also a big experience. Since this knowledge is more technical then purely scientific, there is not too much space dedicated to this problem in this thesis. Nevertheless, some important data are presented in Chapter 10. The experimental techniques used for control of the $\mathrm{Al}_x\mathrm{Ga}_{1-x}\mathrm{N}$ composition, surface morphology, and thickness are described in Chapter 3. Using this knowledge presented here it was possible to produce HEMT structures (on sapphire and also SiC substrates) with the mobility exceeding $1500\,\mathrm{cm}^2\mathrm{V}^{-1}\mathrm{s}^{-1}$ and 2DEG exceeding $1{\times}10^{13}\,\mathrm{cm}^{-2}$. It was also the main aim of the project which, according to the sponsors, has been successfully finished.

Chapter 8 presents a new method (GTS) of GaN deposition on sapphire substrates. The GaN epilayers deposited using this GTS method are highly strained at room temperature. It has been found that this method can be used for production of the particularly good templates for the growth of GaN layers by HVPE technique. It was possible to deposit HVPE layers with thickness exceeding $250\,\mu$m without cracks. It should be also pointed out that this method allows to simplify the growth process. As opposed to the standard two step growth method (described in Chapter 6) the complete growth process can be performed at one temperature and pressure. Additionally, the dislocation density was less or equal to the results obtained using the two step growth method.

Chapter 9 is the natural continuation of the ideas presented in Chapter 8 replacing Ga by Al to deposit the nucleation layer.

Bibliography

[1] W. C. Johnson, J. B. Parson, M. C. Crew, J. Phys. Chem. 36 (10) (1932) 2651.

[2] M. A. Khan, J. N. Kuznia, J. M. V. Hove, N. Pan, J. Carter, APL 60 (24) (1992) 3027–3029.

[3] S. Porowski, I. Grzegory, J Cryst Growth 178 (1-2) (1997) 174–188.

[4] H. Amano, N. Sawaki, I. Akasaki, Y. Toyoda, APL 48 (5) (1986) 353–355.

[5] L. Liu, J. H. Edgar, Mat Sci Eng R 37 (3) (2002) 61–127.

[6] R. F. Davis, T. Gehrke, K. J. Linthicum, P. Rajagopal, A. M. Roskowski, T. Zheleva, E. A. Preble, C. A. Zorman, M. Mehregany, U. Schwarz, J. Schuck, R. Grober, Mrs Internet J N S R 6 (14) (2001) 1–16.

[7] S. Nakamura, Jpn J Appl Phys 2 30 (10A) (1991) L1705–L1707.

[8] S. Keller, B. P. Keller, Y. F. Wu, B. Heying, D. Kapolnek, J. S. Speck, U. K. Mishra, S. P. DenBaars, APL 68 (11) (1996) 1525–1527.

[9] H. P. Maruska, J. J. Tietjen, APL 15 (10) (1969) 327–329.

[10] H. Manasevi, F. M. Erdmann, W. I. Simpson, J Electrochem Soc 118 (11) (1971) 1864.

[11] D. Wickenden, T. Kistenmacher, W. Bryden, J. Morgan, A. Estes Wickenden, Heteroepitaxy of Dissimilar Materials Symposium (1991) 167–172.

[12] H. Amano, I. Akasaki, T. Kozawa, K. Hiramatsu, N. Sawaki, K. Ikeda, Y. Ishii, J Lum. 40-41 (1988) 121–122.

[13] H. Amano, M. Kito, K. Hiramatsu, I. Akasaki, Jpn J Appl Phys 2 28 (12) (1989) L2112–L2114.

[14] S. Nakamura, T. Mukai, M. Senoh, APL 64 (13) (1994) 1687–1689.

[15] T. Mimura, S. Hiyamizu, T. Fujii, K. Nanbu, Jpn J Appl Phys 19 (5) (1980) L225–L227.

[16] J. Klamka, Heterozlaczowe Przyrzady Polprzewodnikowe na Zakres Mikrofal Milimetrowych, Oficyna Wydawnicza “MH”, 2002.

[17] D. C. Look, Electrical characterization of GaAs materials and devices, Design and measurement in electronic engineering, Wiley, Chichester; New York, 1989.

[18] A. G. Milnes, D. L. Feucht, Heterojunctions and metal-semiconductor junctions, Academic Press, New York, 1972.

[19] R. A. Kiehl, P. M. Solomon, D. J. Frank, Ibm Journal of Research and Development 34 (4) (1990) 506–529.

[20] P. M. Koenraad, The influence of ionized impurities on the transport properties of a two-dimensional electron gas, Ph.D. thesis, Technische Universiteit Eindhoven (1990).

[21] C. Skierbiszewski, K. Dybko, W. Knap, M. Siekacz, W. Krupczynski, G. Nowak, M. Bockowski, J. Lusakowski, Z. R. Wasilewski, D. Maude, T. Suski, S. Porowski, Appl Phys Lett 86 (10) (2005) –.

Chapter 2

Basic properties of III-V nitrides

2.1 Crystal structure of III-V nitrides

Depending on the conditions the group III-V nitrides can exist in three different crystal structures: wurzite, zincblende, and rock salt structure (Figure 2.1). This behavior is called polymorphism and is common for wide bandgap semiconductors. The thermodynamically stable structure for bulk AlN, GaN, and InN is wurzite, forced upon by the relatively small size of the nitrogen atom compared to the group III atoms. For epitaxial GaN and AlN layers grown epitaxially on (001) sapphire, the wurzite structure dominates. On the other hand, substrates like GaAs (001), Si (001) and MgO force the III-nitrides into the zincblende structure [1]. In these cases, the natural tendency to form the wurzite structure is suppressed by the topological structure of the substrates. Small inclusions of the zincblende structure are also observed in the low temperature GaN nucleation layer for samples grown on sapphire [2]. These inclusions are not stable at the high growth temperature for the main layer

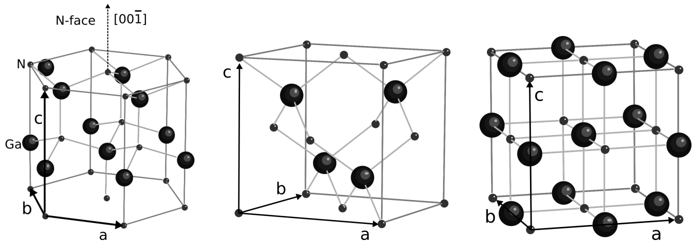

(a) (b) (c)

Figure 2.1: Crystal structures in which III-V nitrides can exist: (a) wurtzite, (b) zinc blende and (c) rocksalt crystal structure.

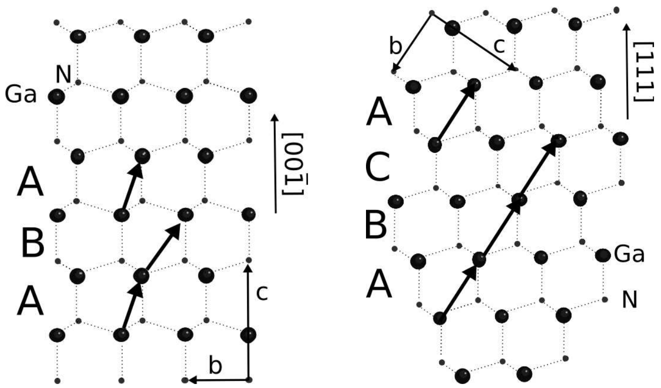

(a) (b)

Figure 2.2: The stacking sequence for the zinc blende (a) and wurzite (b) structures.

because in the epilayer no cubic inclusions are found.

From a crystallographic point of view the zincblende and wurzite structures are very similar. In both cases each nitrogen atom is connected to four group III atoms. The most important difference between these two structures is their stacking sequence. In case of the wurzite structure the stacking sequence of (001) planes is ABCABCABC in the [001] direction, whereas for the zincblende structure the stacking sequence of (111) planes is ABABAB in the [111] direction (Figure 2.2). The last known, and not very abundant structure of GaN, the rocksalt phase, is observable in high pressure experiments (>30 GPa) using Raman scattering [3]. The transition of polycrystalline wurzite GaN to the rocksalt phase is known to take place at a pressure of about 36 GPa [4] - for comparison the same phase transition of AlN is already measured at pressures between 16 and 22.9 GPa [5, 6]. The existence of the rocksalt phase was also reported for epitaxial GaN material [7] - it probably was the result of the stress generated in the sample during the high temperature growth. It should be pointed out that all three GaN structures presented in Figure 2.1 contain polar crystal planes meaning planes terminating with either group III atoms or only nitrogen atoms. For the zinc blende and rocksalt structures the polar crystallographic plane is (111) and for wurzite it is the (001) plane. Since epitaxial growth is mostly performed along the c-axis of GaN there are two possible directions of the growth: [001] or [00$\bar{1}$]. Different chemical properties, such as etching characteristics and oxidation rates, are determined by the polarity of the wurzite GaN structure [8]. In this case the [00$\bar{1}$] direction is chosen to point out from the cation (group III element) to the anion (group V element). The polarity of the GaN epilayer can be controlled by varying the low temperature nucleation layer thickness. The N-polar GaN epilayers are usually very rough and they are covered by hexagonal hillocks. This is the reason

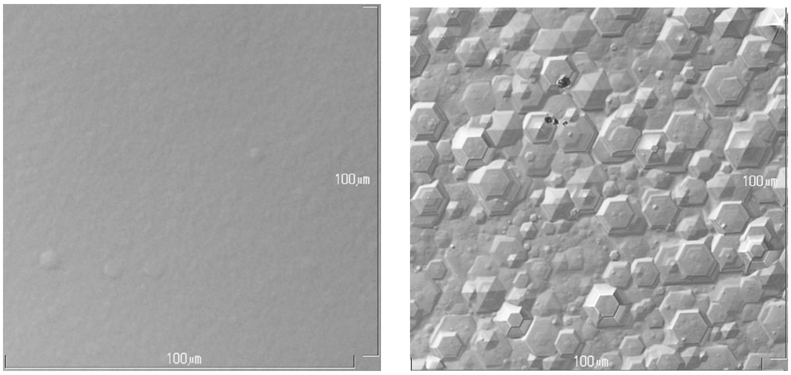

(a) (b)

Figure 2.3: Optical microscopy images ($100\,\mu$m $\times 100\,\mu$m) of Ga-polar (a) and N-polar (b) GaN material. Both $0.5\,\mu$m thick layers were grown using an AlN nucleation layer with different thickness.

why N-polar material is not suited for processing of devices. Figure 2.3 presents two optical microscopy images of GaN epilayers grown on sapphire using different thicknesses of the low temperature AlN NL - the images show Ga and N-polar material.

2.2 Mechanical, optical, and thermal properties of GaN

In general, the data presented for III-V nitrides in scientific literature can be separated into two main groups. The first group contains data that are measured on epitaxial material and the second group of data are measured on bulk material. The difference in defect density for the GaN epitaxial layers and bulk material can exceed 9 orders of magnitude. Strain and defects existing in the samples can distort the physical parameters and therefore, there is a wide spread in the reported values. The most evident example of this phenomenon is observed for InN, where the reported band gap value varies from 0.3 up to 2.05 eV, depending on the sample and on its preparation method. In the case of lattice constants the situation is similar because the data are influenced by the growth conditions, impurity concentration, and film stoichiometry.

In Table 2.1 the physical properties of III-V nitrides are presented. In contrast to the classical III-V materials systems of AlAs and GaAs where the lattice difference is very small, the III group nitrides are characterized by a large variation in lattice parameter between the different members of the family. Thus, there is a large lattice mismatch in heterojunctions involving different groups of III-V nitrides, e.g. for GaN/AlN it is 2 % for a_0 (for AlAs/GaAs it is only 0.1 %). Additionally, due to

	Lattice constants [nm]	Melting point [°C]	Thermal conductivity at 300 K (W $cm^{-1}K^{-1}$)	Band gap Eg (300 K)	Thermal expansion coefficient ($10^{-6}K^{-1}$)
AlN	a0=0.311 c0=0.498	3487 [13]	2.85	6.2	5.3 ‖ c-axis 4.2 ⊥ c-axis
GaN	a_0=0.318 c_0=0.518	2791 [13]	1.3	3.4	3.2 ‖ c-axis 5.6 ⊥ c-axis
InN	a_0=0.354 c_0=0.57	2146[12]	0.8	1.89	3.7 ‖ c-axis 5.7 ⊥ c-axis
AlAs	a_0=0.566	1740	0.91	2.165	5.2
GaAs	a_0=0.565	1240	0.55	1.424	5.73

Table 2.1: Physical properties of III-V nitrides [9].

differences in the thermal expansion coefficient, the lattice mismatch increases at high temperature.

2.3 Sapphire as a substrate for GaN epitaxy

As mentioned before, the lack of GaN free standing crystals forces scientists to use foreign substrates for GaN epitaxial growth. There are three main criteria for choosing substrates for GaN epitaxy: thermal stability, lattice constant, and availability of the material. The epitaxial growth process proceeds at temperatures higher than 1100 °C (for MOCVD), so this is the first condition the substrates should be able to withstand. The crystal quality of epitaxially grown GaN is a strong function of the lattice mismatch between GaN and the substrate. The last criterion is availability of substrates. Although free standing 2 ” GaN wafers were already presented they are not fully commercially available (the main reason is a very high price (10000 € for a 2 ” freestanding GaN wafer) and the quality of crystals). SiC, with a lattice mismatch of only 3 % and high thermal conductivity (Table 2.2), is presented as a very good alternative for free standing GaN substrates. Although

z	Lattice constants [nm]	Melting point [°C]	Thermal conductivity at 300 K (W $cm^{-1}K^{-1}$)	Lattice mismatch [%]	Thermal exp. coef. ($10^{-6}K^{-1}$)	Resistivity (Ω cm)	Price per 2” wafer [€]
Al_2O_3	a_0=0.4765, c_0=1.2982	2030	0.32 ‖ c-axis, 0.35 ‖ a-axis	13	9.03 ‖ c-axis, 5.0 ⊥ c-axis	$> 10^{11}$	40
Si	a_0=0.543102	1414	1.56	17	2.616	$< 5x10^4$	80
4H-SiC	a_0=0.30730, c_0=1.0053	2830	3.0-3.8	3.1	4.2	10	> 3000

Table 2.2: Physical properties of the most common substrates for GaN epitaxy.

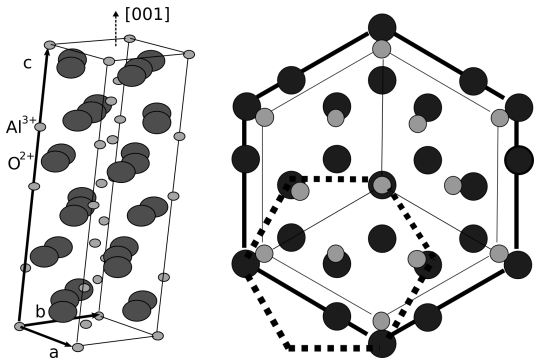

(a) (b)

Figure 2.4: Hexagonal unit cell of Al_2O_3 crystal (a), and orientation of the GaN layer in relation to the sapphire substrate (b).

the quality of the SiC wafers gradually increases over time, there are still problems with appropriate wafer preparation for epitaxial growth. Moreover, the price for a reasonably good quality 2" wafer exceeds 3000 €. As opposed to SiC, silicon is a low cost substrate. Physical properties, high quality (perfect surface finish), and its availability in very large sizes, makes it a very attractive substrate for GaN-based devices. Nevertheless, due to the large lattice constant and thermal expansion coefficient mismatch, the quality of GaN epitaxial layers on silicon is much poorer than that on sapphire or silicon carbide [10]. Moreover, on Si which is an n-type dopant in GaN, it is harder to produce high resistive GaN material for HEMT applications on these substrates.

Sapphire (0001) is the most commonly employed substrate for GaN epitaxy. The crystal structure can be described by a rhombohedral unit cell but also by a hexagonal one (Figure 2.4a) and it is mainly composed of ionic bonds. As opposed to GaN, it is a non-polar material with a dislocation density between 1×10^3-1×10^4 cm^{-2}. The thermal expansion coefficient of sapphire is larger then GaN, therefore producing, as opposed to silicon, a biaxial compressive strain in the layer during cooling down from high deposition temperature. The thermal conductivity of sapphire is very low compared to other substrates (Table 2.2) thus it is a very poor material for dissipating heat, enforcing the use of a thicker buffer layer for a HEMT structure as compared to SiC. Sapphire is an electrically insulating material so the back side of the substrate cannot be used as electrical contact. GaN epitaxy on sapphire (0001) results in c-plane oriented film (Ga or N-polar) with a 30^o rotation of the in-plane GaN crystal with respect to the same orientation of sapphire. As shown in Figure 2.4b this rotation reduces the lattice mismatch to 13 %- without it the lattice mismatch would exceed 30 % [11]. The (001) plane and [$\bar{1}$,0,0] crystallographic direction of the GaN epilayer are parallel to the (001) plain and $[\bar{1},\bar{1},0]$ direction of the Al_2O_3 substrate. An excellent review on substrates for GaN epitaxy is given by Liu and Edgar [10].

2.4 Piezoelectric and spontaneous polarization in III-V nitrides. GaN/AlGaN based HEMT structure

Wurzite and the other low symmetry crystal structures can exhibit spontaneous polarization (SP), as well as piezoelectric polarization (PP) arising from the strain induced in the crystal structure. It is important to note that among all III-V materials only the group III-nitrides possesses a spontaneously induced electrical field. The fixed direction of the SP in wurzite III-V nitrides is the c-direction $\vec{c}$=[001]. Mathematically it is expressed as:

$$\vec{P}_{sp} = P_{sp}\vec{c}, \tag{2.1}$$

In the linear regime the PP effect is described by following mathematical equation:

$$P_{pp} = \sum_j e_{ij}\epsilon_j, \tag{2.2}$$

where ϵ denotes the strain and e_{ij} represents the piezoelectric constants (Table 2.3). In case of the III nitrides, equation 2.2 can be reduced to the following expressions:

$$\begin{aligned} &P_{pp} = e_{33}\epsilon_3 + e_{33}(\epsilon_1 + \epsilon_2), \\ &\epsilon_3 = \tfrac{(c-c_0)}{c_0}, \\ &\epsilon_1 = \epsilon_2 = \tfrac{(a-a_0)}{a_0}. \end{aligned} \tag{2.3}$$

where ϵ_3 is the strain along the c direction, $\epsilon_1$and ϵ_2 represent the in-plain strain, and a_0 and c_0 denote the lattice constants (Table 2.1). However, equation 2.3 does not include the third independent component of the piezoelectric tensor, ϵ_{15}, the one that describes the shear strain. It is assumed that this component is negligible, because in general the growth of epilayers is always in the [001] direction. According to Bernardini et al. [12], the piezoelectric constants for III-V nitrides are one order of magnitude larger than for other III-V materials, and reversed in sign - meaning that for Ga(Al)-face heterostructures the spontaneous polarization is pointing towards the substrate (Figure 2.5). The SP constant of AlN is about three times larger then the constant of GaN, and (on the other hand) the lattice mismatch is 2 % between these

	P_{sp}(C/m^2)	e_{33}(C/m^2)	e_{31}(C/m^2)
GaN	-0.029	0.73	-0.49
AlN	-0.081	1.46	-0.60
InN	-0.032	0.97	-0.57
GaAs	-	-0.12	0.06
AlAs	-	-0.03	0.01

Table 2.3: Spontaneous polarization P_{sp} and piezoelectric constants (e_{33}, e_{31}) for III-V semiconductors [12].

compounds. For comparison, the reverse situation is observed for InN and GaN; these materials have a similar SP constant but their lattice mismatch is larger than 10 % (for a_0) [13]. This implies that for a HEMT structure based on $Al_xGa_{1-x}N$ layers and a GaN buffer, the SP effect is bigger then the PP, while for structures based on $In_xGa_{1-x}N$ the PP effect is prevailing. The polarization induced charge at the interface of a heterojunction is related to the gradient of polarization, which is given by a classical formula:

$$\rho_p = \nabla P. \tag{2.4}$$

Applying this relation to a HEMT structure based on GaN/AlGaN (Figure 2.6), the polarization sheet charge density is given by the following equation [14]:

$$\begin{aligned} \sigma &= P(Al_xGa_{1-x}N) - P(GaN) = \\ &= \left\{P_{sp}(Al_xGa_{1-x}N) + (P_{pp}(Al_xGa_{1-x}N)\right\} - \left\{P_{sp}(GaN)) + P_{pp}(GaN)\right\}. \end{aligned} \tag{2.5}$$

Because the typical thickness of the GaN buffer layer (BL) grown on sapphire exceeds 2 μm, the layer is relaxed (Figure 2.5) and the piezoelectric polarization for the GaN layer equals zero in this equation. Changing from Ga-face to N-face, polarity flips and the spontaneous and piezoelectric polarization vectors change their sign. The band diagram for a standard HEMT structure is presented on Figure 2.6b. For the undoped AlGaN layer the conduction band goes down from the surface to the GaN/AlGaN interface. As a result of the differences in bandgap, a quantum well is formed at the GaN/AlGaN interface. The states in the quantum well are filled by electrons.

On the basis of equation 2.5 it is possible to estimate the sheet charge density induced by the spontaneous and the piezoelectric polarization which will be captured in the quantum well. Regardless of the details, a number of important assumptions must be made. First, it is assumed that the very thin $Al_xGa_{1-x}N$ layer has the same lattice constant as the GaN buffer layer. Because the $Al_xGa_{1-x}N$ layer is so thin, it is assumed that the layer is highly strained but not cracked yet. Second, there is a linear relation between the AlGaN composition and lattice, elastic, piezoelectric

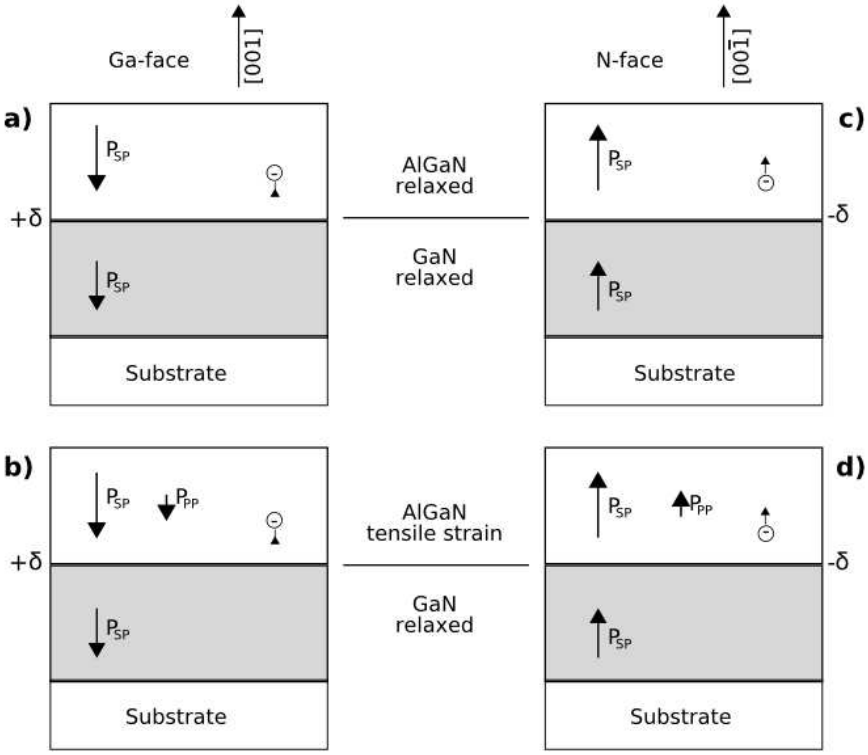

Figure 2.5: Spontaneous and piezoelectric polarization in Ga and N-face for HEMT structure [15].

and spontaneous polarization constants (Vegards law). Finally, applying all these assumptions to equation 2.5 the separate influence of P_{SP} and P_{PP} can be calculated; the results are presented in Figure 2.5. It is clear that charges induced by both types of polarization are of the same order of magnitude; therefore both effects are equally important for the HEMT structure. For an $Al_{0.25}Ga_{0.75}$ top layer the total induced 2DEG equals $1.4\times10^{13}\,m^{-2}$ where at maximum charge induced by spontaneous P_{sp} and P_{pp} equals $6\times10^{12}\,m^{-2}$ and $8\times10^{12}\,m^{-2}$ respectively (this value is in fact very close to the results presented for real HEMT structures).

According to equation 2.5 and equation 2.1, it is possible to induce positive ($+\delta$) or negative ($-\delta$) charge on the GaN/AlGaN interface by changing the polarity of the HEMT structure. If the charge is positive ($+\delta$), free electrons tend to compensate the polarization induced charge (Figure 2.5a) and form a 2DEG. This effect can be enhanced by growing a highly tensile-strained $Al_xGa_{1-x}N$ layer (Figure 2.5b) with a high Al content. The only limiting factor in this case is the small critical thickness

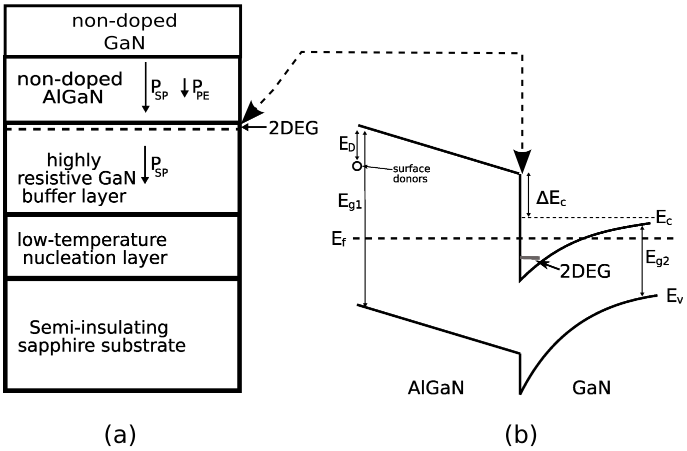

Figure 2.6: Schematic drawing of the standard HEMT structure (a) and corresponding band diagram (b). The vertical arrows on the left image show the direction of spontaneous and piezoelectric polarization in the structure.

of AlN (this it the main reason why the $Al_xGa_{1-x}N$ layer is used) grown on the GaN buffer. For N-polar material the polarization induced charge is negative (-δ) so it will cause an accumulation of holes (Figure 2.5c, d) at the heterojunction interface [15].

The schematic diagram of Figure 2.5(a and b) represents merely the basic model of the perfect HEMT structure based on 2DEG and two-dimensional holes gas (2DHG), respectively. The real construction of the standard HEMT structure based on GaN/AlGaN layer with Ga-polarity grown on a sapphire substrate is presented in Figure 2.6a. The first epilayer, the low temperature GaN (or AlN) NL, is deposited at the beginning of the growth process. This layer consists of many small crystallites, that stimulate the Volmer-Weber growth mode [2]. It improves surface morphology (Figure 2.3) and reduces the number of defects in the high temperature BL. The deposition temperature of that layer is between 400 and 600 °C and it is different for the GaN and the AlN NL. Although this is the thinnest layer in the typical GaN based HEMT structure (only 20-25 nm thick), it has an enormous influence on the properties of the layers deposited on it.

In the next part of this thesis it will be demonstrated that by changing the growth conditions of the NL it is possible to control the electrical properties of the BL. Secondly, the high temperature layer is grown, with an optimal growth temperature between 1130 °C and 1170 °C. Because of the high dissipation of energy in the HEMT device, the thickness of this layer should exceed 2 μm. In typical samples the dislocation density in this layer exceeds 10^9 cm^{-2}. In order to prevent parallel conduction of the HEMT transistors the sheet resistance of the GaN BL should be higher than $10^7\,\Omega$cm . In the following step, the top $Al_xGa_{1-x}N$ layer is deposited with similar growth conditions as the BL. The typical Al content is about 20-30 %

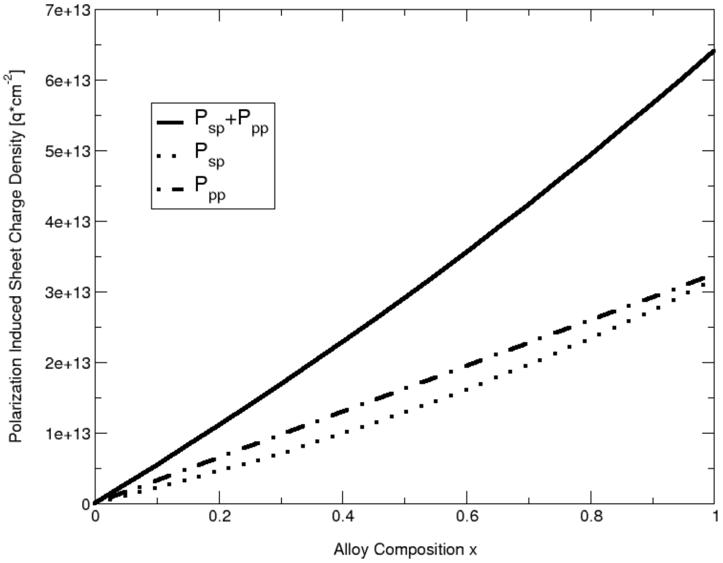

Figure 2.7: Calculated sheet charge density for GaN/AlGaN HEMT structure caused by spontaneous and piezoelectric polarization vs alloy composition of the barrier.

and the thickness is within the range of 25-30 nm. To induce the highest amount of additional strain in order to maximize the PP contribution, the optimal thickness should be just below the critical thickness of $Al_xGa_{1-x}N$ [16]. However, local variation in the material composition, the GaN/AlGaN interface roughness, and the non-uniform strain in the material alter the local distribution of the polarization and reduce the sheet charge density. The 2DEG density for such a HEMT structure is about 1.2×10^{13} cm^{-2} with a mobility around 1200 cm^{2}V^{-1}s^{-1}.

At this point the question about the origin of the electrons emerges. As was already described in section 1.2, for GaAs/AlGaAs counterpart the Si doping in the top layers provides the electrons to the quantum well. In the GaN based HEMT structure it is not necessary to dope the AlGaN layer with silicon to obtain the high density in the 2DEG. The simplified explanation of this phenomena was given by Ibbetson et al. [17]. They assumed that the charge balance equation for the GaN based HEMT structure can be expressed by the following equation:

$$\sigma_{Surface} + \sigma_{AlGaN} - qn_s = 0, \tag{2.6}$$

where $\sigma_{Surface}$ denotes the surface charge due to the ionized surface states, σ_{AlGaN} is the integrated charge due to ionized donors in AlGaN layer, and n_s represents the 2DEG density. The magnitude of BL charge should be as small as possible for well-designed HEMT structures; in this case this parameter can be neglected. Furthermore, it is assumed that the AlGaN layer is undoped (σ_{AlGaN}=0) with the surface states at an energy E_D below the conduction band edge. If the surface states are deep below the Fermi level E_f, no 2DEG is observed since $\sigma_{Surface}$ equals 0. However, in this situation there is a constant electric field in the AlGaN barrier due to the unscreened polarization (spontaneous and piezoelectric) dipole. This is energetically not favorable, thus the conduction and the valance band must be bended from the GaN/AlGaN interface up to the surface (Figure 2.6b). The donor energy is in this case above the Fermi level E_f and therefore, electrons are available to be transferred from the occupied surface states to the empty states in the triangular quantum well.

Another explanation of the source of electrons present in 2DEG can be directly provided based on equation 2.4 [18] applied for interface between air and AlGaN layer. Assuming that in air the vector of polarization equals 0, the sheet charge density $\sigma_{Surface}$ caused by the different total polarizations of AlGaN and air can be expressed as:

$$\sigma_{Surface} = P_{air} - P(Al_xGa_{1-x}N) = -P_{sp}(Al_xGa_{1-x}N) + (P_{pp}(Al_xGa_{1-x}N). \quad (2.7)$$

In this case, because of the spontaneous polarization present in III-V nitrides, there must be a surface charge induced spontaneously in the material. For example: for a relaxed GaN layer (x=0, P_{pp}=0, equation 2.7) the sheet hole density collected on the surface exceeds $n_s=1.8\times10^{13}$ cm^{-2}. For a strained $Al_xGa_{1-x}N$ layer with x=0.3 and a lattice constant equal to GaN (HEMT structure presented on Figure 2.5c) the sheet holes density is equal $n_s=3.5\times10^{13}$ cm^{-2}. These two examples show, that in opposite to HEMT structures based on GaAs/AlGaAs, it is not necessary to dope $Al_xGa_{1-x}N$ layer with Si to increase the 2DEG density. There is enough spontaneous induced charge to fill the GaN/AlGaN quantum well with electrons.

An improved version of the standard HEMT structure was proposed by Shen et al. [19]. In Figure 2.8 a schematic cross section and band diagram of the improved HEMT structure is presented. The new structure consists of the standard GaN and AlGaN layer and with an additional AlN layer (spacer) in between. This additional layer increases the effective band offset discontinuity dE_C between the GaN and AlGaN layers. The effective dE_C increases due to the polarization-induced dipoles in the AlN layer. Since the dE_C is higher, penetration of the electrons in the AlGaN layer decreases, resulting in a better confinement of the electrons in the quantum well. Because AlN is a binary compound, the alloy disorder scattering is strongly reduced and through this, it improves the 2DEG mobility. The 2DEG density for this improved HEMT structure is similar to the standard one, but the mobility increases to above 1500 cm^{2}V^{-1}s^{-1}.

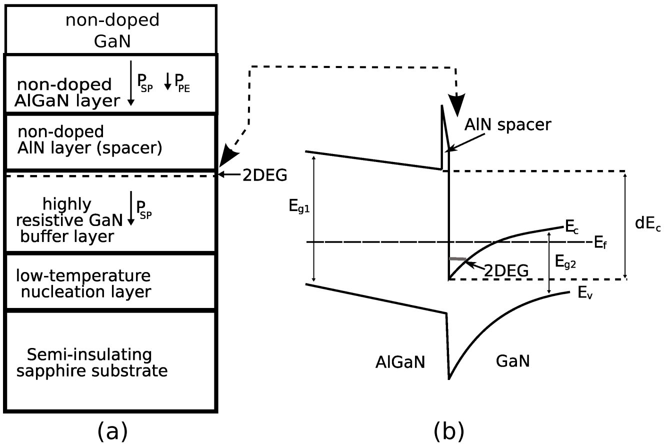
non-doped GaN
non-doped AlGaN layer
P_{SP} P_{PE}
non-doped AlN layer (spacer)
2DEG
highly resistive GaN buffer layer
P_{SP}
low-temperature nucleation layer
Semi-insulating sapphire substrate
(a)
AlN spacer
E_{g1}
E_c
E_f
2DEG
E_{g2}
E_v
dE_c
AlGaN
GaN
(b)

Figure 2.8: Schematic drawing of improved structure of HEMT based on GaN/AlN/AlGaN layers (a) and the corresponding band diagram (b) [19].

Bibliography

[1] M. P. Thompson, G. W. Auner, A. R. Drews, J Electron Mater 28 (10) (1999) L17–L19.

[2] F. Degave, P. Ruterana, G. Nouet, J. H. Je, C. C. Kim, Diam Relat Mater 11 (3-6) (2002) 901–904.

[3] P. Perlin, C. Jauberthiecarillon, J. P. Itie, A. S. Miguel, I. Grzegory, A. Polian, Phys Rev B 45 (1) (1992) 83–89.

[4] H. Xia, Q. Xia, A. L. Ruoff, Phys Rev B 47 (19) (1993) 12925–12928.

[5] I. Gorczyca, N. E. Christensen, P. Perlin, I. Grzegory, J. Jun, M. Bockowski, Solid State Commun 79 (12) (1991) 1033–1034.

[6] M. Ueno, A. Onodera, O. Shimomura, K. Takemura, Phys Rev B 45 (17) (1992) 10123–10126.

[7] M. Lada, A. G. Cullis, P. J. Parbrook, M. Hopkinson, APL 83 (14) (2003) 2808–2810.

[8] J. L. Weyher, S. Muller, I. Grzegory, S. Porowski, J Cryst Growth 182 (1-2) (1997) 17–22.

[9] J. Edgar, Properties of Group III Nitrides, Vol. 11, INSPEC, 1994.

[10] L. Liu, J. H. Edgar, Mat Sci Eng R 37 (3) (2002) 61–127.

[11] W. A. Melton, J. I. Pankove, J Cryst Growth 178 (1-2) (1997) 168–173.

[12] F. Bernardini, V. Fiorentini, D. Vanderbilt, Phys Rev B 56 (16) (1997) 10024–10027.

[13] F. Bernardini, V. Fiorentini, Phys Status Solidi B 216 (1) (1999) 391–398.

[14] O. Ambacher, J. Smart, J. R. Shealy, N. G. Weimann, K. Chu, M. Murphy, W. J. Schaff, L. F. Eastman, R. Dimitrov, L. Wittmer, M. Stutzmann, W. Rieger, J. Hilsenbeck, Journal of Applied Physics 85 (6) (1999) 3222–3233.

[15] O. Ambacher, R. Dimitrov, M. Stutzmann, B. Foutz, M. Murphy, J. Smart, J. R. Shealy, N. G. Weimann, L. F. Eastman, Inst Phys Conf Ser - (166) (2000) 493–497.

[16] H. Amano, I. Akasaki, Opt Mater 19 (1) (2002) 219–222.

[17] J. P. Ibbetson, P. T. Fini, K. D. Ness, S. P. DenBaars, J. S. Speck, U. K. Mishra, APL 77 (2) (2000) 250–252.

[18] P. K. Larsen, G. J. M. Dormans, D. J. Taylor, P. J. v. Veldhoven, J Appl Phys 76 (4) (1994) 2405–2413.

[19] L. Shen, S. Heikman, B. Moran, R. Coffie, N. Q. Zhang, D. Buttari, I. P. Smorchkova, S. Keller, S. P. DenBaars, U. K. Mishra, Ieee Electr Device L 22 (10) (2001) 457–459.

Chapter 3

Characterization techniques

In this chapter the standard techniques used for the characterization of the studied samples presented in this thesis are described. The research is focused on epitaxial growth of the semiconductor, so fast and non-destructive methods are preferred. The exception is the Hall effect measurement - the wafer with the epitaxial layer has to be cut in smaller peaces and processed into suitable samples. On the other hand this is the simplest method that gives informations about the mobility of the majority carriers. In this chapter two of the applied characterization techniques will not be described: photoluminescence and defect selective etching. Photoluminescence is skipped because there is already a dissertation, written by our colleague Victoria Kirilyuk [1], completely devoted to this technique. Defect selective etching is a very simple and fast technique used for investigation of the type and density of the dislocations in the epitaxial layer. A new dissertation by Łukasz Macht [2] deals extensively with this method.

3.1 Hall measurement

Hall measurements using the van der Pauw configuration is the most frequently used method to determine the carrier concentration, sheet resistance and mobility of the majority carriers in semiconductors. The basic physical principle underlying the Hall effect is the Lorentz force (Figure 3.1). The moment an electron moves along a direction perpendicular to an external magnetic field, it experiences a force acting normal to both directions and will be deviated from its original path. For the analysis to be valid, the samples must be homogeneous in thickness, contacts should be sufficiently small and there should not be any isolated holes on the surface [3]. Another important requirement for the Hall measurements is that the contacts should behave ohmic in the used current range. The magnitude of the measured Hall voltage

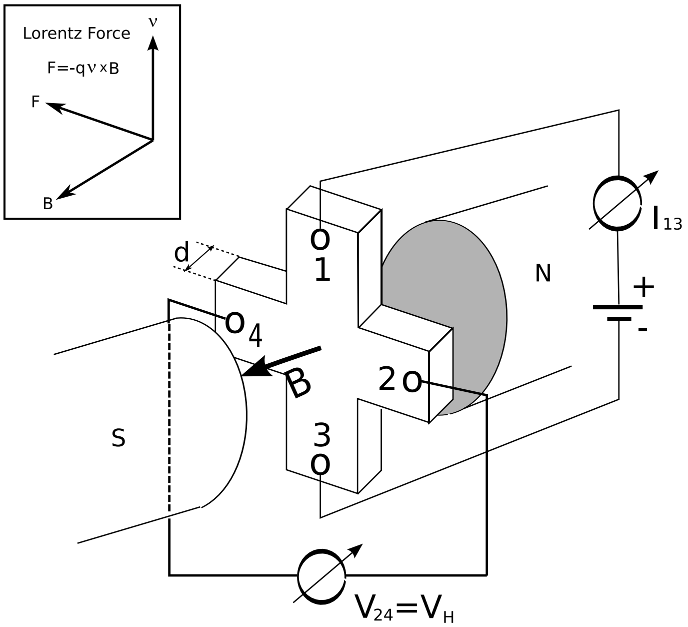

Figure 3.1: Schematic of van der Pauw configuration used in determination of Hall voltage V_H.

V_H (Figure 3.1) equals :

$$|V_H| = I_{13}B/qnd, \tag{3.1}$$

where q (1.602×10^{-19} C) is the elementary charge, I_{13} is the current flowing through the sample, B stands for the magnetic field, d is the thickness of the sample, and n is the bulk density of the charge carriers. Thus, by measuring the Hall voltage and by applying the above mentioned equation (3.1) the bulk carrier concentration (or sheet carrier concentration n_s=nd) can be calculated. To increase the accuracy of the V_H values, the measurements obtained for different combinations of contacts can be averaged. Moreover, to reduce the offset voltage, caused by non-symmetric contact placement, sample shape, and bad contacts, the data are acquired for both positive and negative magnetic field directions and averaged. Another important parameter that can be extracted using the standard Hall setup is the carrier mobility. In order to calculate the mobility of the carriers, the following equation can be applied:

$$\mu = |V_H|/R_sIB = 1/(qn_sR_s), \tag{3.2}$$

where R_s is the sheet resistance of the investigated sample. When the conducting layer thickness is known, the bulk resistivity can be calculated (ρ=R_sd). The most convenient method for R_s measurements was proposed by van der Pauw [3].

According to this author it is necessary to measure two characteristic resistances R_A and R_B:

$$\begin{aligned} R_A &= V_{43}/I_{12}, \\ R_B &= V_{14}/I_{23}, \end{aligned} \tag{3.3}$$

where V_{43} is voltage measured between contacts numbered 4 and 3, and I_{12} is the current applied between contacts 1 and 2 (see Figure 3.1). The value of the characteristic resistances R_A and R_B are related to the sheet resistance R_s through van der Pauw equation:

$$\exp(-\pi R_A/R_S) + \exp(-\pi R_B/R_S) = 1. \tag{3.4}$$

In order to facilitate the solution of R_S from equation 3.4 the following formula can be used:

$$\rho = \frac{\pi d}{2\ln(2)}(R_A + R_B) f(\frac{R_A}{R_B}), \tag{3.5}$$

in which:

$$f \simeq 1 - (\frac{R_A - R_B}{R_A + R_B})^2 \frac{\ln(2)}{2} - (\frac{R_A - R_B}{R_A + R_B})^4 \left\{ \frac{\ln(2)^2}{4} - \frac{\ln(2)^3}{12} \right\}. \tag{3.6}$$

The Hall method is the main technique for the basic evaluation of HEMT structures. Figure 3.2 presents the resistivity, carrier concentration and mobility measured for a HEMT structure in the temperature range between 7-300 K. As opposed to bulk GaN, the carrier concentration in a GaN/AlGaN based HEMT structure is almost constant in a temperature range between 4-300 K. Moreover, the mobility of the electrons exceeds 1000 $\mathrm{cm^2V^{-1}s^{-1}}$ while the mobility measured for non-intentionally doped GaN epilayers is limited within the range 50-550 $\mathrm{cm^2V^{-1}s^{-1}}$ (for samples prepared at the Radboud University in Nijmegen). As opposed to the carrier concentration, the carrier mobility is a strong function of the temperature. Based on these measurements it is possible to extract information about scattering factors like: the interface roughness, polar-optical phonon or piezoelectric scattering [4, 5]. A more thorough interpretation of these data can yield detailed information about the scattering mechanisms present in the semiconductor. However, it lies outside the scope of this study and for that reason it will not be presented here.

3.2 Depletion capacitance-voltage measurements

Capacitance-Voltage (C-V) measurements [6, 7] of a reverse-biased Schottky barrier is a convenient, non-destructive (using a Hg probe), and fast method for determining

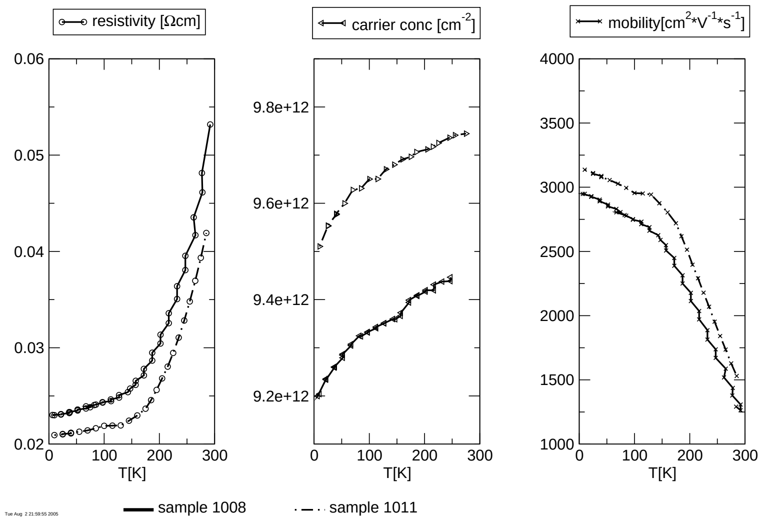

Figure 3.2: Typical characteristics for resistivity, 2DEG density and mobility as a function of the temperature for GaN/AlGaN HEMT structures.

the doping profile in semiconductors (Figure 3.3). For measurements it is necessary to form an ohmic and a Schottky contact on the surface of the sample. In case of the Hg-probe method this is realized by placing two spots of mercury on the sample surface. A small spot with a well defined area is used as Schottky contact and a large one works as an ohmic contact (if the current per unit area is small enough, Schottky contact has an ohmic characteristic). The main disadvantage of this method is that the maximum depletion depth is limited by the electrical breakdown voltage at high reverse bias, especially for highly doped material. In order to measure the C-V profile it is first necessary to apply a reverse DC bias to the Schottky contact, placed on the surface of the sample. That results in formation of a depletion region with a certain depth and thus, a electrical capacitance. Moreover, charges of one sign are induced on the metal site and charges with the opposite sign are induced on the semiconductor site. At the same time the AC signal should be applied to measure the capacitance. The AC capacitance of the Schottky barrier can be defined as a change of charge Q upon the incremental change of bias:

$$C = \frac{dQ}{dV}. \tag{3.7}$$

The amplitude of the AC signal should be much smaller than the value of the DC bias. The C-V method can be also used for study, of deep impurities levels [8, 9]. Depending on the frequency of the applied AC signal, the charge from deep impurity

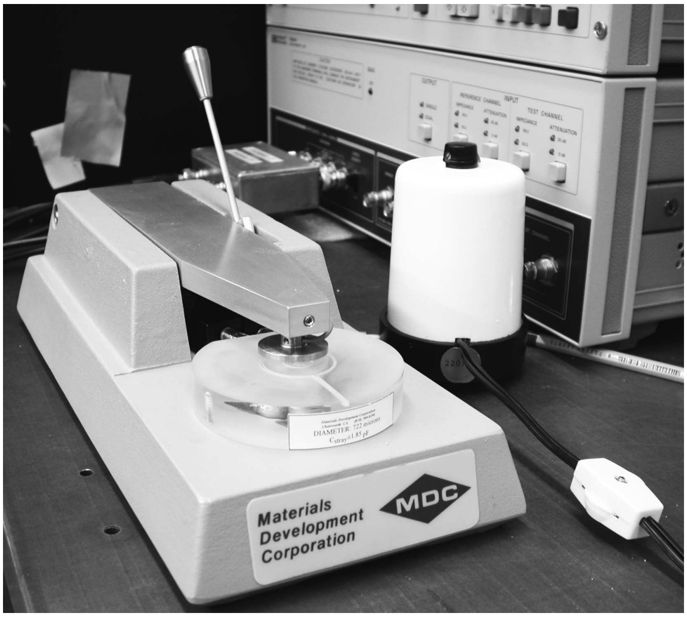

Figure 3.3: Photograph of the Hg-probe used for non-destructive C-V measurements.

levels can follow the AC signal [10, 11]. In such a case, the additionally induced charge will influence the measured value of the capacitance.

To calculate the depletion width, it is necessary to make an assumption that the Schottky barrier behaves like a capacitor with parallel plates with area A, spaced W, and filled with the medium having a dielectric constant equal ϵ_r. The capacitance of such a condensator is expressed by the classical formula:

$$C = \frac{\epsilon_0 \epsilon_r A}{W}. \tag{3.8}$$

Figure 3.4 presents the energy band diagram for a reversed biased Schottky barrier junction made on a n-type semiconductor. It is assumed that the semiconductor is non-degenerated and uniformly doped. To calculate the doping profile of the semiconductor layer, the following equation can be used:

$$[N_D(W) - N_A(W)] = \frac{C^3}{q\epsilon_r\epsilon_0 A^2 \frac{dC}{dV}} = \frac{-2}{q\epsilon_r\epsilon_0 A^2 \frac{d\left(\frac{1}{C^2}\right)}{dV}}. \tag{3.9}$$

Moreover, to simplify the equation 3.9 it is assumed that N_D(W)-N_A(W)≈N_D(W) because for highly doped n-type semiconductors the hole concentration is negligible.

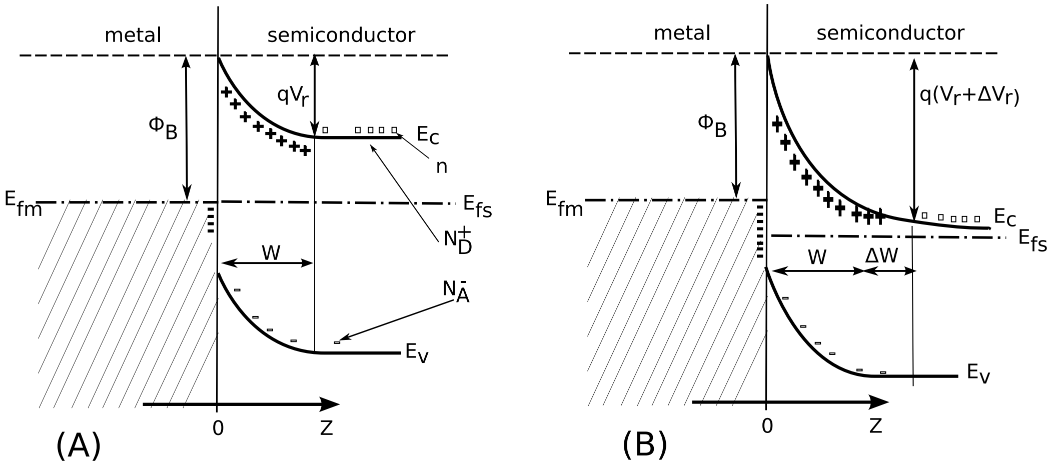

Figure 3.4: Energy band diagram for a Schottky barrier (A) thermal equilibrium situation; (B) reverse bias [8].

Since equation 3.9 is widely used in the characterization of semiconductors a few limitations should be mentioned. In the presented model, it is assumed that the electron concentration is zero (n=0) within the depleted region W (Figure 3.4), and $n = n_0$ outside of it. In practice, the carrier concentration changes from 0 to n_0 over the region of several extrinsic Debye lengths [9] $\lambda_D = \sqrt{\frac{\epsilon_r \epsilon_0 kT}{q^2 n}}$, which equals about 11 nm for GaN samples with a carrier concentration n=1×10^{17} cm^{-3} at room temperature. It means that if the sample has an abrupt doping profile $(N_D - N_A)$ with respect to λ_D, it will be impossible to measure it precisely by the C-V method. Another factor disturbing the doping profile measurements are overlapping depletion regions. When an n-type layer is deposited on a p-type layer or a semi-insulating layer (as is the case of the HEMT structures), an additional depletion region will exist at the interface of these two materials. This depletion region overlaps, at a high enough reversed bias, the depletion layer created by the Schottky barrier. This results in artifacts in the measured C-V profile. In this situation the measured C-V profile will differ from the real doping profile. Another factor causing an error in the measurements is the series resistant effect. As stated earlier, equation 3.9 assumed that the capacitance is the only element present in the measured circuit. In practice, there will always be a series resistance R between the Schottky barrier and the ohmic contact and the relation between the measured capacitance C_m and actual capacitance C is changed to:

$$C_m = \frac{C}{1 + (\omega RC)^2}. \tag{3.10}$$

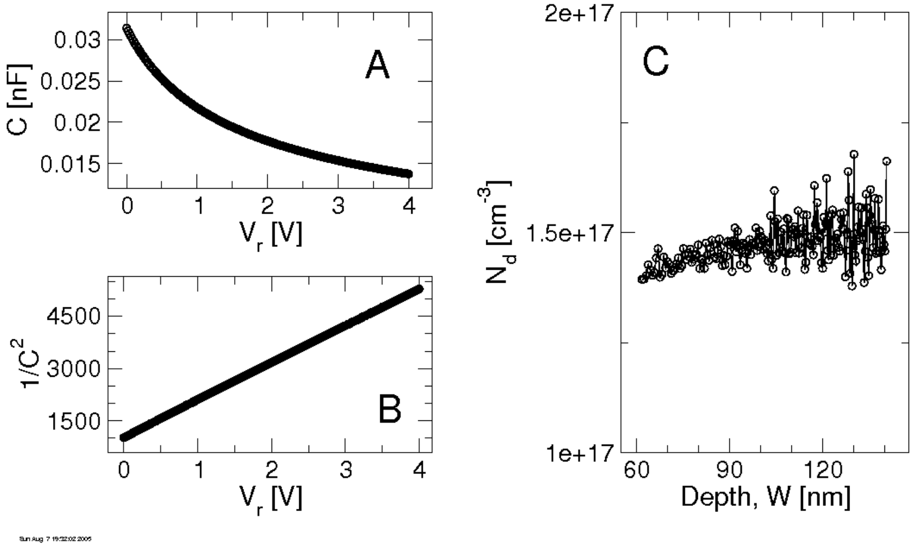

Figure 3.5: The example of the C-V measurement (A) using Hg-probe measured for $2\,\mu$m thick non intentionally doped, n-type GaN sample. A plot $1/C^2$ versus applied voltage (B) should be a straight line with a slope determined by N_d (equation 3.9). The plot (C) presents calculated doping profile using equation 3.9 and equation 3.8.

It is obvious that this series resistance will affect the calculations of the depletion depth value (equation 3.10) if the appropriate correction is not applied. As a rule of thumb it is assumed that if $\omega RC \geq 0.2$ the profile will be distorted. Moreover, if $\omega RC \geq 0.4$ equation 3.9 cannot be applied at all. Now the question arises: is it possible to calculate the 2DEG density based on C-V measurements if a HEMT structure consists of a highly resistive GaN buffer layer, a 1 nm AlN interlayer and the $Al_xGa_{1-x}N$ layer on top. In a HEMT structure there is a large carrier confinement on the GaN/AlGaN interfaces and thus the C-V concentration does not have a direct physical meaning [12]. However, Kroemer et al. [13] showed that if n(z) is a real carrier concentration profile and $\hat{n}(z)$ is the C-V profile, there is still a conservation of the charge, it means:

$$n_s = \int_0^\infty \hat{n}(z)dz = \int_0^\infty n(z)dz. \tag{3.11}$$

Assuming that for a GaN/AlGaN based HEMT structure the GaN layer is highly resistive (compensated), equation 3.11 can be used for 2DEG density calculations using the measured C-V profile (Figure3.6).

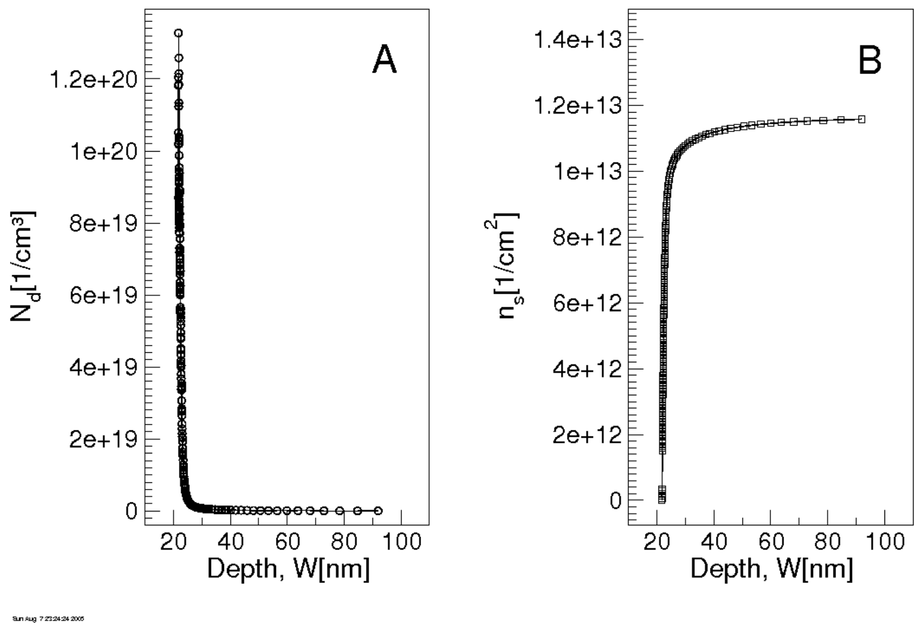

Figure 3.6: The example of the C-V doping profile (A) measured using Hg-probe for $2\,\mu$m thick non-intentionally doped, GaN/AlGaN HEMT. Plot (B) presents the calculated 2DEG density using equation 3.11.

3.3 In-situ reflectance measurements

Because of its easy implementation, a normal incidence reflectance measurement is a basic, standard method for in situ monitoring of the MOCVD growth process. In case of MOCVD, optical techniques are essentially the only viable in situ methods that allow investigating of the growth process in the high pressure, high temperature and chemically reactive deposition environment. Figure 3.7 shows a photograph of the MOCVD reactor with the in situ reflectance measurement setup. The schematic diagram of the in situ reflectance setup is presented on Figure 3.8. The main part of the setup consists of a light source (diode or xenon lamp) and a detector (photo diode or CCD camera). A standard lens is used to focus the light on the sample inside the MOCVD reactor. The data from the detector are collected and analyzed by a computer. During the reflectance measurements light is partially reflected from the investigated sample (Figure 3.9). The fraction of the light intensity being reflected (R), from a single interface between vacuum and bulk material with a refractive index n and an extinction coefficient index k, can be simply described by:

$$R = I_{reflected}/I_{incident} = \left\{(n-1)^2 + k^2\right\} / \left\{(n+1)^2 + k^2\right\}. \tag{3.12}$$

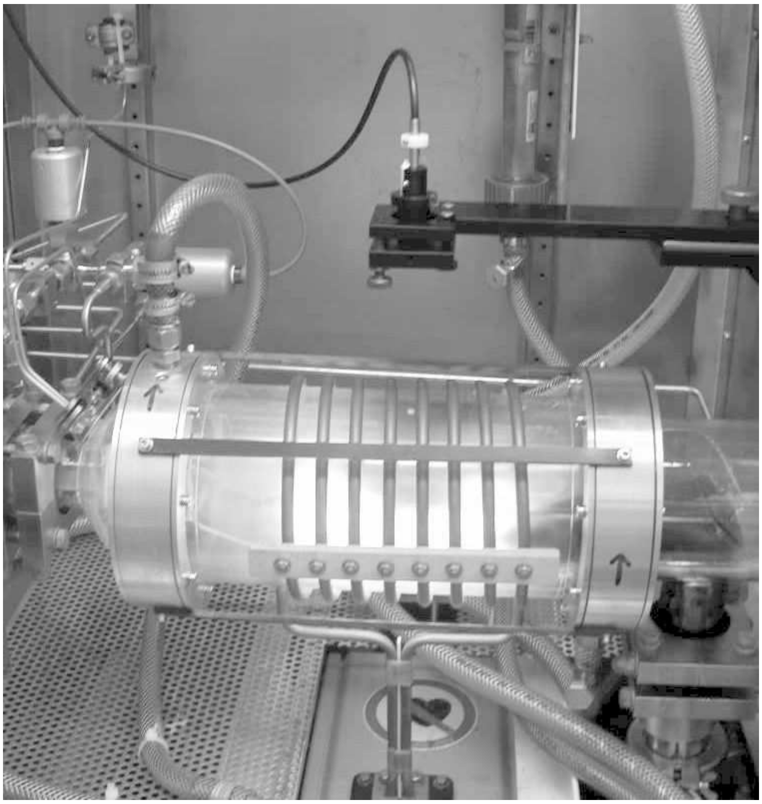

Figure 3.7: MOCVD reactor with in situ reflectance measurement system.

Both parameters n and k show a dispersion as well as a change with the actual substrate's temperature and layer composition. In the simplest case when the investigated sample consists of a substrate and a deposited layer, the most convenient way to calculate the layer thickness is to take the measurements period of the reflectance-transient. For light perpendicularly incident the equation $2nd = i\lambda$ where d is the thickness of the film, λ is the wavelength, and i is an integer must be satisfied. If the sample is transparent or at least partially transparent (for example due to the surface roughness) at the wavelength of the incoming light, the collected signal shows an intensity-modulation, related to the interference effect. One part of the incoming light is partially reflected at the surface. Moreover, another part penetrates the deposited layer (Figure 3.9) and reflects from the substrate/layer interface, and will travel back to the surface. The intensity of the reflected light is then given by a superposition of all reflected beams, and through this a constructive and a destructive interference will occur. The observed intensity-modulation of the light are Fabry-

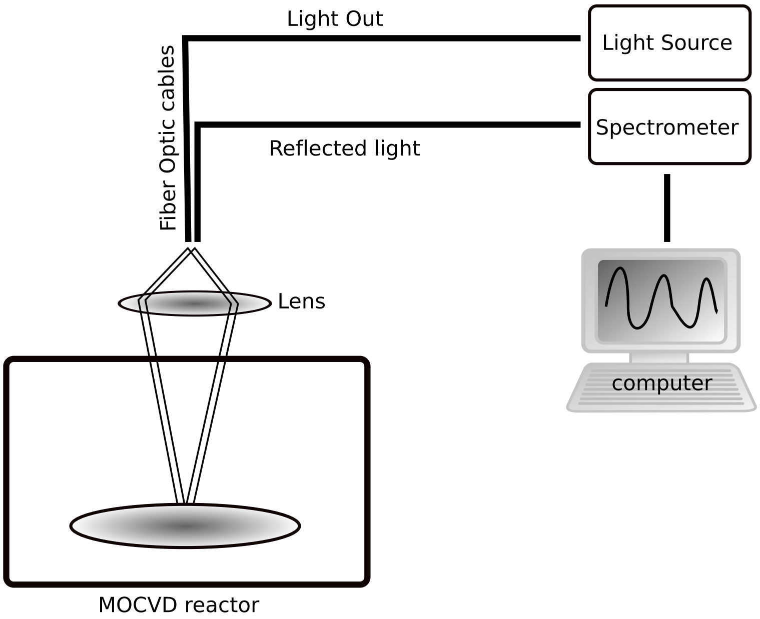
Light Out
Light Source
Fiber Optic cables
Spectrometer
Reflected light
Lens
computer
MOCVD reactor

Figure 3.8: Schematic diagram of in situ reflectance setup used for monitoring the growth process in MOCVD.

Perot oscillations. It should be mentioned that these oscillations can be also observed without the external source of light, when the process is conducted at a temperature above 1000 °C. In this case the sample acts as the source of light itself (Figure 3.10). Calculating the Fabry-Perot oscillations is the simplest way to measure the growth rate during MOCVD process. It is also possible to calculate not only the growth rate, but also the reflectance time trace itself, taken during the semiconductor film deposition, optical constants, and the roughness of the epitaxial layer [14–16] by using more sophisticated methods. Examples of the in situ measurements will be presented in next the chapters.

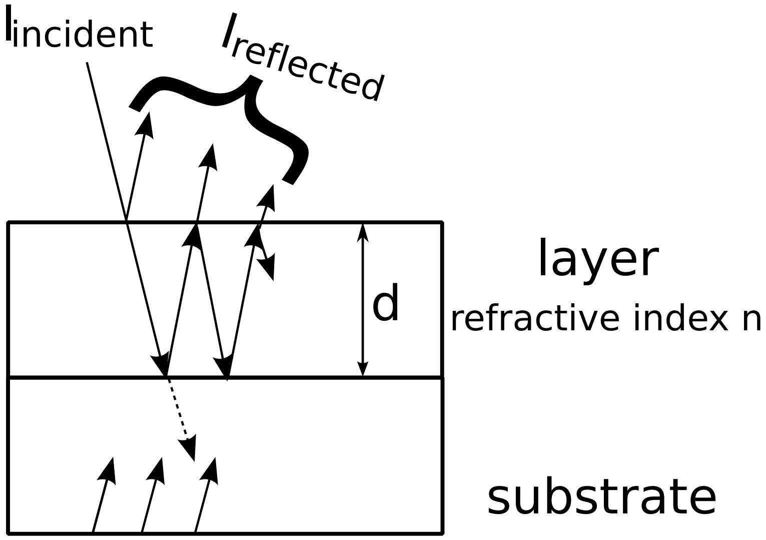

Figure 3.9: Reflection of light at a transparent/semitransparent layer growing on top of a substrate. The intensity of the reflected light is given by the superposition of all reflected beams. If the deposition process is at high temperature above 1000 °C the sample itself can be the source of the light strong enough to observe Fabry-Perot oscillations.

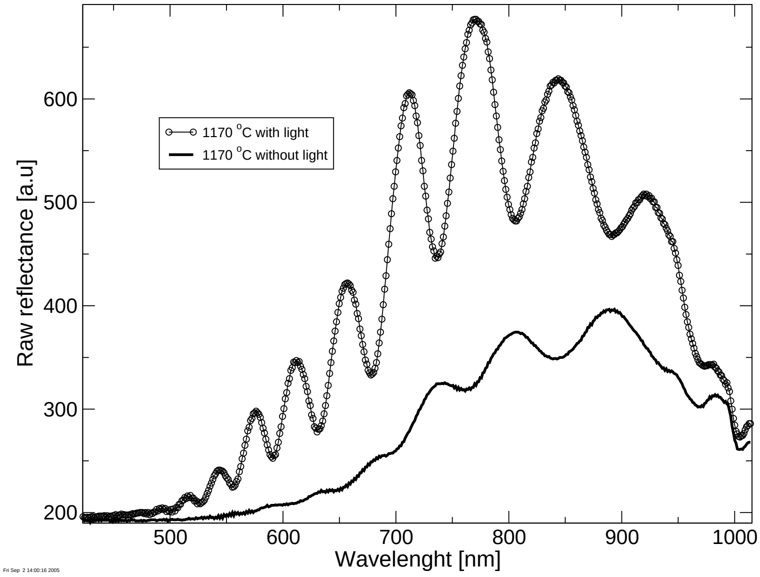

Figure 3.10: Spectrum of the light measured at 1170 °C for the 1.7 μm thick GaN sample with and without external source of light. The difference in the position of the peaks between two plots is caused by slow decomposition of the sample during the measurement.

3.4 Grazing X-ray reflectometry

Since the development of the new III-V materials, there are more and more devices that require deposition of ultra thin layers (nano scale). A good example is the HEMT structure based on GaN/AlN/AlGaN layers. The thickness of the nucleation layer used for the GaN deposition on sapphire is about 20 nm (see Chapter 6). In an ideal model, the AlN layer should be about 1 nm thick, whereas the top AlGaN layer thickness should not exceed 25 nm. In order to control the thickness and roughness of those layers grazing X-ray reflectometry (XRR) technique seems to be a good choice [17]. The main advantages of this method are:

- non-destructive measurement process;
- simple physics beyond it;
- relatively fast measurement process;
- global information about the investigated surface (roughness and morphology) - the signal is collected from the area of 20 mm^2;
- many materials can be investigated (metals, insulators, semiconductors).

The technique is based on the reflection of the X-ray beam from a surface (Figure 3.11). The beam of X-rays is directed toward the surface of the sample through the divergence slit. The beam hits the surface at an angle θ_i and is the reflected to the detector at an angle θ_r. For specular reflected rays $\theta_i = \theta_r$. By changing simultaneously the incident and reflected angle it is possible to collect the intensity vs θ data. The reflection is described by classical rules of physics for

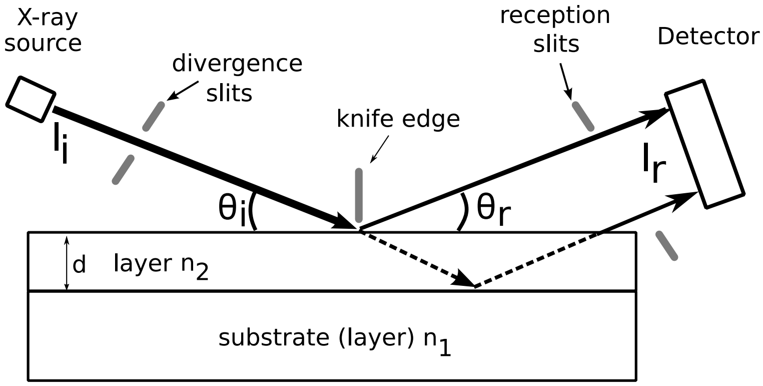

Figure 3.11: Schematic view of X-ray grazing reflectometry experiment.

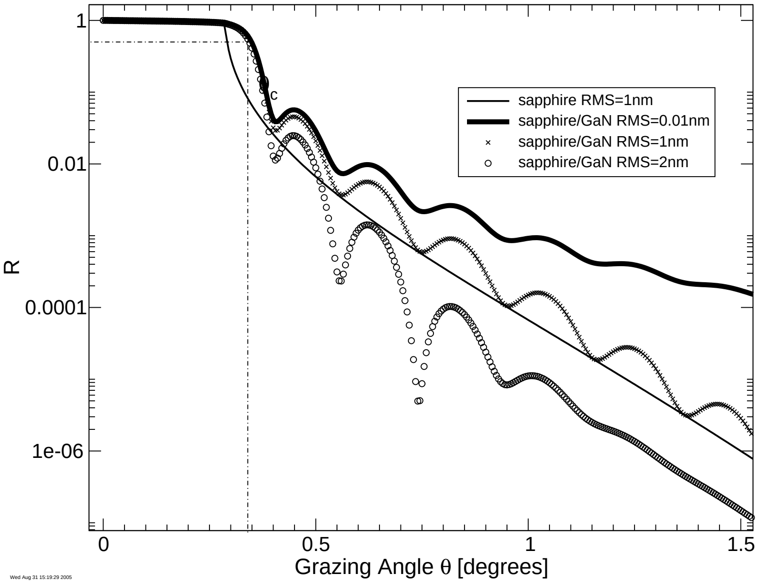

Figure 3.12: Simulated curves for X-ray reflectivity experiments for sapphire and 20 nm thick GaN epilayer deposited on sapphire. The amplitude of X-ray reflectance oscillations is proportional to the RMS roughness of the GaN layer. For just sapphire the oscillations are not observed.

refraction and reflection of light with optical indexes related to the wavelength used in the measurement and to the medium properties. For X-rays the index of refraction can be given by:

$$n = 1 - \delta + i\beta, \tag{3.13}$$

where δ is associated with the dispersion and has a very small value (in order $10^{-5} - 10^{-6}$). β is imaginary part of refraction index related to absorption (usually β is smaller then δ). Figure 3.12 presents a few simulated XRR curves for different samples.

Starting from $\theta = 0$ the total reflection of the X-ray beam by the surface is observed. For incident angles below a critical angle, θ_c, ($\theta < \theta_c$), after total reflection occurs. The critical value θ_c is defined as an angle where intensity falls to 50% of the plateau. By applying Snell's law and small angle approximations ($n_{air} = 1$), the critical angle, θ_c has the following relation to δ:

$$1 - \delta = cos(\theta_c) \approx 1 - \frac{\theta_c^2}{2} \Rightarrow \theta_c = \sqrt{2\delta}, \tag{3.14}$$

if absorption is considered negligible. For incident angles greater then θ_c, the X-ray beam penetrates inside the layer. For a thin GaN layer deposited on sapphire the reflectivity curves for a single layer exhibit fringes (sapphire/GaN Figure 3.12). The fringes are the result of the difference in optical index n between sapphire and GaN which causes constructive interference at each interface. So for a single layer periodicity of the oscillations is directly related to the thickness and X-ray wavelength where the amplitude is related to the surface roughness. The same rules can be applied for multilayer systems. Figure 3.13 shows simulated X-ray reflectance data for 20 nm thick GaN and AlN layers deposited on a sapphire substrate with an surface RMS roughness equal to 1 nm. As should be expected the frequency of oscillations of the reflected beam is about two times higher compared to the single layer system with only 20 nm thick GaN (Figure 3.12). The precision of calculated parameters (thicknesses, roughness) of the layers based on XRR measurements depends strongly on three main issues [17]: the number of layers in the sample, the total thickness of the layers and the relative index variation between each layer and substrate. Higher number of layers increase the number of generated fringes. If the contrast between fringes and the signal to noise ration is high, then up to 15 layers can be assessed using this technique. The limitation for the thickness measurement can be in solving very short periods of oscillations. On the other hand, the spectrum should reveal a few oscillations over the $2\theta = 4$ degrees recording range. So in practice XRR method is applied successfully for the layers with thickness between 5 nm up to 300 nm. The validation of calculated thickness is quite difficult since there is only a limited number of techniques which can be applied to the same range of thickness

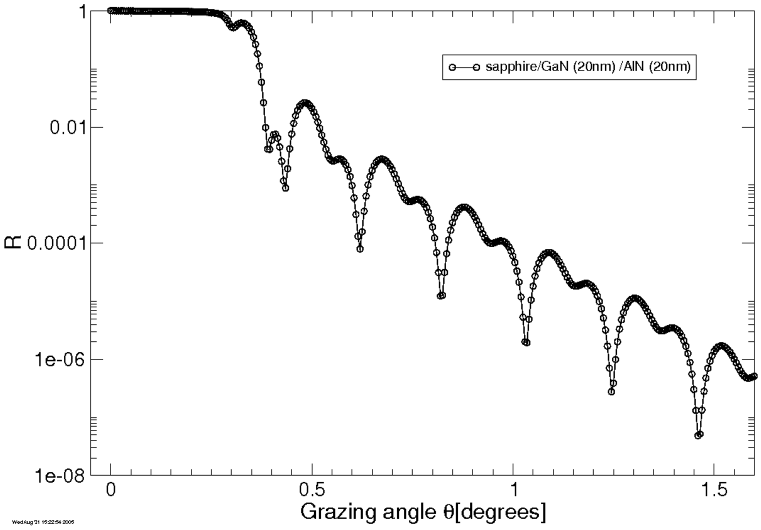

Figure 3.13: Simulated curves for X-ray reflectivity experiments for sapphire sample with 20 nm thick GaN and AlN layer on the top.

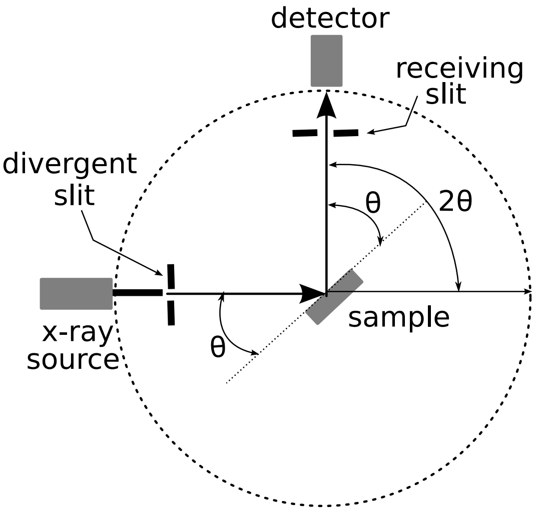

Figure 3.14: Schematic setup for $\theta - 2\theta$ scan. Sample, X-ray source, and detector can be set at any desired angle position.

measurements. However, in case of HEMT structures based on GaN/AlGaN layers the calculated thickness of the $Al_xGa_{1-x}N$ layer shows agreement with capacitance voltage measurements within 25 %. Moreover, RMS roughness values calculated from XRR measurments can be compared with RMS measured using atomic force microscopy (see Table 6.3). The discrepancies between results exceed 30 % but it should be pointed out that there is a large difference between the area investigated by XRR method (0.2x6 mm^2) and atomic force microscopy (50x50 μm^2).

3.5 X-ray diffraction

For the studies described in this thesis the X-ray diffraction equipment (Bruker D8 Discovery) was applied to measure the lattice constant and evaluate the quality of epitaxial layers. The wavelength used for measurements was λ =1.54060 Å. This machine is used mostly for measuring rocking curves or $\theta - 2\theta$ scans, yielding information about the exact sample composition and the crystal quality. Figure 3.14 presents a schematic drawing of the X-ray setup. The main part of it, is a X-ray source, detector, sample holder and system for controlling the angular position of the detector and X-ray lamp. To improve the measurement precision additional slits are applied. By varying θ and measuring signal at 2θ, the interference takes place for all planes parallel to the sample holder. Constructive interference is observed if the Bragg law is satisfied:

$$n\lambda = 2d \cdot \sin(\theta), \tag{3.15}$$

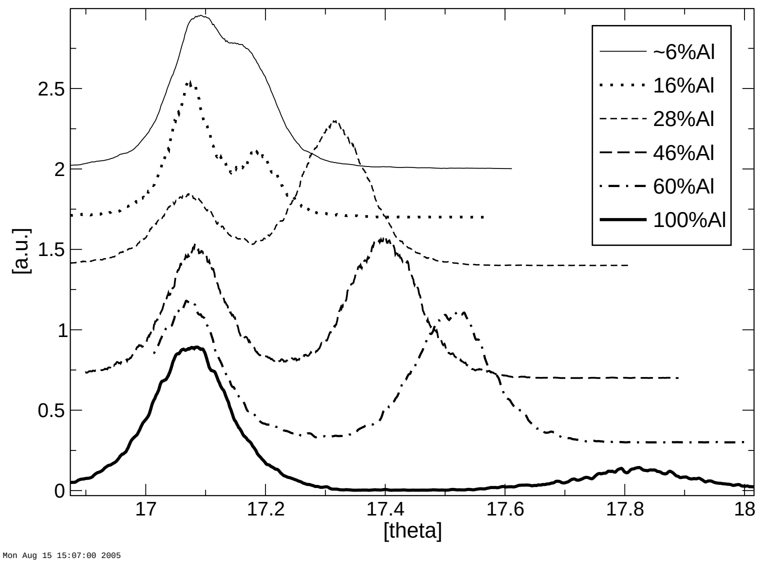

Figure 3.15: Rocking curve, measured for GaN/Al$_x$Ga$_{1-x}$N samples ((002) peaks) grown on sapphire with different Al content. The first peak from the left side represent the GaN layer.

where d is the lattice constant of the crystal and n the order of diffraction. From the peak position it is possible to calculate the lattice constant of the crystal and through this also information about the strain can be extracted. Figure 3.15 presents series of X-ray rocking curves for GaN/Al$_x$Ga$_{1-x}$N samples grown on sapphire. On every curve there are two (002) peaks visible: the first (from the left) is due to the GaN layer and the second is caused by the Al$_x$Ga$_{1-x}$N epilayer. According to Paduano et al. [18] the Al content can be estimated by the X-ray diffraction method through measurements of the a and c lattice constants. The authors compared results obtained from X-ray diffraction measurements with X-ray energy dispersive spectroscopy data. The agreement in results was between 1 to 3 %. Moreover, by measuring several different (hkl) reflections from a single crystal and calculating the rocking curve linewidth, it is possible to estimate the dislocation density. For this purpose the model proposed by Ayers [19] can be employed. The usefulness of this method for GaN material was demonstrated in publication [20].

The rocking curves measurements are very fast and non-destructive for checking the composition and quality of the epitaxial layers. A broad range of sample sizes (from less than 1 mm^2 up to few centimeters) can be measured. On the other hand, a disadvantage of this method is a low spacial resolution and sometimes a low sensitivity. For very complicated $\theta - 2\theta$ scans the direct interpretation of the data can be also difficult.

3.6 Scanning electron microscopy

The scanning electron microscope (SEM) is a type of electron microscope capable of producing high resolution images of a sample surface. In typical SEM configuration (Figure 3.16) the electrons emitted from a electron gun consisting a tungsten filament and anode. The electron beam, which typically has an energy ranging from a few keV to < 50 keV, is collimated by condenser lenses into a beam with a diameter about 5 nm. The electron beam passes through the objective lens, where pairs of scanning coils deflect the beam over a rectangular area of the sample surface and then it is focused by an objective lens. The primary imaging method is by collecting secondary electrons, with an energy below 50 eV. Because these electrons have a low energy, they are generated within a few tenths of a nanometer below the surface of the sample. The penetration depth is strongly dependent on the energy of the incident beam. The intensity of the signal measured by detector depends on the surface area that is exposed to the primary beam. For the samples with uniform chemical composition, a flat area placed perpendicularly to the primary beam makes the detected signal relatively small. For steep surfaces and edges the signal tends to be stronger. By collecting the signal from every point of the investigated area an image with three-dimensional contrast can be created. The magnification produced by SEM is usually in the range between 10 to 2×10^5 times and the resolution is between 4 to 10 nm.

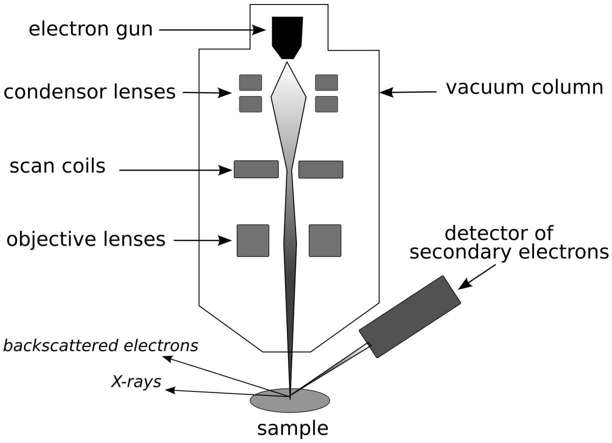

Figure 3.16: Schematic diagram of SEM setup.

In addition to the secondary electrons, backscattered electrons can also be detected. Because the probability of backscattering is a weak function of atomic number, this technique may be used to detect both topological and compositional details of the sample. Moreover, the energy of the back scattered electrons is much higher then the energy of the secondary electrons, they may be scattered deep within the sample. With the use of an additional detector (usually silicon doped with lithium) it is possible to perform energy dispersive X-ray (EDX) spectroscopy measurements. The chemical composition of the sample (see Chapter 9) can be resolved by determining the energies of the X-rays emitted from the area excited by the electron beam (qualitative analysis). The quantitative analysis following from analyzing the rate of detection of the characteristic X-rays. This method cover the full range of elements from Boron to Uranium. The main advantages of SEM over conventional light microscopy include greater magnification and much greater depth of field which allows a large amount of the sample to be in focus. Moreover, SEM produces images with high resolution and also the preparation of the samples is relatively easy. The main disadvantage of SEM is the fact that all measurements are done in vacuum and also the samples should be conductive. Imaging and analysis of insulating materials is difficult due to the excessive charge built-up. This effect can be reduce by deposition a thin layer of conductive material like carbon or gold but in such cases, the SEM method is sometimes destructive for the sample. Despite all these disadvantages, conventional SEM still remains the main tool for investigation in modern science.

3.7 Atomic force microscopy

The atomic force microscope (AFM) is a very powerful technique, derived from the scanning tunneling microscope, invented by Binnig, Quate and Gerber in 1986 [21]. The AFM consists of a cantilever with a sharp tip at its end, typically composed of silicon or silicon nitride. The tip, sizes in the order of nanometers, is placed so close to the surface that the atoms of the tip and the surface are influenced by interatomic forces. These forces lead to a deflection of the cantilever according to Hooke's law,where the spring constant of the cantilever is known. As the tip is scanned across the surface, it reproduces the contours of the surface topography. The displacement of the tip is measured via a laser beam that is reflected from the cantilever into a array of photodiodes (Figure 3.17).

Over the years several modes of operation have been developed for the AFM. The primary modes of operation are contact mode and tapping mode [22].

In contact mode AFM operates by scanning a tip attached to the end of a cantilever across the surface. At the same time, the change in cantilever deflection is analyzed. A feedback loop maintains a constant (at the setpoint) deflection between the cantilever and the sample by adjusting the z position of a scanner. Based on the x,y and z position of the tip the topography of the sample can be calculated.

In the tapping mode AFM operates by scanning a tip attached to the end of an

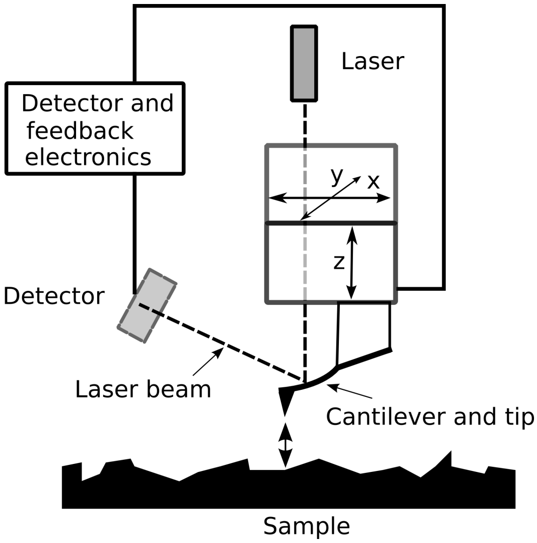

Figure 3.17: Schematic diagram of AFM setup.

oscillating cantilever. The cantilever is externally oscillated close to its resonance frequency, with an amplitude ranging typically from 20 nm to 100 nm. The oscillation gets modified by the tip-sample interaction. The feedback loop modifies the z position of the cantilever to keep (at the setpoint) the root mean square value of the oscillation signal acquired by the detector constant. AFM measurements in tapping mode can be done in ambient and liquid environments. In the liquid, the oscillations need to be at the cantilever resonance. The AFM has several advantages over the SEM. As opposed to the SEM, which provides only two-dimensional image of a sample, the AFM provides a true three-dimensional surface profile. Moreover, AFM is a non-destructive method, and the samples, except for the cleaning of a surface, do not require any special treatment. Unlike the SEM the electrical properties of samples do not influence the quality of the images. The main disadvantage of the AFM is a scanned image size. The SEM can show an area in the order of $1{\times}1\,mm^2$ and depth in the order of 1 mm. Contrarily, the AFM can show only a maximum height on the order of μm and a maximum area of around $100{\times}100\,\mu\mathrm{m}^2$. Moreover, the AFM cannot scan images as fast as an SEM. It may take several minutes for a typical region to be scanned with the AFM, however an SEM is capable of scanning at near real-time, although at a relatively low quality.

Bibliography

[1] V. Kirilyuk, Optical Characterization of Gallium Nitride, PhD thesis, RUN, 2002.

[2] L. Macht, J. Kelly, J. Weyher, A. Grzegorczyk, P. Larsen, J Cryst Growth 273 (3-4) (2005) 347–356.

[3] L. J. v. d. Pauw, Philips Technical Review 20 (59) (1958) 220.

[4] B. K. Ridley, B. E. Foutz, L. F. Eastman, Phys Rev B 61 (24) (2000) 16862–16869.

[5] D. Zanato, S. Gokden, N. Balkan, B. K. Ridley, W. J. Schaff, Semicond Sci Tech 19 (3) (2004) 427–432.

[6] P. Blood, Semicond. Sci. Technol. (1) (1986) 7–27.

[7] S. M. Sze, Physics of semiconductor devices, 2nd Edition, Wiley, New York, 1981.

[8] B. L. Sharma, Metal-semiconductor Schottky barrier junctions and their applications, Plenum Press, New York, 1984.

[9] D. C. Look, Electrical characterization of GaAs materials and devices, Design and measurement in electronic engineering, Wiley, Chichester; New York, 1989.

[10] G. I. Roberts, C. R. Crowell, Solid State Electron 16 (1) (1973) 29–38.

[11] W. Shockley, W. T. Read, Phys Rev 87 (5) (1952) 835–842.

[12] O. Ambacher, J. Smart, J. R. Shealy, N. G. Weimann, K. Chu, M. Murphy, W. J. Schaff, L. F. Eastman, R. Dimitrov, L. Wittmer, M. Stutzmann, W. Rieger, J. Hilsenbeck, Journal of Applied Physics 85 (6) (1999) 3222–3233.

[13] H. Kroemer, W.-Y. Chien, J. S. Harris, J. D. D. Edwall, Appl Phys Lett 36 (4) (1980) 295–297.

[14] W. G. Breiland, K. P. Killeen, Journal of Applied Physics 78 (11) (1995) 6726–6736.

[15] R. S. Balmer, C. Pickering, A. J. Pidduck, T. Martin, J Cryst Growth 245 (3-4) (2002) 198–206.

[16] D. E. Aspnes, Journal of the Optical Society of America a-Optics Image Science and Vision 10 (5) (1993) 974–983.

[17] C. Schiller, G. M. Martin, W. W. Vanderhoogenhof, J. Corno, Philips J Res 47 (3-5) (1993) 217–234.

[18] Q. Paduano, D. Weyburne, S. Q. Wang, Phys Status Solidi A 188 (2) (2001) 821–824.

[19] J. E. Ayers, J Cryst Growth 135 (1-2) (1994) 71–77.

[20] A. Pelzmann, M. Mayer, C. Kirchner, D. Sowada, T. Rotter, M. Kamp, K. J. Ebeling, S. Christiansen, M. Albrecht, H. P. Strunk, B. Hollander, S. Mantl, Mrs Internet J N S R 1 (1-46) (1996) art. no.–40.

[21] G. Binnig, C. F. Quate, C. Gerber, Phys Rev Lett 56 (9) (1986) 930–933.

[22] Q. Zhong, D. Inniss, K. Kjoller, V. B. Elings, Surf Sci 290 (1-2) (1993) L688–L692.

Chapter 4

Growth of GaN epilayers on Si(111) substrates using multiple buffer layers

[*]

We present a study of the growth of high quality GaN films on Si (111) substrates by MetalOrganic Chemical Vapor Deposition technique. In order to improve the quality of the epitaxial films we introduced different nucleation or buffer layers and combinations of them. Our results obtained on an optimized AlN nucleation layer will serve as reference point. In order to improve the quality of the epitaxial films we introduced different combinations of nucleation and intermediate layers. The first combination consists of an optimized AlN nucleation layer followed by a 1 μm thick GaN film, on which we deposited Si_xN_y/GaN intermediate layers. Based on the optimized AlN nucleation layer, we introduced AlGaN/GaN superlattices or AlN intermediate buffer layers. Additionally, we present results on the modification the Si (111) surface with NH_3 to promote nucleation from selective GaN islands. In all experiments the total thickness of the GaN epilayers was 3 μm. X-ray diffraction, photoluminescence, Hall measurements and atomic force microscopy were used in order to elucidate the effectiveness of these growth processes. For the most successful deposition scheme, the one with the Si_xN_y/GaN intermediate layers, the resulting GaN layers are of high quality as compared to the other methods. The donor bound exciton, which dominates the photoluminescence spectrum, showed a full width at half maximum (FWHM) of about 50 meV at room temperature and 10 meV at 4 K. The FWHM of the symmetric (0002) rocking curves in w-scan is about 640 arcsec.

---

[*] based on P.R. Hageman, S. Haffouz, A. Grzegorczyk, V. Kirilyuk and P.K. Larsen, Mat. Res. Symp. Proc. 693 (2002)

The root-mean-square roughness, as measured by atomic force microscopy, does not exceed 10 Å.

4.1 Introduction

Silicon is considered to be one of the best candidates as an alternative, inexpensive and large substrate for depositing GaN despite of the well-known difficulties in this material system. These difficulties are caused by a lattice mismatch of 17%, the combination of an a-polar substrate with a polar epilayer and by thermal expansion coefficient incompatibility. The difference in thermal expansion coefficient between GaN and Si, 5.59 and $3.59\times10^{-6}\,K^{-1}$ (300 K) respectively [1], leads to tensile stress in GaN and thus to crack formation upon cooling down from growth temperature. Future applications, like the integration of silicon-based electronics with GaN opto-electronic devices, and the possible growth of GaN on large wafers are the motivation for this research. Since GaN is not suitable as a nucleation layer on Si(111) substrates due to wetting problems, we have investigated the use of AlN nucleation layers to grow GaN epilayers (layer thicknesses $\approx 3\,\mu$m) on Si (111) substrates. Since the physical properties of these layers are inferior compared to the layers grown on sapphire we have extented our research to different combinations of nucleation and intermediate layers based on the AlN nucleation layer. We will present results on layers grown with a SiN intermediate layer after $1\,\mu$m of GaN growth, with the insertion of low temperature AlN layers as well as GaN/AlN with superlattices. We also modified the silicon surface with an NH_3 treatment to promote the selective island nucleation [2, 3]. The results on this alternative approaches will be compared with those obtained with the AlN nucleation layer.

4.2 Experimental details

GaN layers thickness with about $3\,\mu$m were grown in a horizontal MOCVD reactor on Si (111) substrates [4]. Ammonia (NH_3), trimethylgallium (TMG), trimethylaluminium (TMA), and silane (Si_3H_4), diluted to 50 ppm with H_2 , were used as precursors. The on-axis Si (111) substrates were degreased in organic solvents and etched in a buffered 10% HF solution before growth, then in situ thermally cleaned at 1100 °C in a hydrogen atmosphere. Photoluminescence (PL) measurements were carried out at 4 K; the 325 nm line from a HeCd laser provided optical excitation with an excitation density of about $25\,Wcm^{-2}$. The luminescence was dispersed by a 0.65 m monochromator and detected by a cooled GaAs photomultiplier. High-resolution, X-ray diffraction (XRD) w-scans measurements (rocking-curves) were performed on a Bruker D8 instrument.

4.3 Results and discussion

Our standard GaN is grown on Si (111) substrates, which are first thermally treated at 1100 °C in a hydrogen flow to remove the native oxide. After cooling down from this thermal-cleaning step, the deposition of an AlN nucleation layer takes place. After the depositing the nucleation layer, using a TMAl flow of 20 mmol/min and a NH_3 flow of 4.1×10^{-2} mol/min, the temperature is raised. Immediately after reaching the growth temperature (1170 °C), GaN is deposited using a TMG flow of 63 μmmol/min and an NH_3 flow of 0.1 mol/min resulting in a GaN growth rate of 1.65 μm/h. The AlN nucleation layer has been optimised with respect to the growth time and growth temperature, i.e. 5 minutes growth at 850 °C, resulting in a layer of about 10 nm thick. The 3 μm thick GaN layer showed rocking curve full width at half maximum (FWHM) of the symmetric (0002) and a-symmetric (105) reflections of 832 ” and 702 ”, respectively. Optically, the FWHM of the D^oX peak was found to be 17.6 meV. These results are indicative for good material quality, certainly for the layer thicknesses under investigation. A serious problem in this material system is the formation of cracks. Due to the large difference in thermal expansion coefficient between GaN and Si tensile stress is introduced in the GaN epilayer during cooling down from growth temperature. To have more detailed information on this aspect, we have performed a series of experiments with different thicknesses of the GaN epilayers. From these experiments, it appeared that the tensile stress, even for layers with a thickness of 0.4 μm, is large enough to introduce cracks in the epilayer. Rocking curve measurements showed that for a layer with a thickness of 1.2 μm the FWHM are the smallest for both the symmetric and a-symmetric reflections, being 670 ” and 569 ”, respectively. The quality of GaN grown on sapphire can be remarkably improved by using a so-called selective island nucleation layer [5,6]. These selective islands are formed by depositing the low temperature GaN nucleation layer on a in situ grown Si_xN_y mask. This 30 nm thick GaN nucleation layer is deposited at 525 °C and during heating up to growth temperature (1170 °C), the GaN nucleation layer, deposited on the Si_xN_y mask, transforms from a smooth layer to nano-scale GaN islands, acting as centers for lateral overgrowth [5,6]. First, we tried to demonstrate this original process on silicon substrates and so we treated the silicon substrates with NH_3 for different times. After this NH_3 treatment we deposited our low temperature GaN nucleation layer on it. During heating up to growth temperatures this nucleation layer should transform in selective island of regular shape, size and distribution as was shown for sapphire substrates [2–6]. The results of these experiments are given in Figure4.1 where scanning electron microscope (SEM) pictures are given of these nucleation layers deposited on NH_3 treated silicon for different times. The deposited buffer layer has been cooled down immediately after heating up to growth temperatures. As is obvious from Figure 4.1,

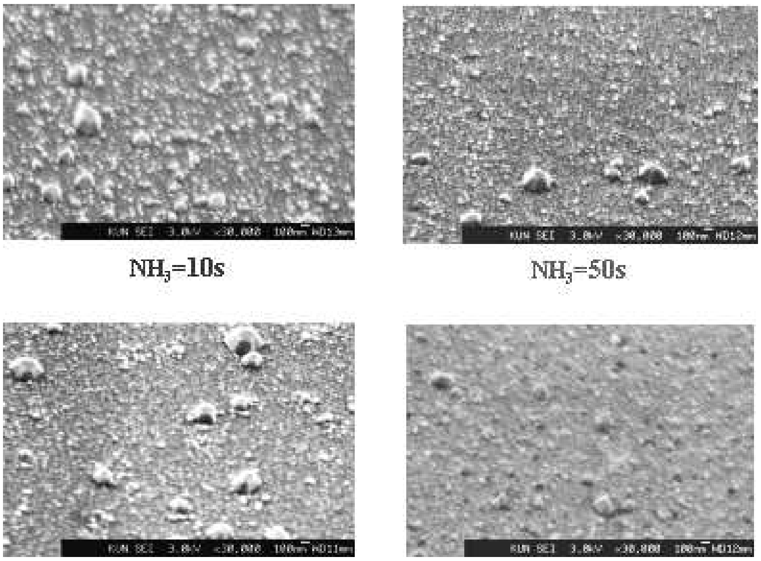

NH_3=10s NH_3=50s

NH_3=20s NH_3=120s

Figure 4.1: SEM pictures of Si (111) substrates treated for different times with NH_3, after heating up the low temperature (525 °C) GaN nucleation layer to growth temperatures (1170 °C).

the very inhomogeneous size distribution of the islands makes this approach not suitable for the deposition of high quality GaN.

In order to reduce the dislocation density and to enhance the general quality of the GaN grown on Si (111), we inserted a Si_xN_y mask after $1\,\mu$m GaN growth. This mask is in situ grown as described above [2, 3]. On this mask a low temperature GaN nucleation layer was deposited and transformed into selective island during heating up. For this procedure the same parameters were used as for GaN on sapphire [2, 3]. On these selective islands nucleation layer a $2\,\mu$m GaN epilayer was grown. This structure is schematically depicted in Figure 4.2a. This new method resulted in a remarkably improvement of the material properties. In figure 3 the PL spectra are given of a $3\,\mu$m GaN layer grown on our AlN nucleation layer and of a GaN layer grown with the inserted Si_xN_y mask. From this figure it is quit obvious that the optical properties have changed dramatically for the better as is demonstrated by the increase of 2.5 times of the PL intensity and the reduction of the FWHM of the D^oX peak from 17.6 to 10 meV. Additionally, the betterment of the structural properties is significant as illustrated by the reduction FWHM of the HR-XRD w-scans from 832 ” to 669 ” for the symmetric and from 702 ” to 547 ” for the a- symmetric reflection. At the same time the free carrier concentration was decreased with one order of magnitude to $2\times10^{16}\,cm^{-3}$. This implies that both the Si_xN_y mask and the silicon substrate are

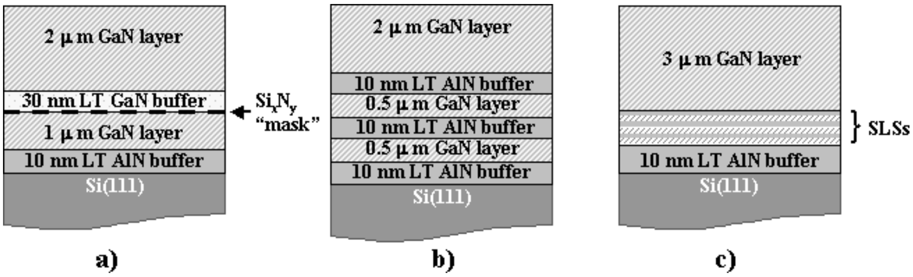
2 µ m GaN layer
30 nm LT GaN buffer
1 µ m GaN layer
10 nm LT AlN buffer
Si(111)
Si_xN_y "mask"
a)
2 µ m GaN layer
10 nm LT AlN buffer
0.5 µ m GaN layer
10 nm LT AlN buffer
0.5 µ m GaN layer
10 nm LT AlN buffer
Si(111)
b)
3 µ m GaN layer
SLSs
10 nm LT AlN buffer
Si(111)
c)

Figure 4.2: Schematic cross sections of the layer structures used in this paper for growing GaN on Si (111)

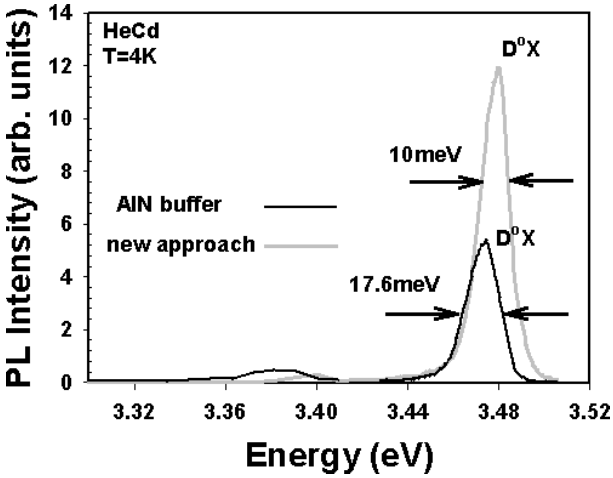

Figure 4.3: PL spectrum of a GaN sample grown on Si (111) with the AlN nucleation layer (black line) and one grown on an AlN nucleation layer with an additional Si_xN_y layer (grey line). Both spectra were recorded at T=4 K.

stable during growth, thereby preventing the incorporation of silicon in the growing layer. Also the surface roughness could be reduced from 1.0 nm to 0.8 nm (RMS) as was shown by AFM measurements on an area of 18.7×18.7 mm^2. The introduction of low temperature GaN or AlGaN buffer layers in the thick GaN layer can reduce the dislocation density considerably and can diminish the tensile stress in the layer [7, 8]. The insertion of such low temperature buffer layers can thus prevent cracking of the layer. According to this principle we introduced an AlN low temperature buffer layer (10 nm, 850 °C growth temperature) after growing 0.5 μm GaN on the AlN nucleation layer, and repeated this sequence once again. As top layer 2 μm GaN was deposited to ensure a total GaN thickness of 3 μm for fair comparisons with the previous experiments. A schematically drawn cross section of this layer sequence is depicted in Figure 4.2b. A different approach to prevent cracking is the insertion of a GaN/AlN superlattice [9]. After the deposition of the AlN nucleation layer we deposited a AlN/GaN superlattices at the usual growth temperature of 1170 °C. On top of this structure 3 μm GaN was deposited for the same reasons as mentioned before (see Figure 4.2c). The layer of Figure 4.2b is not crack free at all and also the HR-XRD w-scans indicate a reduced structural quality as compared to the layers grown like Figure 4.2a), the FWHM of the symmetric reflection increases from 669 ” to 843 ” and the a- symmetric one from 547 ” to 950 ”. In contrast, the Hall measurements indicate an improvement of the electrical properties, n=3.3×10^{15} cm^{-3} and m=150 cm^{2}V^{-1}s^{-1}. The superlattice did not reduce the density of cracks as compared to layers without it but the HR-XRD w-scans gave pretty good values of 641 ” and 648 ” for the symmetric and a-symmetric reflections, respectively. These experiments give a good indication in what direction the research should go in order to grow crack free GaN on Si. To our opinion the three methods discussed above should be optimised and combined to ensure the growth of high quality, crack free GaN layers on silicon substrates.

4.4 Conclusions

Structural properties of GaN layers grown Si (111) substrates were investigated in this paper. Firstly, results on 3 μm thick GaN layers grown an AlN nucleation layer were presented. Although of good quality, the insertion of a Si_xN_y intermediate layer significantly improves the optical and structural properties. It results in a reduction of the D^oX FWHM to 10 meV and a 2.5 fold increase of its luminescence intensity. The FWHM of symmetric and a-symmetric w-scans are reduced from 832 ” to 669 ” and from 702 ” to 547 ”, respectively. This makes our new approach very promising for further improvement of GaN on Si(111) substrates. In order to prevent cracking of the layer, different schemes of buffer and insertion layers were tested. From these experiments it can be concluded that both the insertion of low temperature AlN buffer layers in the GaN layer and the insertion of an AlN/GaN superlattice are not successful in reducing the crack density, but an improvement of the structural quality is found for the latter experiment.

4.5 Acknowledgements

This work was partly financially supported by the Dutch Technology Foundation (STW). Philips Semiconductors kindly provided the silicon substrates.

Bibliography

[1] H. H. Landolt, R. Brnstein, K. Schaifers, P. Biermann, H. H. Voigt, Numerical Data and Functional Relationships in Science, Vol. 17, Springer-Vlg, Berlin ; New York, 1982.

[2] S. Haffouz, V. Kirilyuk, P. R. Hageman, L. Macht, J. L. Weyher, P. K. Larsen, APL 79 (15) (2001) 2390–2392.

[3] P. R. Hageman, S. Haffouz, V. Kirilyuk, L. Macht, J. L. Weyher, A. Grzegorczyk, P. K. Larsen, Phys Status Solidi A 188 (2) (2001) 659–662.

[4] F. K. de Theije, A. R. A. Zauner, P. R. Hageman, W. J. P. van Enckevort, P. K. Larsen, J Cryst Growth 197 (1-2) (1999) 37–47.

[5] S. Haffouz, H. Lahreche, P. Vennegues, P. d. Mierry, B. Beaumont, F. Omnes, P. Gibart, Appl Phys Lett 73 (9) (1998) 1278–1280.

[6] P. Vennegues, B. Beaumont, V. Bousquet, M. Vaille, P. Gibart, J Appl Phys 87 (9) (2000) 4175–4181.

[7] M. Iwaya, S. Terao, N. Hayashi, T. Detchprohm, H. Amano, I. Akasaki, A. Hirano, C. Perrot.

[8] C. C. Yang, M. C. Wu, C. H. Lee, G. C. Chi, J Appl Phys 87 (9) (2000) 4240–4242.

[9] E. Feltin, B. Beaumont, M. Laugt, P. De Mierry, P. Vennegues, M. Leroux, P. Gibart, Phys Status Solidi A 188 (2) (2001) 531–535.

Chapter 5

Structural properties of maskless epitaxial lateral overgrown MOCVD GaN layers on Si (111) substrates

[*]

We report on the maskless epitaxial lateral overgrowth of GaN on structured Si (111) substrates and on its structural properties using transmission electron microscopy (TEM) and photo-electrochemical (PEC) etching techniques. The structured silicon substrates are achieved using photolithography and dry etching; 4 μm-deep holes of 1.5 μm in diameter, each separated by 2.5 μm, are etched in the (111) Si surface. The growth process is started by depositing a 10 nm thick AlN buffer layer at 850 °C and then followed by the growth at high temperature (1170 °C) of the GaN epilayer. The deposition of GaN takes place first on the Si (111) surface covered with AlN in between the holes, i.e. no deposits are formed in the holes. During the growth the GaN layer extends vertically and laterally over the holes until complete coalescence. Transmission electron microscopy shows that regions over the holes contain only dislocations in the basal plane resulting from the bending of dislocations nucleated at the Si/AlN interface and at the coalescence boundary between the two laterally overgrown layers. This results in a drastic decrease of dislocation density in these areas of the films. The revelation of dislocations is also achieved by PEC etching technique.

---

[*] S. Haffouz, A. Grzegorczyk, P.R. Hageman, P Vennegues, E.W.J.M. van der Drift, P.K. Larsen, J Cryst Growth 248 (2003) 568

5.1 Introduction

Despite the difficulties in the growth of high-quality GaN on silicon substrates caused by a lattice mismatch of 17 % and by a thermal expansion coefficient incompatibility, silicon is considered as a good candidate for depositing GaN for electronic applications. The low cost, large-scale availability, good thermal and electrical conductivities and the feasibility of removing the silicon substrates with wet etching are the main motivations for optimizing the growth of III-nitride material on this substrate. The standard growth process of GaN on Si (111), which uses only a low-temperature AlN buffer layer, still results in a high density of dislocations [1]. The use of multiple buffer layers [2] or a SiN_x [3] intermediate layer improved the optical and structural quality of the overgrown GaN films but the dislocations density is still as high as a few $10^9\,cm^{-2}$. However, as recently reported by various research groups [4, 5], an improvement of the physical quality of GaN layers grown by metal organic chemical vapor deposition (MOCVD) can be achieved using the epitaxial lateral overgrown (ELO) technique via selective mask. Although this technique has been proven to be very efficient to reduce the density of dislocations down to $5\times10^7\,cm^{-2}$ [2] using silicon substrates, it still needs a multiple regrowth steps procedure and an ex situ processing step. Recently, Strittmatter et al. [6] have successfully demonstrated a maskless, single-step ELO of GaN on structured Si (111) substrates. The substrates are structured with parallel grooves along or perpendicular to the Si $\left\langle 1\bar{1}0 \right\rangle$ direction.

In the present paper, we will report on the ELO of GaN epilayers using hole openings in Si (111) surface and on structural properties of epitaxial layer using transmission electron microscope, high resolution XRD ω-scans and photo-electrochemical (PEC) etching techniques.

5.2 Experimental details

The GaN epilayers were deposited on (111)-oriented silicon substrates by the MOCVD technique (AIX200). Trimethylgallium (TMG), trimethylaluminum (TMA) and ammonia (NH_3) were used as the precursors of gallium, aluminum and nitrogen, respectively.

The substrates have been patterned by a sequence of dry etching steps using successively inductively coupled plasma (ICP) etching technique (Alcatel METLAB system operating at 13.56 MHz) and electron cyclotron resonance (ECR) plasma (Alcatel DECR200 system operating at 2.45 GHz). Both systems are equipped with a variable temperature chuck (-150 °C to 25 °C). Reactive ion etching (RIE) is carried out with a Leybold Heraeus LH 400 RIE system operating at 13.56 MHz, with a

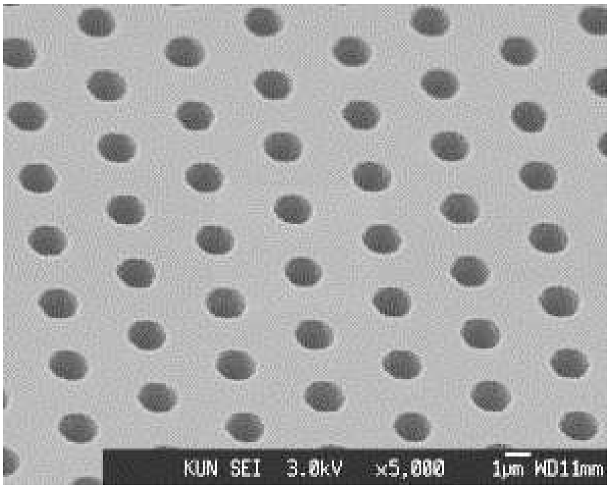

Figure 5.1: Top view SEM image of the structured Si (111) substrate. The pattern consists of 4 μm deep holes of 1.5 μm in diameter, each separated by 2.5 μm.

water-cooled quartz substrate electrode. The silicon substrates were first patterned by an oxide mask deposited in an ICP plasma of C4F8 during 5 min. The flow of the gas was 33 sccm. The corresponding power, pressure and substrate bias were, respectively, 200 W, 0.5 Pa and -150 V. Then a RIE-oxygen plasma was applied to the surface of substrates to remove the organic residues. Finally, the silicon etch is carried out in SF6/O2 ECR plasma at a microwave power of 400 W. The etching pressure, temperature and bias were, respectively, 0.2 Pa, -20 V and -80 °C. The flow of SF_6 and O_2 gases were, respectively, 20 and 2 sccm. Using these conditions, the typical silicon etch rate is about 300 nm/min. The formed pattern consists of 4 μm deep holes of 1.5 μm in diameter, each separated by 2.5 μm as shown in Figure 5.1. TEM specimens have been prepared by a conventional combination of mechanical thinning and ion milling. TEM observations have been conducted on a JEOL 2010 FEG [7] microscope.

High-resolution XRD ω-scans (rocking curves) were performed on a Bruker D8 instrument. PEC etching was performed in a stirred KOH solution (0.004 M) at room temperature. The UV illumination was provided by 450 W Xe lamp. A 100 nm thick Ti layer was used to assure photocurrent conduction.

5.3 Results and discussion

Before loading into the reactor, the silicon substrates were first degreased in organic solvents, etched in a buffered 10 % HF solution, and spin dried. After loading, an in situ thermal cleaning procedure was applied to the surface during 10 min at 1100 °C in a hydrogen atmosphere. After cooling down from this thermal-cleaning step, the deposition of the AlN nucleation layer is started at 850 °C using 20 μmol/min TMA and 4.1×10^{-2} mol/min NH_3. Different growth temperatures and layer thicknesses have been investigated in order to find out the optimum deposition conditions. The optimum thickness of AlN buffer layer was about 10 nm. After the AlN nucleation layer has been deposited, the sample is heated to the GaN growth temperature. Immediately after reaching the high growth temperature (1170 °C), GaN is deposited using 63 μmol/min TMG and 0.1 mol/min NH_3 . Hydrogen was used as carrier gas (3.5 slm). The regrowth pressure was 50 mbar. Figure 5.2a shows a scanning electron microscopy image of a 2 μm thick GaN layer. Clearly observable is that the deposition starts first between the holes, i.e. on the surface of the AlN film; no deposits are formed in the holes. These holes are intentionally etched deeply in order to avoid nuclei formation at the ridges or at the bottom of these structures. For incomplete coalescence we observe inverted pyramidal holes. The two-dimensional evolution of the deposition is schematized in Figure 5.2b. This anisotropy is well known in GaN, which refers to the fact that the vertical extension (in $\langle 0001\rangle$) is much faster than in lateral direction (in $\left\langle 00\bar{1}1\right\rangle$) resulting in a pyramidal shape [8]. In this study, the surface to be overgrown is about 1.5 μm wide, which makes complete coalescence possible only after 3 um thick GaN deposition without changing the other growth conditions like III/V ratio, growth temperature, NH_3 flow and without introduction of impurities like magnesium (Mg) in order to enhance the lateral extension [9]. However, using our growth conditions, we observed the existence of small holes at the surface due to the non-perfect planarization. Contrary to the work of Sano et al. [10], the impurity contamination from the thermal decomposition of silicon substrate was not observed. During growth, the GaN layer deposited between holes extends laterally and vertically over the holes until complete coalescence. This area has been closely studied by TEM. Figure 5.3 shows (002) and $(11\bar{2}0)$ dark field cross-section TEM images of GaN laterally grown over the opening in the silicon substrate. Whereas only dislocations with a vertical line are observed above the Si substrate, the dislocations in the laterally overgrown regions are basal plane dislocations. It could clearly be seen that these dislocations result from the bending of vertical dislocations nucleated over the Si substrate close to the hole. This phenomena of the bending of dislocations is similar to what is observed in classical ELO growth. When a vertical dislocation encounters a lateral facet, it bends to adopt a direction in the basal plane. This mechanism is characteristic of lateral growth in GaN [11]. Most of the observed dislocations are a-type dislocations (Burger's *vector* $= \frac{1}{3}\left\langle 11\bar{2}0\right\rangle$). Some vertical dislocations are also observed in the coalescence boundaries between two overgrown regions.

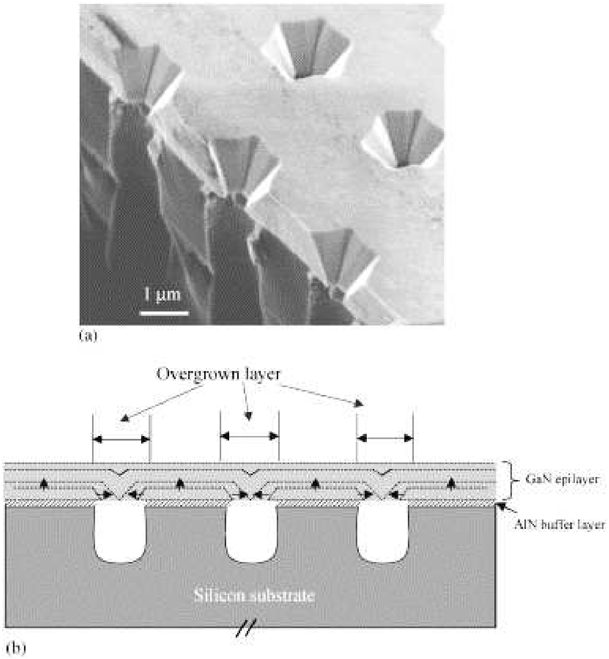

Figure 5.2: SEM image of $2\,\mu$m thick GaN layer (a) and schematization of the two-dimensional evolution of the deposition (b).

Using this ELO process, we observed the apparition of cracks at the surface of GaN layer only after $2\,\mu$m thick, which is a good improvement compared to our standard process using AlN buffer layer. Using standard process, we noticed crack formation with a thickness of $0.4\,\mu$m [3]. The high resolution XRD diffraction measurements show the same trend, an improvement of the structural quality of the GaN layer grown by ELO process which reflected by the reduction of the full-width at half-maximum (FWHM) of the rocking curve of the symmetric (0002) reflection down to 594 arcsec. Using standard process and for the same thickness of the GaN layer this value was 832 arcsec [3]. Figure 5.4 shows a SEM image of the GaN epitaxial layer after PEC etching in a stirred KOH solution (0.004 M) at room temperature and under UV illumination. Straight whisker-like etch features are observed at the surface which reveals the distribution of dislocations in the epitaxial layer [12]. However, these whiskers are formed only between the holes, i.e. not at the surface of the overgrown area. This could be explained by the fact that the PEC etching reveals only dislocations in $< 0001 >$ direction but not those in the basal plane.

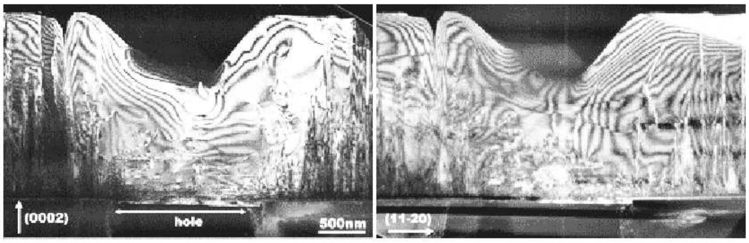

Figure 5.3: (0002) and (11$\bar{2}$0) dark field cross-section TEM images of GaN laterally grown over the opening in the silicon substrate.

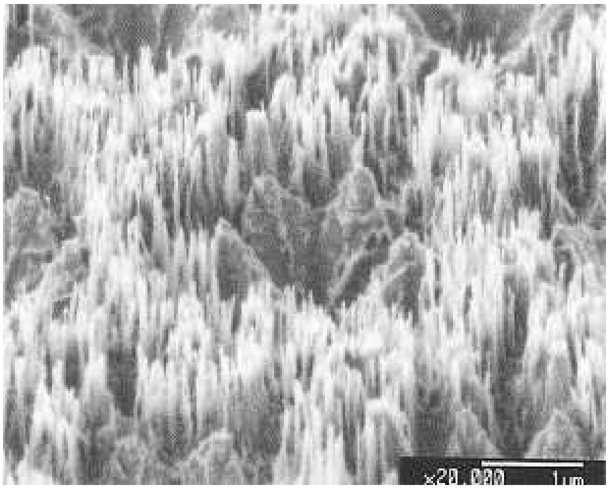

Figure 5.4: SEM image of GaN epitaxial layer after PEC etching.

5.4 Conclusions

We reported on the maskless ELO of GaN by MOCVD technique using structured silicon substrates prepared by conventional photolithography and dry etching techniques. Transmission electron microscope proved a drastic decrease of dislocation density in the overgrown areas of the GaN films. The photo-electrochemical etching technique has revealed only the presence of the dislocations in left angle < 0001 > direction.

5.5 Acknowledgements

The authors grateful to L. Macht and J.L. Weyher for PEC experiments. This work is financially supported by the Dutch Technology Foundation (STW).

Bibliography

[1] A. Watanabe, T. Takeuchi, K. Hirosawa, H. Amano, K. Hiramatsu, I. Akasaki, J Cryst Growth 128 (1-4) (1993) 391–396.

[2] E. Feltin, B. Beaumont, M. Laugt, P. De Mierry, P. Vennegues, M. Leroux, P. Gibart, Phys Status Solidi A 188 (2) (2001) 531–535.

[3] P. R. Hageman, S. Haffouz, V. Kirilyuk, A. Grzegorczyk, P. K. Larsen, Phys Status Solidi A 188 (2) (2001) 523–526.

[4] H. Marchand, N. Zhang, L. Zhao, Y. Golan, S. J. Rosner, G. Girolami, P. T. Fini, J. P. Ibbetson, S. Keller, S. Den Baars, J. S. Speck, U. K. Mishra, Mrs Internet J N S R 4 (2) (1999) art. no.–2.

[5] E. Feltin, B. Beaumont, P. Vennegues, M. Vaille, P. Gibart, T. Riemann, J. Christen, L. Dobos, B. Pecz, J Appl Phys 93 (1) (2003) 182–185.

[6] A. Strittmatter, S. Rodt, L. Reissmann, D. Bimberg, H. Schroder, E. Obermeier, T. Riemann, J. Christen, A. Krost, Appl Phys Lett 78 (6) (2001) 727–729.

[7] M. T. Otten, W. M. J. Coene, Ultramicroscopy 48 (1-2) (1993) 77–91.

[8] B. Beaumont, S. Haffouz, P. Gibart, Appl Phys Lett 72 (8) (1998) 921–923.

[9] S. Haffouz, B. Beaumont, P. Gibart, Mrs Internet J N S R 3 (8) (1998) art. no.–8.

[10] S. Sano, T. Detchprohm, S. Mochizuki, S. Kamiyama, H. Amano, I. Akasaki, J Cryst Growth 235 (1-4) (2002) 129–134.

[11] P. Vennegues, B. Beaumont, V. Bousquet, M. Vaille, P. Gibart, J Appl Phys 87 (9) (2000) 4175–4181.

[12] S. Haffouz, V. Kirilyuk, P. R. Hageman, L. Macht, J. L. Weyher, P. K. Larsen, APL 79 (15) (2001) 2390–2392.

Chapter 6

Influence of the nucleation layer morphology and epilayer structure on the resistivity of GaN films grown on c-plane sapphire by MOCVD

*

The influence of hydrogen and nitrogen carrier gases used during the preparation of the nucleation layer on the structural and electrical properties of GaN layers has been investigated. The GaN was grown on sapphire substrates using metal organic chemical vapor deposition. The nucleation layer morphology strongly depends on the carrier gas affecting the electrical properties of GaN epitaxial films through changes of the ratio of edge to mixed and screw-type threading dislocations. X-ray diffractometry, X-ray reflectometry, atomic force microscopy, and defect selective etching were employed to study the structural properties of both the nucleation layer and the GaN epilayers deposited on top of this. It is found that the density of edge-type dislocations determines the resistivity of GaN epilayers and that one key factor for varying the density of these dislocations is the morphology of the nucleation layer, i.e. the morphology of the GaN epilayer can be controlled by the type of carrier gas used in the preparation of the nucleation layer. The electrical resistivity of our GaN epilayers is typically about $0.5\,\Omega\,\mathrm{cm}$ and more than $3\times10^4\,\Omega\,\mathrm{cm}$ with nucleation

---

[*] A.P. Grzegorczyk, L. Macht, P.R. Hageman, J.L. Weyher, P.K. Larsen, J. Cryst. Growth 273 (2005) 424

layers grown using hydrogen and nitrogen carrier gases, respectively.

6.1 Introduction

GaN is a very promising material for high-power and high-frequency electronics due to the wide bandgap, high thermal stability, and high breakdown voltage. The technological potential of the group III nitrides, in particular the GaN/AlGaN system, has already been demonstrated. During the last few years, extensive efforts have been devoted to the growth of high-quality GaN layers using metal organic chemical vapor deposition (MOCVD), especially with respect to the electrical properties of this material. Among the parameters that control the performance of AlGaN/GaN high electron mobility transistors (HEMTs), one of the most important is the resistivity of the GaN layer. Highly resistive GaN layers avoid parallel conductivity, thereby enhancing the device pinch-off voltage.

In general, there are two significant methods of growing resistive GaN layers by MOCVD. The first method is based on acceptor doping (Fe, Mg, Zn) [1, 2] of the GaN layer. For application in HEMT devices this method is not desirable because of the reduction of the mobility due to introduction of additional scattering centers. The second method achieves a high resistivity by optimizing the growth conditions and, through this, by tailoring the specific structure of GaN epilayers. Bougrioua et al. [3] measured the influence of the nucleation layer (NL) recrystallization time and the growth rate of GaN layers deposited on c-plane sapphire substrates. It was found that shorter recrystallization times and higher growth rates (higher temperatures) led to high resistivities, however, also to an increase of hillocks. These could be avoided by changing the epilayer growth parameters during deposition. Wickenden et al. [4] showed that the resistivity of GaN films grown on a-plane sapphire in a H_2 ambient may be controlled over more than eight orders of magnitude by varying the growth pressure during the growth of the GaN epilayers. With increasing growth pressure, the GaN films exhibit an increasing grain size and a decreasing density of threading dislocations (TDs) with an edge component, together with a decreasing carbon and oxygen content and a decreasing resistivity. The highest resistivity values of $10^{10}\,\Omega\,\mathrm{cm}$ were obtained at pressures at and below 100 Torr with a decrease to $10^{2}-10^{4}\,\Omega\,\mathrm{cm}$ at 500 Torr. The observations were explained by assuming that carbon impurities segregate at edge-type TDs, acting as compensating acceptor states. In our MOCVD reactor the growth of GaN layers on c-plane sapphire substrates in a H_2 ambient generally led to low-resistivity films over the whole pressure range of our reactor, from 20 to 100 Torr. Above this limit the roughness of the surface starts to increase. It should be noted that results can depend on the type of the growth system and therefore may not be transferable. The reactor used in our experiments differ from the shower head reactors used by both Bougrioua et al. and Wickenden et al. (see Section 6.2). There are a number of publications about the influence of the carrier gas on the main GaN layer growth (e.g. [5–10]), but only a few of these describe its influence on the GaN NL [11, 12]. Halidou et al. [11] presented AFM images of NL grown using different carrier gas. The authors observed similar relations between carrier gas and and NL surface morphology as presented in this paper. It suggests that the method of GaN resistivity control by using different carriers during NL growth can be transferable to different growth systems. To the best of our knowledge no publication exists which connects the type of carrier gas during NL deposition with the electrical properties of GaN layer.

In this paper we present a method which allows one to control the resistivity of GaN epilayers over more than four orders of magnitude while keeping the growth parameters for the GaN epilayer constant during the growth, with a small increase of the total number of dislocations in the epitaxial layer and leading to a smooth surface morphology. Table 6.2 shows that the total number of dislocations is higher for resistive samples than for conductive ones. It is similar to the observation presented in Ref. [4]. This allows the growth of an AlGaN/GaN heterostructure with a high sheet carrier density of up to 1.5×10^{13} cm^{-2} and very good pinch-off characteristics.

6.2 Experimental details

The GaN layers were deposited on 2 “ diameter, (0001)-oriented and commercially available sapphire substrates by MOCVD using a RF heated, AIXTRON AIX-200, low-pressure horizontal reactor (Figure 6.1 and Figure 3.7). Trimethylgallium and ammonia were used as Ga and N precursors, respectively.

The growth procedure was started by annealing the substrate for 10 minutes at a high temperature (1150 °C) in a H_2 atmosphere and at a total reactor pressure of 50 mbar. Then, for samples #1N, #3N, #5N, #7N, and #9H (see Table 6.1) the carrier gas was changed to N_2 keeping all other parameters constant. For the other samples discussed in this paper, H_2 remained the carrier gas. Next, a 45 s nitridation step was carried out using 2 slm of NH_3 at a temperature of 1125 °C and parallel, the carrier gas flow was reduced to keep the total flow constant. This ammonia gas flow was kept constant till the end of the growth process and used in all forthcoming steps after the nitridation including cooling down. After the nitridation, the temperature was decreased to 560 °C, the pressure raised to 500 mbar, and a thin GaN NL was deposited. All growth parameters are summarized in Table 6.1.

Next, the wafer was brought to high temperature (1130 °C) and annealed for 25 s. In this step the recrystallization of the crystallites in NL takes place [13]. Finally, a 1 mm thick GaN epilayer was deposited at a total reactor pressure of 50 mbar with

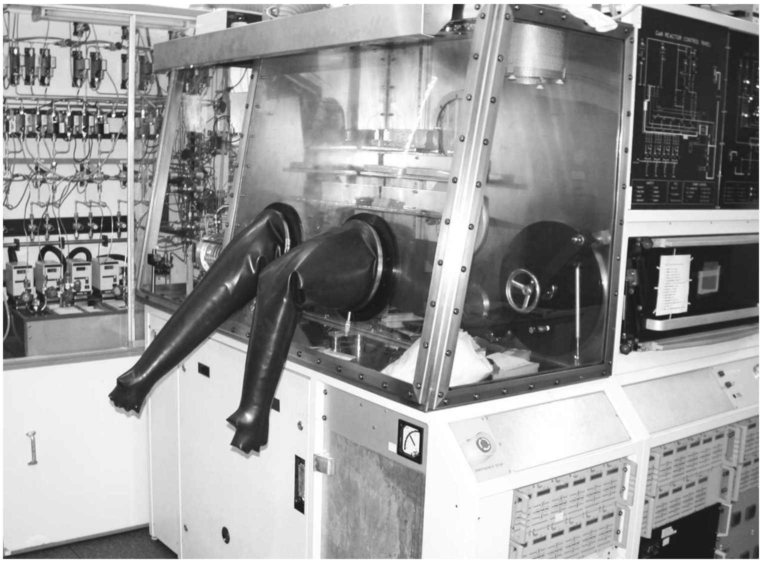

Figure 6.1: The MOCVD equipment built on the basis of AIX-200 reactor.

a V/III ratio of 1400. For every sample H_2 was used as a carrier gas during the deposition of the main GaN layer.

In the case of samples #3N, #4H, #7N, and #8H, the growth process was interrupted just before the deposition of the main layer and the reactor was immediately cooled down to room temperature. Sample #9H was grown in the same condition as #8H and immediately cooled down from 560 °C so there was no annealing after the NL had been deposited. All samples had specular and smooth surfaces. The average growth rate of the main GaN layer was determined to be about 2.6 μm/h from in situ reflectance measurements. The structural quality of the epitaxial layer was assessed by taking the full-width at half-maximum (FWHM) of the symmetric [002] and asymmetric [105] low-angle diffraction peaks of the rocking curve with a high resolution XRD Bruker-D8 instrument. For visualization of the surface morphology of the different nucleation layers, tapping-mode atomic force microscopy (AFM) was used. Thickness and roughness of the nucleation layer was investigated by grazing incidence X-ray reflectometry (XRR) [14, 15]. To visualize the defects of the GaN epilayers, orthodox etching in the KOH–NaOH eutectic mixture was performed at 400 °C for 4 min [16].

Ti/Al ohmic contacts made without any special surface treatment were used for resistivity measurements in the van der Pauw geometry. After deposition, the contacts were annealed in 600 °C for 2 min. The estimated value of resistivity for highly resistive samples was more than $3\times10^{4}\,\Omega\,\mathrm{cm}$.

Table 6.1: Composition of the carrier gas and growth time of nucleation layer for different samples

Sample id	Nitridation carrier gas	NL carrier gas	NL growth time (min)	NL annealing carrier gas	GaN top layer carrier gas
#1N	N_2	N_2	3	N_2	H_2
#2H	H_2	H_2	3	H_2	H_2
#3N	N_2	N_2	3	N_2	-
#4H	H_2	H_2	3	H_2	-
#5N	N_2	N_2	3:30	N_2	H_2
#6H	H_2	H_2	3:30	H_2	H_2
#7N	N_2	N_2	3:30	N_2	-
#8H	H_2	H_2	3:30	H_2	-
#9N	H_2	H_2	3:30	-	-

6.3 Results and discussion

The structural and electrical properties of the GaN epilayers (deposited as described in Table 6.1) are summarized in Table 6.2. The differences of the resistivity and defect density were induced by the use of different carrier gases, H_2 or N_2 , during the NL growth. Samples #1N and #5N, which were grown on the NL formed with N_2 as a carrier gas, have orders of magnitude higher resistance than the samples which were grown on a NL using H_2 as a carrier gas (samples #2H, #6H). Figure 6.2 presents XRR data measured for the NL described above. In these XRR curves the distance between peaks is inversely proportional to the thickness of the sample. A higher roughness of the sample is responsible for a decreased intensity of the reflection and thereby for a decreased amplitude of the oscillations. The area of the sample probed by the X-rays has a width of 0.2 mm. The length is determined by the angle of the incident beam and is about 6 mm. The fitting to the experimental data was performed using the Bruker REFSIM simulation software, which includes a fitting optimization algorithm. In the theoretical model two layers were included: a sapphire substrate layer and on top of it the GaN NL. Calculated values of roughness and thickness of

Table 6.2: Full-width at half-maximum of the symmetric [002] and asymmetric [105] X-ray rockingcurves, the resistivity of 1 mm thick GaN epilayers, and the resultingnumber of defects calculated on the base of AFM images

Sample id	FWHM [002](”)	FWHM [105](”)	Resistivity (Ω cm)	Screw and mix defects density (cm^{-2})	Edge defects density (cm−2)
#1N	665	559	Highly resistive	1.7×10^8	2.4×10^9
#2H	345	291	43	1.9×10^8	1.4×10^9
#5N	230	248	Highly resistive	2.5×10^8	2.3×10^9
#6H	349	216	0.5	2.2×10^8	1.6×10^9

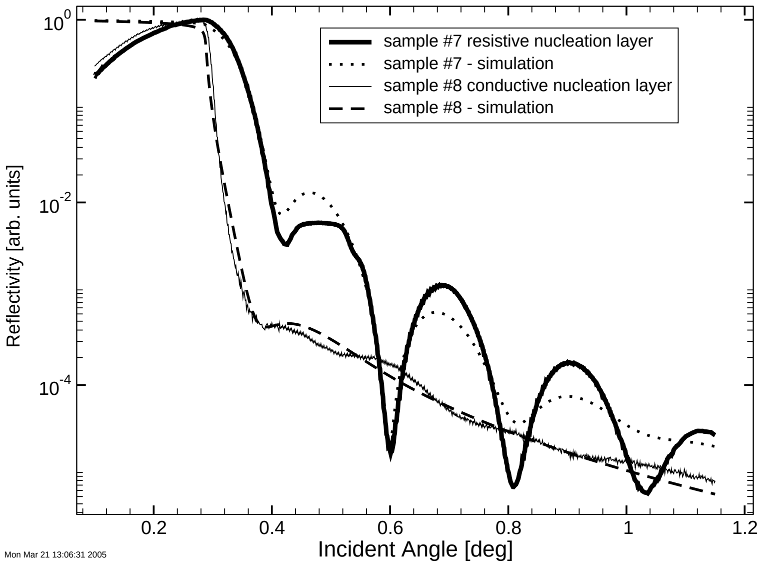

Figure 6.2: X-ray reflectometry data for nucleation layers #7N and #8H. Similar curves were observed for samples #3N and #4H.

the different NL are presented in Table 6.3. The NLs grown in a N_2 atmosphere are

Sample id	XRR (RMS) (nm)	Thickness (nm)	AFM (RMS) (nm)
#3N	2.2	16.2	1.8
#4H	4.2	6.9	5.7
#7N	2	17.7	1.9
#8H	5.4	7.4	7.5
#9H	2.9	13	-

Table 6.3: Calculated value of roughness and thickness based on XRR data for nucleation layer and RMS values measured by AFM

thicker and smoother compared to the samples grown in a H_2 atmosphere (compare #3N with #4H, and #7H with #8H). This effect is due to the decomposition of GaN in the NL during annealing at the high temperature [17].

Furtado et al. [18] studied the decomposition behavior of undoped and Zn-doped GaN epitaxial layers. Annealing in pure N_2 at 1070 °C for 2 h 30 min led to a decomposition of the surface, while annealing in a H_2 atmosphere at 950 °C produced traces of liquid gallium droplets after 2 h. To verify this effect, sample #9H was not annealed after the growth of the NL. It turned out that the thickness of this sample was indeed higher then that of sample #8H, which was grown in H_2 atmosphere and

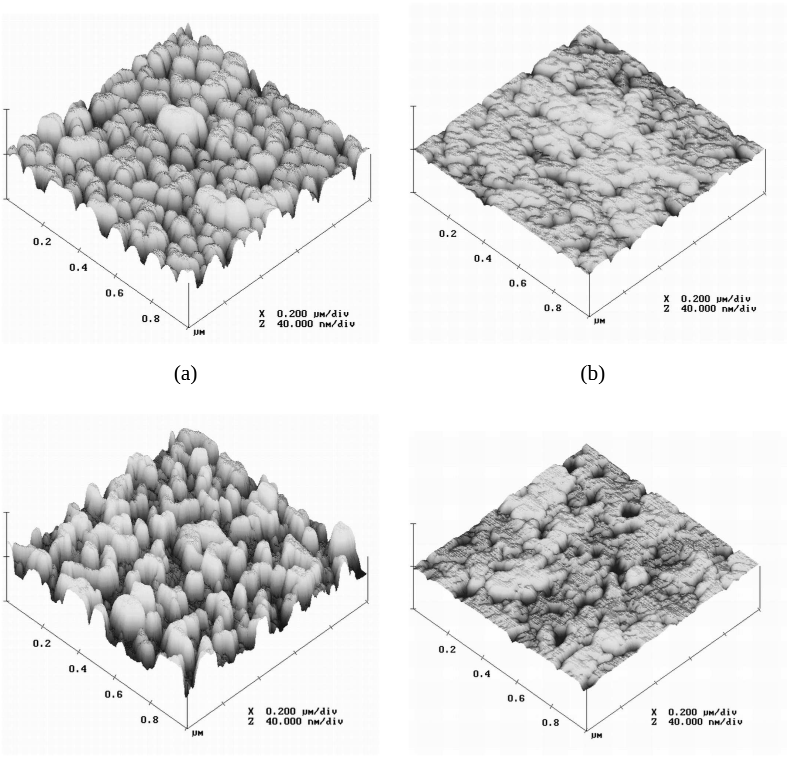

(a) (b)

(c) (d)

Figure 6.3: AFM images for nucleation layer: (a) #4H, 3 min, RMS=5.7 nm, (b) #3N, 3 min, RMS=1.8 nm, (c) #8H, 3:30 min, RMS=7.5 nm, (d) #7N, 3:30 min, RMS=1.9 nm.

annealed at 1130 °C and lower than that of sample #7N which was grown in N_2 and also annealed at 1130 °C.

The roughness of the samples grown in H_2 increased with the annealing time (sample #8H and #9H). Root-mean square (RMS) roughness values of the surface, calculated on the basis of $25\times25\,\mu m^2$ AFM images, is 1.8 nm for sample #3N and 5.7 nm for sample #4H. This value corresponds very well with XRR data presented in Table 6.3.

Figure 6.3 shows $1\times1\,\mu m^2$ AFM images for NLs grown with H_2 and N_2 , respectively. The NL grown in the presence of H_2 clearly possesses a columnar structure as opposed to the samples grown in N_2. Vennegues et al. [19] observed a similar effect on samples grown with a mixture of H_2 and N_2 as a carrier gas.

We found that the structure of the NLs correlates closely to the GaN film resistivity. The GaN films #5N and #1N, grown on a NL with a flat morphology, are highly resistive (ρ $>3\times10^4\,\Omega\,cm$), whereas GaN films #6H and #2H, in which the NL is columnar, have a low resistivity. A similar effect was observed by Twig et al. [20] for AlN nucleation layers grown on a-plane sapphire. Based on the AFM images presented in Figure 6.3, we can conclude that the NL grown in H_2 atmosphere has a lower density of islands, with statistically larger diameter than the samples grown in N_2 atmosphere. A higher density of islands leads to a smoother surface and more grain boundaries in the NL. According to Weimann et al. [21], the boundaries between islands contain arrays of dislocations along the interface between two islands. Böttcher et al. [22] showed that the average grain diameter is inversely proportional to the threading dislocation density.

To reveal the type and density of the dislocations, in the GaN films, the samples were etched in the KOH–NaOH eutectic mixture. It is known that each type of defect has a different rate of etching [23, 24]. For edge, screw, and mixed-type dislocations, the Burgers vector $\vec{b}$ is given by [25] equation 6.1

$$\begin{aligned} \vec{b}_1 &= \tfrac{1}{3}\langle 11\bar{2}0\rangle, \quad |\vec{b}_1|^2 = a^2, \\ \vec{b}_2 &= \tfrac{1}{3}\langle 0001\rangle, \quad |\vec{b}_2|^2 = \tfrac{8}{3}a^2, \\ \vec{b}_3 &= \tfrac{1}{3}\langle 11\bar{2}3\rangle, \quad |\vec{b}_3|^2 = \tfrac{11}{3}a^2 \end{aligned} \tag{6.1}$$

where a and b are the lattice constants of GaN.

According to Cabreras theory, during etching of the containing dislocations material, the change in chemical potential is given by [26] equation 6.2

$$\Delta\mu^* = \frac{2\pi^2\gamma^2\Omega}{G|\vec{b}|^2\alpha} \tag{6.2}$$

where α is a parameter describing the mixed character of dislocation, γ is the edge free-energy, Ω the volume occupied by each atom, and G is the shear modulus. From Boltzmann statistics, the rate of etch-pit nucleation is proportional to $\exp(-\Delta G_p^*/kT)$, where ΔG_p^* is the work done for the formation of the nucleus which is proportional to $(\Delta\mu^*)^{-1}$. As a consequence of Eq. 6.2, edge-type dislocations are expected to have the lowest etch rate among the types of dislocations present in GaN; hence they should be revealed as small pits after the etching process. Figure 6.4 presents an AFM image of the GaN surface after selective etching. Large etch pits represent screw and mixed dislocations while small ones represent edge dislocations.

Highly resistive samples have a higher density of defects (Table 6.2) compared with the conductive ones. Sample #5N, the one with the narrowest [002] symmetric peak (Table 6.2), has a higher density of dislocations as compared to samples #2H and #6H. A similar relationship holds for the asymmetric peak [105] which is more sensitive for the defect density [27]. This phenomenon suggests that in case of resistive and non-resistive samples, different types of defects are created in the crystal

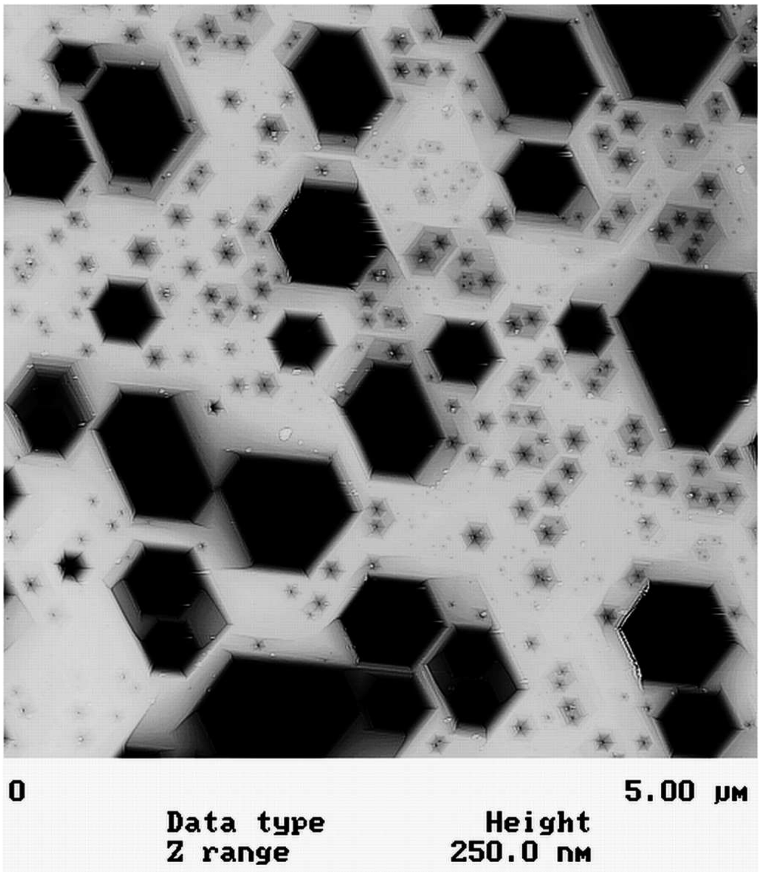

Figure 6.4: AFM image of sample #2H etched in the KOH-NaOH eutectic mixture at 400 °C for 4 min.

lattice [28]. This trend is reflected in Table 6.2 and is similar to that reported for the GaN layer grown on a-plane sapphire [20].

Screw dislocations are identified as a path of electrical conductivity so they should increase the electrical conductivity of the GaN layers [22]. Mixed dislocation is identified as electrically inactive or not highly conductive [29–31]. According to the model proposed by Wiemann et al. [21], edge dislocations work as acceptor-like trap levels. Cho et al. [29] experimentally confirmed this model using deep-level transient spectroscopy measurements. Simpkins et al. [31] identified edge dislocation as negatively charged and not highly conductive. The present results therefore suggest that the increased number of edge dislocations (see Table 6.2) compensates GaN layers and makes it highly resistive.

On the basis of the presented method, we managed to grow AlGaN/GaN HEMT structures with sheet carrier densities of up to $1.5 \times 10^{13} cm^2$ and pinch-off voltage 3.5 V*. The results will be presented in detail in the future.

6.4 Conclusions

In summary, we have demonstrated that the carrier gas strongly influences GaN NL morphology. The growth condition which provides the high density of small-diameter islands that increases the resistivity (from $0.5\,\Omega\,\mathrm{cm}$ up to more than $3\times10^4\,\Omega\,\mathrm{cm}$) can be achieved by changing the carrier gas from H_2 to N_2 during the growth process of NL. X-ray reflectometry is a very valuable method for the investigation of the GaN NL structure and with the help of simulations it allows one to determine the roughness and thickness of the NL measured over a large area. It is found that simulated RMS values agree with values measured by AFM. Our results provide evidence that control of type of defects (edge, screw, or mix), which are introduced in the GaN layers, is a key factor in defining the electrical properties of GaN.

Bibliography

[1] S. Heikman, S. Keller, T. Mates, S. P. DenBaars, U. K. Mishra, J Cryst Growth 248 (2003) 513–517.

[2] N. I. Kuznetsov, A. E. Nikolaev, A. S. Zubrilov, Y. V. Melnik, V. A. Dmitriev, APL 75 (20) (1999) 3138–3140.

[3] Z. Bougrioua, I. Moerman, N. Sharma, R. H. Wallis, J. Cheyns, K. Jacobs, E. J. Thrush, L. Considine, R. Beanland, J. L. Farvacque, C. Humphreys, J Cryst Growth 230 (3-4) (2001) 573–578.

[4] A. E. Wickenden, D. D. Koleske, R. L. Henry, M. E. Twigg, M. Fatemi, J Cryst Growth 260 (1-2) (2004) 54–62.

[5] O. Ambacher, H. Angerer, R. Dimitrov, W. Rieger, M. Stutzmann, G. Dollinger, A. Bergmaier, Phys Status Solidi A 159 (1) (1997) 105–119.

[6] Y. Kobayashi, T. Akasaka, N. Kobayashi, Jpn J Appl Phys 2 37 (10B) (1998) L1208–L1210.

[7] D. D. Koleske, A. E. Wickenden, R. L. Henry, J. C. Culbertson, M. E. Twigg, J Cryst Growth 223 (4) (2001) 466–483.

[8] Y. Kobayashi, N. Kobayashi, J Cryst Growth 190 (1998) 301–304.

[9] O. Schon, B. Schineller, M. Heuken, R. Beccard, J Cryst Growth 189-190 (1998) 335–339.

---

[*] Private communication with M.C.J.C.M. Kramer, Technische Universiteit Eindhoven

[10] H. X. Wang, Y. Amijima, Y. Ishihama, S. Sakai, J Cryst Growth 233 (4) (2001) 681–686.

[11] I. Halidou, T. Boufaden, A. Touhami, A. Rebey, B. El Jani, Phys Status Solidi A 184 (1) (2001) 263–271.

[12] M. Sumiya, N. Ogusu, Y. Yotsuda, M. Itoh, S. Fuke, T. Nakamura, S. Mochizuki, T. Sano, S. Kamiyama, H. Amano, I. Akasaki, J Appl Phys 93 (2) (2003) 1311.

[13] T. Ito, M. Sumiya, Y. Takano, K. Ohtsuka, S. Fuke, Jpn J Appl Phys 1 38 (2A) (1999) 649–653.

[14] C. Schiller, G. M. Martin, W. W. Vanderhoogenhof, J. Corno, Philips J Res 47 (3-5) (1993) 217–234.

[15] Y. M. Le Vaillant, R. Bisaro, J. Olivier, O. Durand, J. Y. Duboz, S. Ruffenach-Clur, O. Briot, B. Gil, R. L. Aulombard, Mat Sci Eng B-Solid 50 (1-3) (1997) 32–37.

[16] G. Kamler, J. L. Weyher, I. Grzegory, E. Jezierska, T. Wosinski, J Cryst Growth 246 (1-2) (2002) 21–24.

[17] D. D. Koleske, M. E. Coltrin, A. A. Allerman, K. C. Cross, C. C. Mitchell, J. J. Figiel, APL 82 (8) (2003) 1170–1172.

[18] M. Furtado, G. Jacob, J Cryst Growth 64 (2) (1983) 257–267.

[19] P. Vennegues, B. Beaumont, S. Haffouz, M. Vaille, P. Gibart, J Cryst Growth 187 (2) (1998) 167.

[20] M. E. Twigg, D. D. Koleske, A. E. Wickenden, R. L. Henry, S. C. Binari, APL 79 (26) (2001) 4322–4324.

[21] N. G. Weimann, L. F. Eastman, D. Doppalapudi, H. M. Ng, T. D. Moustakas, J Appl Phys 83 (7) (1998) 3656–3659.

[22] T. Böttcher, S. Einfeldt, S. Figge, R. Chierchia, H. Heinke, D. Hommel, J. S. Speck, APL 78 (14) (2001) 1976–1978.

[23] J. L. Weyher, P. D. Brown, J. L. Rouviere, T. Wosinski, A. R. A. Zauner, I. Grzegory, J Cryst Growth 210 (1-3) (2000) 151–156.

[24] J. L. Weyher, L. Macht, F. D. Tichelaar, H. W. Zandbergen, P. R. Hageman, P. K. Larsen, Mat Sci Eng B-Solid 91 (2002) 280–284.

[25] D. Hull, D. J. Bacon, Introduction to dislocations, 3rd Edition, International series on materials science and technology, 37, Pergamon, Oxford, 1984.

[26] K. Sangwal, Etching of crystals: theory, experiment, and application, Defects in solids, 15, North-Holland, Amsterdam, 1987.

[27] B. Heying, X. H. Wu, S. Keller, Y. Li, D. Kapolnek, B. P. Keller, S. P. DenBaars, J. S. Speck, APL 68 (5) (1996) 643–645.

[28] J. E. Ayers, J Cryst Growth 135 (1-2) (1994) 71–77.

[29] H. K. Cho, K. S. Kim, C. H. Hong, H. J. Lee, J Cryst Growth 223 (1-2) (2001)

38–42.
[30] E. G. Brazel, M. A. Chin, V. Narayanamurti, APL 74 (16) (1999) 2367–2369.
[31] B. S. Simpkins, E. T. Yu, P. Waltereit, J. S. Speck, J Appl Phys 94 (3) (2003) 1448–1453.

Chapter 7

Resistivity control of unintentionally doped GaN films

[*]

GaN epilayers were grown on sapphire substrates via low temperature GaN and AlN nucleation layers (NL) by metalorganic chemical vapor phase epitaxy (MOCVD). The morphology of the individual NLs strongly depends on the carrier gas used during the growth and recrystallization and this is the key factor for control of the resistivity of the GaN layer grown on it. The GaN nucleation layer grown in presence of N_2 has a higher density of islands with a statistically smaller diameter than the samples grown in H_2 atmosphere (see Chapter 6). Introduction of an additional intermediate (IL) low temperature (GaN or AlN) nucleation layer changes the GaN epilayer resistivity to about $50\,\Omega\,\mathrm{cm}$, regardless of the carrier gas used during the growth of the IL. Defect selective etching demonstrated that control of the type and density of the dislocations in GaN enables the growth of highly resistive layers without any intentional acceptor doping (Mg, Zn).

7.1 Introduction

The technological potential of the group III nitrides, in particular the GaN/AlGaN system, has already been demonstrated [1]. During the last few years, extensive efforts have been devoted to the growth of high quality GaN layers using Metal-Organic Chemical Vapor Deposition (MOCVD), especially with respect to the electrical properties of this material. AlGaN/GaN High Electron Mobility Transistors

---

[*] A. P. Grzegorczyk, L. Macht, P. R. Hageman, M. Rudzinski, and P. K. Larsen, phys. stat. sol. (c), 14 (2005)

(HEMTs) need for optimal performance highly resistive GaN layers to avoid parallel conductivity, thereby enhancing the device pinch-off. In general, there are two distinct methods of growing resistive GaN layers by MOCVD: using acceptor doping (Fe, Mg, Zn) [2, 3] or optimizing growth conditions [4]. For application in HEMT devices the first method is not desirable because of the reduction of the mobility due to introduction of additional scattering centers. Up to now there are only a few publications [5, 6] in which a correlation between the growth conditions of the nucleation layer (NL) and the electrical properties of GaN epilayers is described. The purpose of this report is to demonstrate a new method of GaN resistivity control by using different carrier gas during NL deposition. Although there are many publications about the influence of the carrier gas on the main GaN layer growth (e.g. [7–11]), only a few of those describe its influence on the GaN NL [12, 13].

7.2 Experimental details

The GaN layers were deposited on 2 inch diameter, (0001)-oriented and commercially available sapphire substrates by MOCVD using a RF heated, low pressure horizontal reactor with trimethylgallium, trimethylaluminium and ammonia as source of gallium, aluminum, and nitrogen respectively [14].

After nitridation of the sapphire, a GaN or AlN nucleation layer was deposited at 560 °C or 420 °C respectively, at 500 mbar using H_2 or N_2 as carrier gas. Next, the wafer was brought to high temperature (1130 °C) and annealed for 25 seconds. In this step the recrystallization of the crystallites in the NL takes place. Finally, a 1 μm high temperature (HT) GaN epilayer was deposited at a total reactor pressure of 50 mbar with a V/III ratio of 1400. In case of samples #1HN, #2HH, #3HNA, #4HHA first a 0.5 um HT layer was grown, then a second nucleation layer was deposited and on top of this a 0.5 um thick layer was grown. All details of the experiments are presented in Table 7.1. For every sample H_2 was used as a carrier gas during the deposition of the main HT GaN layer.

To visualize the nucleation layer morphology the growth processes were stopped just before deposition of appropriate HT layer and the samples were cooled down in ammonia atmosphere. The structural quality of the epitaxial layer was assessed by determining the [002] and [105] reflections in an X-ray rocking curve. For visualization of the surface morphology of different nucleation layers, tapping-mode atomic force microscopy (AFM) was used. To visualize the dislocations of the GaN epilayers, orthodox etching in the KOH-NaOH eutectic mixture was performed for 4 minutes at 400 °C [15]. Ti/Al ohmic contacts made without any special surface treatment were used for resistivity measurements in the van der Pauw geometry.

Table 7.1: Composition of the carrier gas and growth time of nucleation layer for different samples. The last column presents resistivity value for every examined sample measured using van der Pauw method.

Sample id	NL (carrier gas)	GaN layer thickness [μm]	IL (carrier gas)	GaN layer thickness [μm]	Resistivity [Ω cm]
#1HN	GaN (H_2)	0.5 μm	GaN (N_2)	0.5 μm	0.7
#2HH	GaN (H_2)	0.5 μm	GaN (H_2)	0.5 μm	0.6
#3HNA	AlN (H_2)	0.5 μm	AlN (N_2)	0.5 μm	577
#4HHA	AlN (H_2)	0.5 μm	AlN (H_2)	0.5 μm	222
#5H	GaN (H_2)	1 μm	-	-	0.5
#6N	GaN (N_2)	1 μm	-	-	$>3\times10^4$
#7HA	AlN (H_2)	1 μm	-	-	>700
#8NA	AlN (N_2)	1 μm	-	-	>700

7.3 Results and discussion

Table 7.2 presents structural properties for samples #5H and #6N. The differences of the resistivity and dislocation density were induced by the use of different carrier gases, H_2 or N_2 , during the NL growth. The number of dislocations in the both samples is similar, as indicated by the FWHM of the [105] reflection rocking curve and the number of defects from etched samples. Table 7.2 shows that there is a small but significant difference between edge dislocation densities for high and low resistive samples. The same relation is observed for screw and mixed dislocations.

Table 7.2: Full width at half maximum of the symmetric [002] and asymmetric [105] X-ray rocking curves, the resistivity of 1 μm thick GaN epilayers, and the number of dislocations deduced from AFM images.

Sample id	FWHM [002]	FWHM [105]	Screw & mixed defects density [cm^{-2}]	Edge defects density [cm^{-2}]
#5H	349”	216”	2.2×10^8	1.6×10^9
#6N	230”	248”	2.5×10^8	2.3×10^9

Such small differences in number of dislocations are observed very often, especially when we compare samples with the same NL thickness. This was also reported by Twigg et al. [6].

In order to find the differences in NL morphology, AFM imaging was performed. The NLs grown in N_2 consist of smaller diameter grains compared to the samples grown in H_2. These results can be correlated with resistivity data presented in Table 7.1. The resistivity of all samples appears to be proportional to the size and density of the grains in the layer (e.g. sample #5H, #6N Table 7.1 and image Figure 6.3a and b in Chapter 6).

In case of a GaN NL thus appears to be possible just by changing carrier gas to

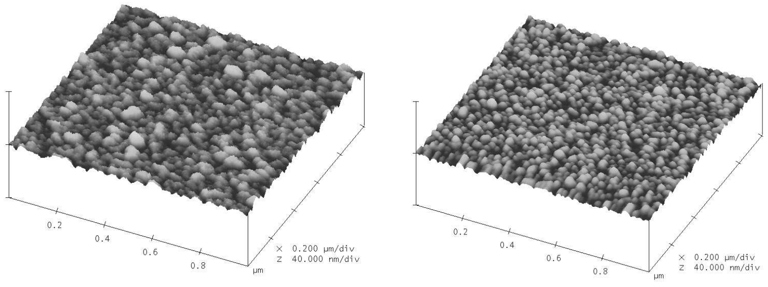

(a) (b)

Figure 7.1: AFM image and root mean square (RMS) values of (a) AlN NL grown in H_2 , RMS=1.4 nm; (b) AlN NL grown in N_2 , RMS=1 nm. The AFM images for GaN NL grown in H_2 and N_2 are presented in Chapter 6 Figure 6.3a and b.

control the resistivity of the samples. The AlN NL morphology is more resistant to carrier gas composition so resistivity of both samples #7HA and #8NA is very high.

Figure 7.2 presents a series of AFM images for GaN and AlN NL grown on 0.5 μm thick HT GaN layer. We observe the same dependence of NL morphology on carrier gas composition as for the samples presented on Figure 7.1. In general, a single grain has a bigger diameter compared to the analogous NL grown directly on sapphire. Experiments showed that the resistivities of investigated samples #1HN, #2HH, #3HNA and #4HHA are lower compared to the samples grown with a single NL. It can be assumed that the first HT 0.5 μm layer of #4HHA sample has the same resistivity as sample #7HA pointing to the fact that the total resistivity of #4HHA sample is decreased due to introduction of a second NL. The same conclusion is valid for sample #5H and #1HN. Boundaries between misoriented islands contain arrays of edge dislocations [16] along the interface and these edge dislocations work as acceptor-like trap levels [17]. Bottcher et al. [18] showed that the average grain diameter is inversely proportional to the threading dislocation density. Screw dislocations are identified as a path of electrical conductivity so they should increase the electrical conductivity of the GaN layers [19]. Mixed dislocations are electrically inactive or not highly conductive [19–21]. Due to the fact that for conductive and resistive samples the number of edge defects is very similar, the ratio between screw and mixed dislocations is altered. By increasing the edge and decreasing the screw dislocation density it is possible to grow highly resistive GaN layers. By growing a second nucleation layer we introduce to the structure grains which are not misaligned so the number of edge dislocation is decreased and total resistivity of the samples decreased as well. Another possible explanation is that the total number of dislocations is reduced [22] and electrically active point defects start to be dominant. However, because all HT layers were grown in the same conditions and total number

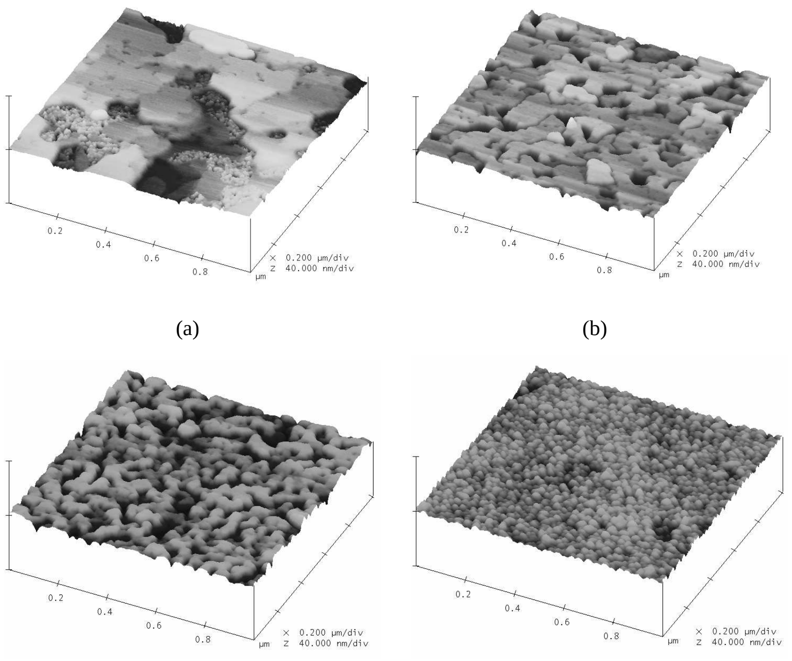

(a) (b)

(c) (d)

Figure 7.2: AFM image and RMS values of NL grown on 0.5 μm thick HT GaN layer (a) GaN NL grown in H_2 , RMS=1.2 nm; (b) GaN NL grown in N_2 , RMS=1.7 nm; (c) AlN NL grown in H_2 RMS=1.1 nm; (d) AlN NL grown in N_2 , RMS=1.2 nm.

of dislocations is similar, we assume that the number of point defects is equal for all the samples.

7.4 Conclusions

In summary, we have demonstrated that the carrier gas (H_2 or N_2) strongly influence the GaN/AlN NL morphology. The growth condition, which provides the high density of small diameter islands that increase the resistivity (from 0.5 Ω cm up to 3×10^4 Ω cm for GaN NL) can be achieved by changing the carrier gas from H_2 to N_2 during the growth process of NL. The presented results suggest that control of the type of defects (edge, screw or mixed), which are present in the GaN layer, is a key factor in defining the electrical properties of GaN.

Bibliography

[1] S. Nakamura, M. Senoh, S. Nagahama, N. Iwasa, T. Yamada, T. Matsushita, H. Kiyoku, Y. Sugimoto, T. Kozaki, H. Umemoto, M. Sano, K. Chocho, Jpn J Appl Phys 2 36 (12A) (1997) L1568–L1571.

[2] S. Heikman, S. Keller, T. Mates, S. P. DenBaars, U. K. Mishra, J Cryst Growth 248 (2003) 513–517.

[3] N. I. Kuznetsov, A. E. Nikolaev, A. S. Zubrilov, Y. V. Melnik, V. A. Dmitriev, APL 75 (20) (1999) 3138–3140.

[4] A. E. Wickenden, D. D. Koleske, R. L. Henry, M. E. Twigg, M. Fatemi, J Cryst Growth 260 (1-2) (2004) 54–62.

[5] Z. Bougrioua, I. Moerman, N. Sharma, R. H. Wallis, J. Cheyns, K. Jacobs, E. J. Thrush, L. Considine, R. Beanland, J. L. Farvacque, C. Humphreys, J Cryst Growth 230 (3-4) (2001) 573–578.

[6] M. E. Twigg, D. D. Koleske, A. E. Wickenden, R. L. Henry, S. C. Binari, APL 79 (26) (2001) 4322–4324.

[7] O. Ambacher, H. Angerer, R. Dimitrov, W. Rieger, M. Stutzmann, G. Dollinger, A. Bergmaier, Phys Status Solidi A 159 (1) (1997) 105–119.

[8] Y. Kobayashi, T. Akasaka, N. Kobayashi, Jpn J Appl Phys 2 37 (10B) (1998) L1208–L1210.

[9] D. D. Koleske, A. E. Wickenden, R. L. Henry, J. C. Culbertson, M. E. Twigg, J Cryst Growth 223 (4) (2001) 466–483.

[10] Y. Kobayashi, N. Kobayashi, J Cryst Growth 190 (1998) 301–304.

[11] O. Schon, B. Schineller, M. Heuken, R. Beccard, J Cryst Growth 189-190 (1998) 335–339.

[12] I. Halidou, T. Boufaden, A. Touhami, A. Rebey, B. El Jani, Phys Status Solidi A 184 (1) (2001) 263–271.

[13] M. Sumiya, N. Ogusu, Y. Yotsuda, M. Itoh, S. Fuke, T. Nakamura, S. Mochizuki, T. Sano, S. Kamiyama, H. Amano, I. Akasaki, J Appl Phys 93 (2) (2003) 1311.

[14] F. K. de Theije, A. R. A. Zauner, P. R. Hageman, W. J. P. van Enckevort, P. K. Larsen, J Cryst Growth 197 (1-2) (1999) 37–47.

[15] G. Kamler, J. L. Weyher, I. Grzegory, E. Jezierska, T. Wosinski, J Cryst Growth 246 (1-2) (2002) 21–24.

[16] P. Fini, X. Wu, E. J. Tarsa, Y. Golan, V. Srikant, S. Keller, S. P. Denbaars, J. S. Speck, Jpn J Appl Phys 1 37 (8) (1998) 4460–4466.

[17] N. G. Weimann, L. F. Eastman, D. Doppalapudi, H. M. Ng, T. D. Moustakas, J Appl Phys 83 (7) (1998) 3656–3659.

[18] T. Böttcher, S. Einfeldt, S. Figge, R. Chierchia, H. Heinke, D. Hommel, J. S. Speck, APL 78 (14) (2001) 1976–1978.

[19] H. K. Cho, K. S. Kim, C. H. Hong, H. J. Lee, J Cryst Growth 223 (1-2) (2001) 38–42.

[20] E. G. Brazel, M. A. Chin, V. Narayanamurti, APL 74 (16) (1999) 2367–2369.

[21] B. S. Simpkins, E. T. Yu, P. Waltereit, J. S. Speck, J Appl Phys 94 (3) (2003) 1448–1453.

[22] J. Chaudhuri, J. T. George, D. D. Kolske, A. E. Wickenden, R. L. Henry, Z. Rek, J Mater Sci 37 (7) (2002) 1449–1453.

Chapter 8

Influence of sapphire annealing in trimethylgallium atmosphere on GaN epitaxy by MOCVD

[*]

The microscopic evolution of GaN layers, grown by metal-organic chemical vapor deposition using a new Ga treatment method was investigated. With the help of in situ reflectance measurements the coalescence and overgrowth of GaN epilayers was observed. The sample morphology was ex situ characterized by atomic force microscopy, scanning electron microscopy, and optical microscopy. By using orthodox etching in molten KOH-NaOH eutectic the dislocation density and N-polar inclusion density were revealed. Photoluminescence measurements were performed in order to determine the optical properties of the GaN layers. The experimental results demonstrated that by annealing the c-plane sapphire in trimethylgallium it is possible to control the GaN epitaxial layer polarity.

The ratio between N and Ga polarity in the deposited GaN layers can be adjusted by means of changing the annealing time in TMG atmosphere of the sapphire substrate. For an annealing time of 20 min the layers are completely N-polar and for a time of 60 min Ga-polar epilayer are grown.

---

[*] A.P. Grzegorczyk, P.R. Hageman, J.L. Weyher, P.K. Larsen, J Cryst Growth, 283 (1-2) (2005) 72-80

8.1 Introduction

GaN is a very promising material for high power and high-frequency electronics (see Figure 1.3) due to its wide bandgap, high thermal stability, and high breakdown voltage. Since Manasevit et al. in 1971 [1] for the first time succeeded in growing III-V nitrides by metal-organic chemical vapor deposition (MOCVD), a lot of efforts were made towards the improvement of the structural quality and the surface morphology of the GaN epilayers. Products like light emitting diodes (LED), laser diodes (LD), and detectors based on GaN material are already available on the market. Despite this fact, the structural quality of the GaN epilayers is still far from that of Si and GaAs. The production of single crystals, although possible, is still very expensive, and not large enough to meet the market needs. Therefore, sapphire, silicon (Si), and silicon carbide (SiC) remain the most popular substrates for GaN heteroepitaxy. Due to the differences in lattice constants and thermal expansion coefficients GaN epilayers suffer from the presence of a large number of threading dislocations. The average density for MOCVD films grown on sapphire often exceeds $2{\times}10^9\,\mathrm{cm}^{-2}$, while for SiC substrates it is only a few times lower (high $10^8\,\mathrm{cm}^{-2}$ dislocations). Despite this high initial dislocation density, some devices (LED) function satisfactorily; however, their properties could be improved through the reduction of dislocations. Since the first demonstration of the MOCVD growth of GaN a lot of different methods were invented to improve the structural and optical properties of GaN epilayers grown on both sapphire and SiC substrates.

GaN epitaxial layers grown directly on c-plane sapphire by MOCVD are N-polar with the surface covered by characteristic hillocks [2]. In 1986 Amano et al. [3] reported the improvement of the optical, morphological, and crystalline properties of the GaN main layer (ML) by introducing a low temperature (LT) AlN nucleation layer (NL) (also called the buffer layer). A few years later [2] applied a similar method in which the GaN NL was used instead of an AlN NL. The author demonstrated that a 10 nm thick LT GaN layer (grown at temperatures between 450 and 600 °C) increased the carrier mobility up to $600\,\mathrm{cm}^2\mathrm{V}^{-1}\mathrm{s}^{-1}$ at 300 K. As a natural continuation, the above mentioned idea was applied by Kachi et al. [4] who proposed an InN NL grown at 600 °C. All the above described methods, commonly called the “two-step growth methods”, introduced an additional layer grown at a temperature lower than the growth temperature of the GaN main layer. In 1996 Keller et al. [5] demonstrated that a short nitridation of the sapphire substrate before depositing the NL strongly affects the nucleation layer structure thereby reducing the threading dislocation density in the main layer. Moreover, Haffouz et al. [6] showed that an additional in situ SiN treatment step, just after the sapphire nitridation, can also considerably improve the optical properties and reduce the density of threading dislocations. It should be pointed out that these nitridation and SiN treatment methods were to date successful only when applied together with the low temperature nucleation layer. In all publications mentioned above, a precise control of the nucleation sites in the NL is a critical factor in the growth process of high quality GaN films suitable for device fabrications.

In literature there are only a few publications describing the use of a Ga annealing step before the GaN epitaxy; Naniwae et al. [7] observed that pretreatment of the sapphire by Ga+HCL gas reduces the pit density and improves the crystalline quality of the GaN films grown by the hydride vapor phase epitaxy (HVPE). In other publications [8, 9] a Ga pretreatment procedure was used in the growth grow of thick GaN layers by HVPE. Moreover, Kim et al. [10] investigated the influence of nitridated metal gallium films as buffer layers for Si-doped GaN layers grown by molecular beam epitaxy (MBE). The authors observed an efficient stress relief in the heteroepitaxial GaN layers and Ga metal in the nitridated Ga metal buffer layer. In addition, Ploog et al. [11] demonstrated that subsequent in situ cleaning via several cycles of Ga deposition and flash-off at 800 °C gives smooth surface morphology of the SiC(0001) substrates used for epitaxial growth of GaN by MBE and plasma-assisted MBE. It should be stressed that the best results were obtained when the GaN growth was initiated directly, i.e. without any specific nucleation layer.

In this paper the influence of a Ga Treatment Step (GTS) of the sapphire substrate and its impact on GaN epitaxial growth are presented. A comparison between the standard two-step growth method and new GTS method is made. For the purpose of studying the growth process, in situ optical reflectance measurement (using a wavelength of 781 nm) is applied as method for investigation of the evolution of the growth of the GaN epilayer. The theory regarding the optical information and extraction of the growth rates has been discussed in detail by Breiland et al. [12]. Moreover, there are also many other publications concerning the influence of the nucleation layer morphology on the GaN growth dynamics and its impact on a in situ reflectance measurements [13–18].

8.2 Experimental details

The GaN layers were deposited on 2 inch diameter, (0001)-oriented, and commercially available sapphire substrates by MOCVD using a RF heated, AIXTRON AIX-200, low pressure horizontal reactor. Trimethylgallium and ammonia were used as Ga and N precursors, respectively. The growth procedure for all samples (see Table 8.1) was started by annealing the substrate for 5 minutes at high temperatures (1150 °C) in a H_2 atmosphere and at a total reactor pressure of 350 mbar (Figure 8.1 A).

Next, a 45 seconds nitridation step was carried out using 2 slm of NH_3 at a

Table 8.1: Details of the substrate annealing procedure (indicated by C, D and E in Figure 8.1) and growth times (F in Figure 8.1) of the samples studied, together with the observed polarity of the surface.

Sample id	NL growth time[min] (C)	TMG annealing time [min] (D)	NH_3 annealing time [min] (E)	TMGa+NH_3 main layer growth time [min] (F)	Polarity
#1	3:30	8	0	36	Ga
#2	-	8	0	36	N
#3	-	4	0	36	N
#4	-	20	0	36	N
#5	-	60	0	36	Ga
#6	-	90	0	36	Ga
#7	-	90	0	72	Ga
#8	-	90	26	36	N/Ga
#9	-	120	0	36	Ga

temperature of 1125 °C (Figure 8.1 B) and reducing at the same time the carrier gas flow to keep the total flow constant. After this nitridation step, the temperature was decreased to 560 °C, the GaN nucleation layer (NL) was deposited at pressure raised to 500 mbar (Figure 8.1 C) and then only for sample #1 a LT NL was deposited. For the other samples the temperature and pressure decreased in the same fashion and for the same time as for sample #1, however the TMG source was not switched on, so there was no LT NL deposition. Next, the wafer was brought to high temperature (1170 °C) in an ammonia atmosphere and the pressure was decreased to 35 mbar. In the meantime, the flow of precursors was adjusted (V/III ratio was 1400) to grow the main GaN layer. When reaching 1170 °C, the NH_3 gas was replaced with H_2 and, at the same time, all samples were exposed to 8-120 min TMG atmosphere (64 μmol of TMG per minute). This annealing time (Figure 8.1D) varied between 8 and 120 min. Then, except for the sample #8, the ammonia gas was switched on to grow the main GaN layer using the same TMG flow. Sample #8 was additionally annealed 26 minutes (Figure 8.1E) in NH_3 (TMG was switched off) and then the main GaN epilayer was deposited (Figure 8.1 F). The average growth rate of the main GaN layer was determined to be about 1.6 μm/h from in situ reflectance measurements. The growth parameters are summarized in Table 8.1. For visualization of the surface morphology, tapping-mode atomic force microscopy (AFM), scanning electron microscope (SEM), and optical microscopy were used. In order to reveal defects in the GaN epilayers, orthodox etching in molten KOH-NaOH eutectic with 10 % MgO powder (E+M etch) was performed at 400 °C for 4 minutes [19]. Photoluminescence (PL) spectra were measured at 4 K using a 100 cm long SPEX 1704 monochromator, and ISA CCD camera for detection and a HeCd laser for excitation. The carrier concentration was calculated based on capacitance-voltage (C-V) measurements using a Hg probe.

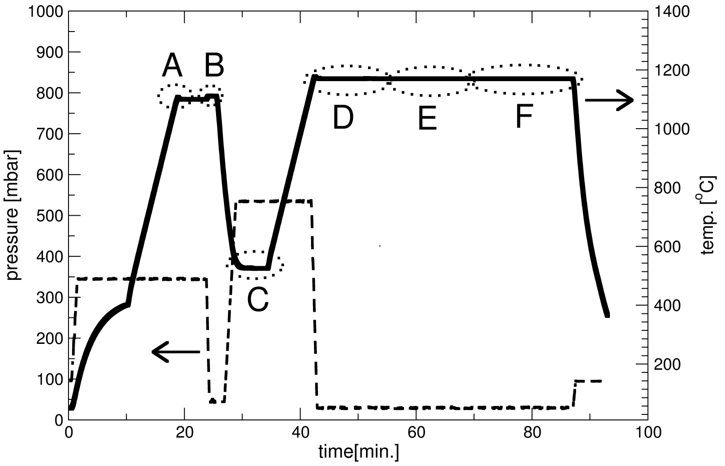

Figure 8.1: The temperature (full line) and pressure (dashed line) variation during the epiataxial process. (A) annealing the substrate in H_2 for 5 minutes at 1150 °C (all samples); (B) a 45 seconds nitridation step at 1150 °C (all samples); (C) sample #1: 3:30 min of deposition GaN at 560 °C, for samples #2 to #8 no GaN was deposited; (D) annealing in TMG at 1170 °C for various times (see Table 8.1); (E) sample #8 additionally annealed in ammonia; (F) main GaN layer deposition (all samples).

8.3 Results and discussion

The in situ reflectance measurements for samples annealed in TMG atmosphere are presented in Figure 8.2. For sample #3 that was grown on sapphire and annealed for 4 minutes in TMGa, the amplitude of the in situ reflectance oscillations decreased rapidly with the time. At this point, the surface appears dim and shows no specular reflectivity. The surface of the sample was covered by the characteristic hillocks (indicative of N-polar material) deteriorating the reflected light intensity. The results are similar to those presented in a publication by [2], for samples grown directly on sapphire. When the annealing time increases up to 20 min, the decreases of the amplitude with time become smaller (sample #2 and #4) suggesting an improvement of the surface morphology [20]. However, this growth procedure still results in N-polar material.

In order to observe the influence of the standard low temperature NL on GaN growth, sample #1 was prepared. As expected, the GaN epilayer grown on a standard low temperature NL which was additionally annealed for 8 min in TMG resulted in Ga-polar (in opposite to the sample #2) material with a smooth surface (Figure 8.3). The reflectance data observed for sample #1 are similar to these observed for similar

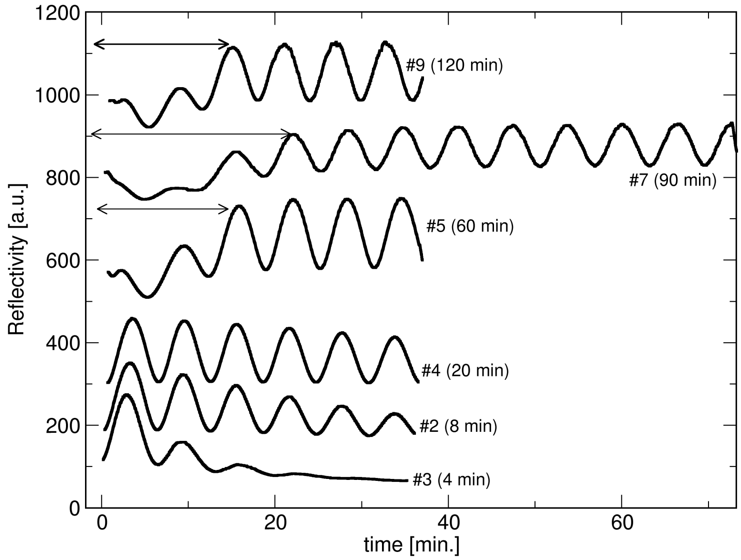

Figure 8.2: In-situ reflectance measurements during GaN growth (after the sapphire annealing treatments). The horizontal arrows indicate the transition time from the beginning of the 3D growth mode to the beginning of the 2D growth mode. The data are arbitrarily shifted along the vertical axis.

processes but without annealing. The amplitude of reflectance oscillation remains constant from the beginning of the growth process. It means that GaN grows directly in step flow mode (or 2D mode) [14]. Similar effect is observed in case of samples #2, #3 and #4 in which the GaN deposition process also starts from 2D growth mode but after few minutes the amplitude decreases indicating deterioration the surface morphology (due to formation of hillocks). However, for samples #5, #7 and #9 annealed in TMG for 60, 90, and 120 min respectively, the amplitude of the signal stayed constant or slowly increased resulting in Ga-polar material with a mirror-like surface. For these processes, the epitaxy begins with the deposition of 3D islands resulting in a decrease of the reflectance just after the start of the GaN growth process (Figure 8.2). The average roughness of the epilayer increases as long as the grain size stays below the nucleation site spacing, which becomes apparent in an additional decrease of the reflectance signal.

With the start of coalescence the reflectivity signal increases again and begins to oscillate due to interference in the GaN layer. After 15 min and 20 min for sample #5 and #7 respectively, the 3D growth mode [14, 21] was changed to 2D growth mode (Figure 8.2 -horizontal arrows). To illustrate this point more clearly, it is useful to compare the surface morphology (Figure 8.4) of sample #6 (1 μm thick) and #7 (2 μm thick) using optical microscopy. Due to the fact that in horizontal types of reactors

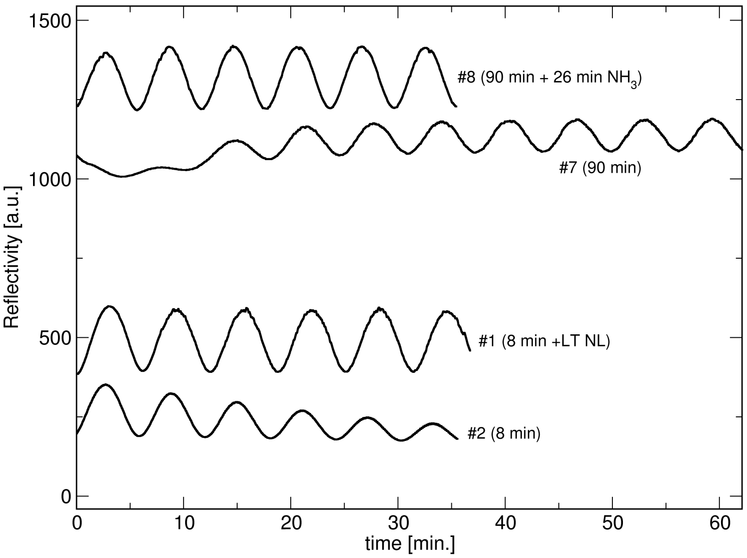

Figure 8.3: In-situ reflectance measurements for GaN samples grown on sapphire annealed in TMG atmosphere. Samples #1 and #2 were both annealed 8 min in TMG at a high temperature; in addition for sample #1 standard low temperatures NL was deposited. Sample #7 and #8 were both annealed 90 min in TMG. Sample #8 was additionally annealed in ammonia for 26 min just before main GaN layer deposition. The data are arbitrarily shifted along the vertical axis.

the growth rate is sometimes slightly higher in the middle of the wafer than near the edge, the complete coalescence of the GaN epitaxial film should be observed in the middle part of the wafer first and then near the edge. The two phases (before and after complete coalescence) are clearly visible on the left part of the 2 inch wafer of sample #6 presented on Figure 8.4. The right part of the wafer (sample #7) shows a 2 μm thick GaN film with a uniform surface morphology indicating complete transformation from 3D growth mode to 2D. The 2D growth mode was also confirmed by AFM (Figure 8.5), where atomic steps are clearly visible (sample #5). Interesting results were observed for sample #8 as well; this sample was grown with the same conditions as sample #7, except for an additional annealing in ammonia atmosphere, which was performed after the GTS. It was observed that (in opposite to the sample #7) the 2D growth mode started immediately just after the GaN main layer deposition had begun. It means that transition from annealing step to the main GaN layer growth is also a critical factor in growth process.

To reveal the dislocation density and the film polarity of the GaN layers, samples #7 and #8 were etched in the KOH-NaOH eutectic (Figure 8.6). The density of dislocations in sample #7 was about $1.3\times10^{9}\,\mathrm{cm}^{-2}$. This value of defect density is comparable with GaN samples grown on sapphire by two-step growth method [22]

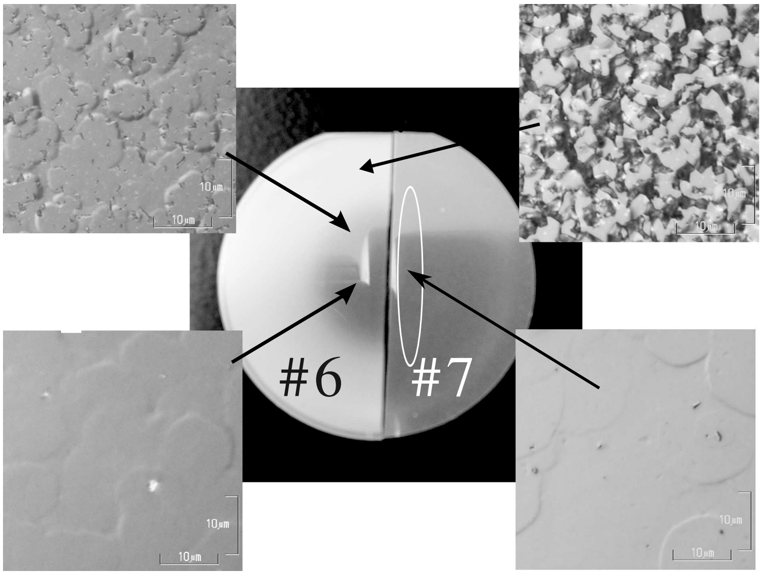

Figure 8.4: Optical images at position indicated by the arrows on a 1 μm thick sample #6 and a 2 μm thick sample #7, both prepared under identical conditions. Due to the radial distribution of the GaN epilayer thickness, the different stages of film coalescence are observed on the thinner sample (#6).

but it should be pointed out that the above described processes were not optimized toward the reduction of dislocations. For sample #8 it was not possible to establish the density of defects after E+M etching, because N-polar material etches much faster then Ga-polar GaN [22]. This effect is clearly visualized in Figure 8.7, where the N-polar inclusions are etched away. It may suggest that the TMG annealing process was still too short to obtain GaN material with only Ga-polarity. The quickly etched N-polar inclusions constitute effective sources of steps, which propagate on the Ga-polar matrix and “sweep” the dislocation-related etch pits. This is the reason why defects itself are not clearly visible in Figure 8.7. Figure 8.8 shows the PL spectra taken on samples #1, #2 and #6 at 4 K. The spectrum for sample #1 is very similar to the standard (without TMG annealing) samples grown using the two-step growth method. This Ga-polar sample exhibits a well-defined spectrum showing a donor bound exciton (D_0X) peak at 3.482 eV and the free exciton A (X_A) at 3.488 eV. On the other hand, the PL spectrum from sample #2 shows an extremely broad peak centered at 3.463 eV, which is typical for N-polar material [23]. The PL spectrum observed for sample #6 differs from the two other samples - the peak shifted to 3.495 eV suggests that the sample is under compressive strain [10, 24]. The broadening of this peak suggests that GaN epilayer is non uniform within the PL laser spot. Considering that the carrier concentration, as measured by CV, was 1.1×10^{17} cm^{-3} and 1.3×10^{17} cm^{-3}

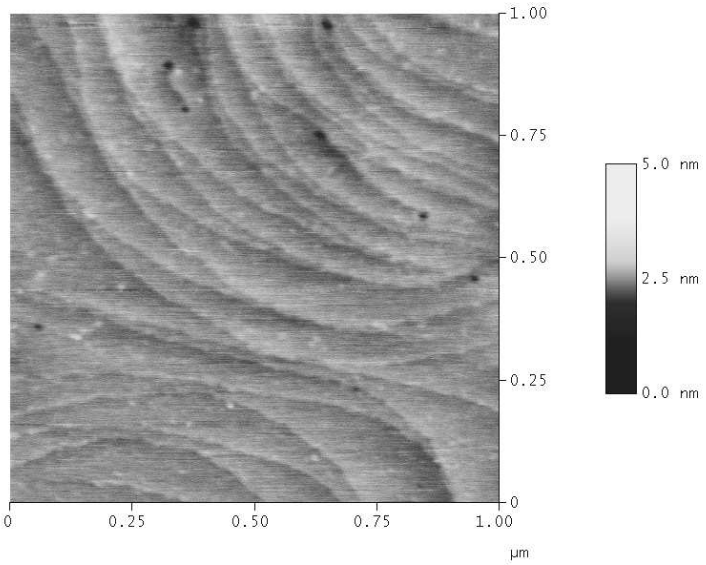

Figure 8.5: AFM image of as-grown sample #5. Clearly visible atomic steps indicate the 2D growth mode.

for sample #1 and #6 respectively, the difference in intensity between both samples can be the result of different defect densities [25]. Moreover, it should be mentioned that for all the presented samples no Ga droplets were observed. In order to check whether Ga droplets were formed on sapphire, a process similar to #7 was performed, with the only exception that the main GaN layer was not deposited and the sample was immediately cooled down after 90 min of annealing in TMG. X-ray reflectance measurements did not show any extra layer on the top of the sapphire wafer. The total weight of the sapphire was the same before and after process. Therefore, it can be concluded that there was no remarkable deposition of Ga in the form of sizable droplets or continuous layer exceeding the atomic scale. In order to explain all the observed phenomenon the following growth model can be proposed: during the TMG annealing a few atomic layers of Ga metal are deposited (Figure 8.9A).

The Ga layer probably does not cover the sapphire surface completely and it forms 2D Ga clusters. If the distance between Ga clusters is too large (Figure 8.9A1) it results in the N-polar material (Figure 8.9C1) growth (sample #2, #3, #4). When the distance between the Ga-clusters is small enough, the non covered places are overgrown by a Ga-polar material by inducing the 3D growth (Figure 8.9B; sample #5, #6, #7, #9). The GaN material deposited on the Ga-clusters forms crystallites similar to those observed for a standard low temperature NL. During the epitaxial

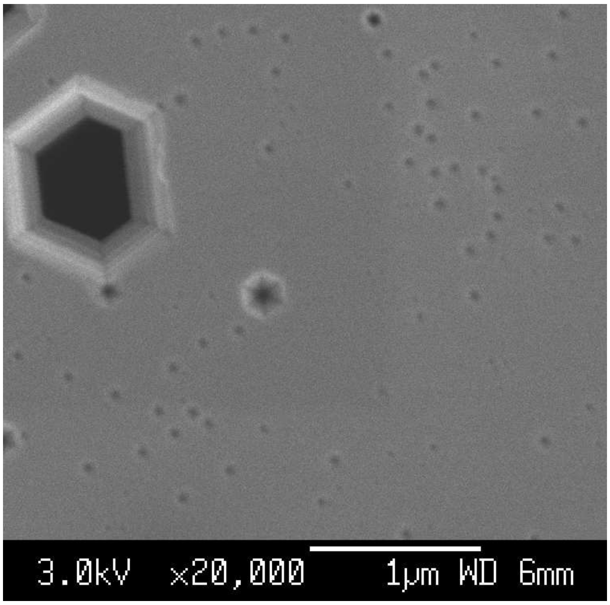

Figure 8.6: SEM image of sample #7 etched in the KOH-NaOH eutectic mixture at 400 °C for 4 minutes.

process the complete coalescence of the crystallites occurs and at the same time the GaN film overgrows non Ga-covered sapphire places. After coalescence of the islands 2D growth mode is induced (Figure 8.9C). By annealing the sapphire wafer first in TMG and then in ammonia (sample #8), the Ga clusters are directly transformed into a thin GaN layer (Figure 8.9D). This layer will grow in a 2D growth mode (Figure 8.9E) right from the start. Since GaN grown directly on sapphire is N-polar the spaces between the Ga clusters are consequently filled by N-polar material.

8.4 Conclusions

In summary, the influence of the Ga based nucleation layer on the GaN epitaxial growth has been investigated. It is demonstrated that by the deposition of a thin Ga layer on sapphire, Ga-polar GaN material with a smooth surface morphology can be grown. Moreover, it was shown that by using an additional ammonia treatment, 2D growth mode can be stimulated. The main disadvantage of the new GTS method is a long annealing time and the use of expensive Ga precursors. Contrarily, the main advantage is the simplification of the growth procedure and through this, an improvement of the epitaxial process reproducibility. In opposite to the two-steps growth method, the GTS procedure enables deposition of GaN at one temperature

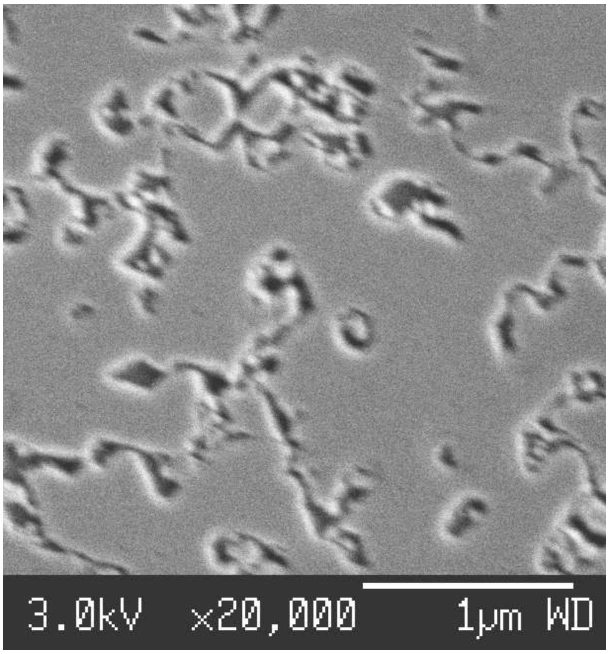

Figure 8.7: SEM image of sample #8 etched in the KOH-NaOH eutectic mixture at 400 °C for 4 minutes. The dark spots depth (measured by AFM) exceeds 900 nm - this indicates the inclusions of N-polar material [22].

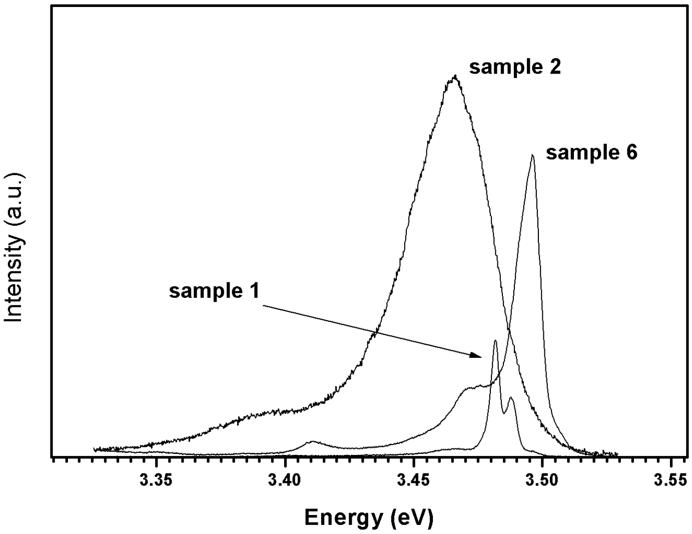

Figure 8.8: PL spectra for samples #1, #2 and #6.

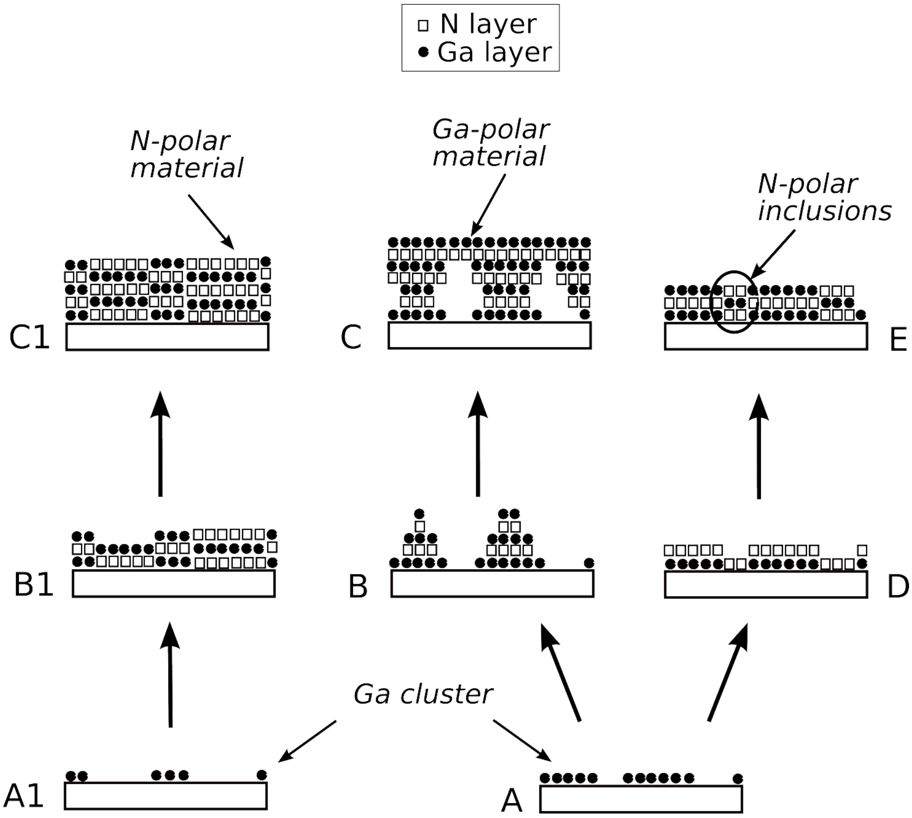
□ N layer
● Ga layer
N-polar material
Ga-polar material
N-polar inclusions
C1
C
E
B1
B
D
Ga cluster
A1
A

Figure 8.9: Growth model for the observed deposition of GaN epilayers.

and at one pressure. It is found that the GTS procedure introduces compressive strain in GaN layers. The defect density is found to be comparable with that observed in samples grown by the standard two-step growth method. However, in order to thoroughly compare the standard growth method with the proposed GTS method, further experiments towards the optimization of the process are necessary.

Bibliography

[1] H. Manasevi, F. M. Erdmann, W. I. Simpson, J Electrochem Soc 118 (11) (1971) 1864.

[2] S. Nakamura, Jpn J Appl Phys 2 30 (10A) (1991) L1705–L1707.

[3] H. Amano, N. Sawaki, I. Akasaki, Y. Toyoda, APL 48 (5) (1986) 353–355.

[4] T. Kachi, K. Tomita, K. Itoh, H. Tadano, APL 72 (6) (1998) 704–706.

[5] S. Keller, B. P. Keller, Y. F. Wu, B. Heying, D. Kapolnek, J. S. Speck, U. K. Mishra, S. P. DenBaars, APL 68 (11) (1996) 1525–1527.

[6] S. Haffouz, A. Grzegorczyk, P. Hageman, P. Vennegues, E. van der Drift, P. Larsen, J Cryst Growth 248 (2003) 568–572.

[7] K. Naniwae, S. Itoh, H. Amano, K. Itoh, K. Hiramatsu, I. Akasaki, J Cryst Growth 99 (1-4) (1990) 381–384.

[8] D. Gogova, H. Larsson, R. Yakimova, Z. Zolnai, I. Ivanov, B. Monemar, Phys Status Solidi A 200 (1) (2003) 13–17.

[9] R. J. Molnar, W. Gotz, L. T. Romano, N. M. Johnson, J Cryst Growth 178 (1-2) (1997) 147–156.

[10] Y. Kim, N. A. Shapiro, H. Feick, R. Armitage, E. R. Weber, Y. Yang, F. Cerrina, APL 78 (7) (2001) 895–897.

[11] K. H. Ploog, O. Brandt, R. Muralidharan, A. Thamm, P. Waltereit, Journal of Vacuum Science & Technology B 18 (4) (2000) 2290–2294.

[12] W. G. Breiland, K. P. Killeen, Journal of Applied Physics 78 (11) (1995) 6726–6736.

[13] P. Vennegues, B. Beaumont, S. Haffouz, M. Vaille, P. Gibart, J Cryst Growth 187 (2) (1998) 167.

[14] S. Figge, T. Bottcher, S. Einfeldt, D. Hommel, J Cryst Growth 221 (2000) 262–266.

[15] D. D. Koleske, M. E. Coltrin, A. A. Allerman, K. C. Cross, C. C. Mitchell, J. J. Figiel, APL 82 (8) (2003) 1170–1172.

[16] D. Koleske, M. Coltrin, K. Cross, C. Mitchell, A. Allerman, J Cryst Growth 273 (1-2) (2004) 86–99.

[17] R. S. Balmer, C. Pickering, A. J. Pidduck, T. Martin, J Cryst Growth 245 (3-4) (2002) 198–206.

[18] J. Han, T. B. Ng, R. M. Biefeld, M. H. Crawford, D. M. Follstaedt, APL 71 (21) (1997) 3114–3116.

[19] G. Kamler, J. L. Weyher, I. Grzegory, E. Jezierska, T. Wosinski, J Cryst Growth 246 (1-2) (2002) 21–24.

[20] O. Briot, J. P. Alexis, M. Tchounkeu, R. L. Aulombard, Mat Sci Eng B-Solid 43 (1-3) (1997) 147–153.

[21] I. V. Markov, Crystal growth for beginners: fundamentals of nucleation, crystal growth and epitaxy.

[22] J. L. Weyher, L. Macht, G. Kamler, J. Borysiuk, I. Grzegory, phys. stat. sol.(c) 0 (3) (2003) 821–826.

[23] L. Macht, J. L. Weyher, P. R. Hageman, M. Zielinski, P. K. Larsen, J Phys-Condens Mat 14 (48) (2002) 13345–13350.

[24] B. Gil, O. Briot, R. L. Aulombard, Phys. Rev. B 52 (24) (1995) 17028–17031.

[25] S. Haffouz, V. Kirilyuk, P. R. Hageman, L. Macht, J. L. Weyher, P. K. Larsen, APL 79 (15) (2001) 2390–2392.

Chapter 9

Influence of sapphire annealing in trimethylaluminum atmosphere on GaN epitaxy by MOCVD

*

The microscopic evolution of GaN layers grown by metal-organic chemical vapor deposition on sapphire using a new Al treatment method replacing traditional techniques was investigated. With the help of in situ reflectance measurements the coalescence and overgrowth of GaN epilayers were examined and the sample morphology was ex-situ characterized by scanning electron microscopy. For characterization of the GaN layers, energy dispersive X-ray spectroscopy and X-ray diffraction were used for chemical and structural analysis, respectively. The experimental results demonstrated that it is possible to control the GaN epitaxial layer polarity and to induce a stable growth mode by depositing a thin Al based nucleation layer on the c-plane sapphire instead of using the classical two-step growth method. It was found, that during the annealing in trimethylaluminum at 1170 °C some amount of carbon is incorporated into the layer. The X-ray diffraction measurement revealed traces of Al_4C_3 in the nucleation layer. In GaN epilayers with thickness exceeding 300 nm, inclusions of probably misoriented crystallites or of cubic GaN were observed.

---

[*] A.P. Grzegorczyk, J.L. Weyher, P.R. Hageman, and P.K. Larsen, Submitted to Thin Solid Films

9.1 Introduction

Gallium nitride-based semiconductors have demonstrated the potential to serve as the basis of a new generation of optoelectronic, high-temperature, and high-power electronics. Products like light-emitting diodes (LED), laser diodes (LD), and detectors based on GaN material are already offered on the market. Since the first application of the metal-organic chemical vapor deposition (MOCVD) technique for III-V nitrides [1], a great deal of work was made towards the improvement of the surface morphology, and the structural and optical quality of the GaN epilayers. Despite these effects, the structural quality of the GaN epilayers is still far from that of Si and GaAs. The production of free standing GaN wafers, although possible, is still very expensive, and moreover not large enough to meet the market needs. Therefore, sapphire, silicon carbide, and silicon remain the most popular substrates for GaN epitaxy. Because of the differences in lattice constants and thermal expansion coefficients, GaN epilayers deposited on these substrates suffer from the presence of a large number of threading dislocations. The average density of these dislocations for MOCVD films grown on sapphire often exceeds $2\times10^{9}\,\mathrm{cm}^{-2}$, while for SiC substrates it is only a few times lower (high $10^{8}\,\mathrm{cm}^{-2}$ dislocations). Even though this initial high dislocation density, some devices based on GaN heteroepitaxy (LED) function satisfactorily. However, their properties could be improved through the reduction of dislocations.

From the time of the first demonstration of the MOCVD growth of GaN many different methods were applied to improve the structural and optical properties of GaN epilayers grown on both sapphire and SiC substrates. Low temperature AlN [2], GaN [3], and InN [4] nucleation layers or a Si_3N_4 treatment [5] are just some standard techniques that allow to improve the GaN quality. In a previous article [6] we have reported a new technique for GaN growth using a Ga treatment step (GTS) method. The main advantage of this method is its very simple growth procedure still resulting in high quality GaN epilayers. As a natural continuation of ideas presented in that publication, series of experiments with Al treatment step (ATS) were conducted and which are described in this paper. In literature there is a large number of publications describing the properties of Al deposited on a sapphire surface [7–10], however, in most of them the experimental conditions are different from those observed during a typical MOCVD GaN deposition experiment. Brown et al. [7] used a MBE reactor to deposit Al on (0001) sapphire, GaN/sapphire, and AlN/sapphire substrates. The authors observed a characteristic striation suggesting a step flow growth mode for the Al layer deposited on sapphire at 200 °C. Moreover, Vermeersch et al. [8] used Auger spectroscopy and energy electron diffraction to investigate Al layers evaporated on a-Al_2O_3. They observed that aluminum evaporation onto a sapphire crystal at 720 °C generates a uniform etching of the substrate. The effect of etching of the sapphire substrate was also reported in other publications [9, 10]. However, Levi and Kaplan [11] presented sessile drop wetting experiments of liquid Al on sapphire conducted at low pressure (10^{-3} Torr) in a controlled Ar atmosphere as a function of the oxygen partial pressure. They showed that two different dominant processes occur at the liquid Al sapphire interface. Below 1100 °C epitaxial growth of new a-Al_2O_3 layers takes place and above 1100 °C dissolution of the sapphire substrate is observed. According to our knowledge there are no publications concerning the growth of a GaN layer by MOCVD using only Al as a nucleation layer. In literature there are several authors describing the use of a Ga annealing step before the GaN deposition [6, 12–15]. All of them except Grzegorczyk et al. [6] use hydride vapor phase epitaxy (HVPE) or molecular beam epitaxy (MBE) techniques for the GaN deposition.

In this paper the influence of the Al Treatment Step (ATS) on the sapphire substrate and its impact on the GaN epitaxial growth are presented. The main differences between this ATS and the GTS method are pointed out as well. For the purpose of studying the growth process, in situ optical reflectance measurement (using a wavelength of 781 nm) was applied as a method for investigation of the growth evolution of the GaN epilayer. Breiland et al. [16] have already discussed in detail the theory regarding the optical information and extraction of the growth rates from in situ optical reflectance measurement. To visualize the surface morphology scanning electron microscopy (SEM) was used. Additionally, X-ray diffraction (using a BRUKER D8 diffractometer) and energy dispersive X-ray (EDX) measurements were applied in order to investigate the chemical composition and structural properties of the layers, respectively.

9.2 Experimental details

The GaN layers were deposited on 2 inch diameter, (0001)-oriented, commercially available sapphire substrates by MOCVD using a RF heated, AIXTRON AIX-200, low pressure horizontal reactor. Trimethylgallium (TMG), trimethylaluminum (TMA) and ammonia were used as Ga, Al and N precursors respectively. The growth procedure for all samples was started by increasing the temperature to 1170 °C and decreasing the pressure to 35 mbar - these conditions were kept constant until the end of the epitaxial process. During the entire process of epitaxy H_2 was used as a carrier gas. All samples grown using the ATS method (Table 9.1) were first annealed for 7 minutes to clean the surface of the sapphire substrate (Figure 9.1-A). After the cleaning procedure, the samples were exposed (Figure 9.1-B) to a TMA atmosphere (16 or $32\,\mu mol$ of TMA per minute) for 7-35 minutes to deposit a nucleation layer (NL). Then, except for the samples #1-#3, TMA was switched off and immediately ammonia gas was switched on for 10 minutes (Figure 9.1-C). After this nucleation

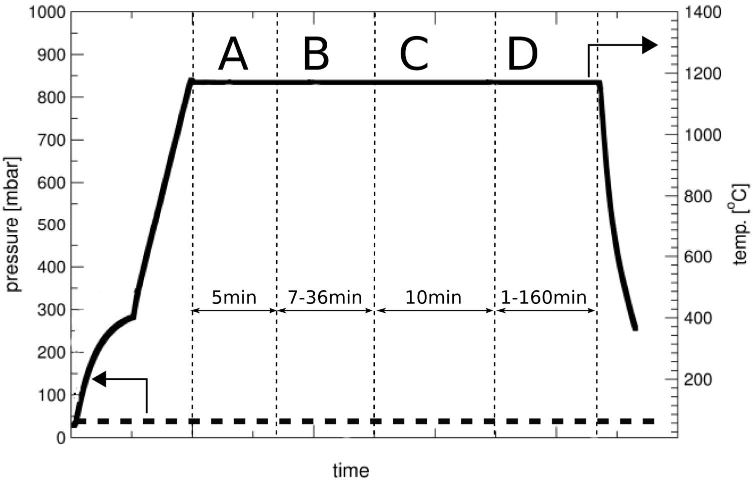

Figure 9.1: Temperature (full line) and pressure (dashed line) variation during the epitaxial process. A) annealing the substrate in H_2 for 5 minutes (all samples) - cleaning procedure; B) annealing in TMA at 1170 °C for 7-36 min; C) annealing in ammonia sample #4-#7; D) main GaN layer deposition (all samples).

layer process the TMG flow (52 *µmol* of TMG per minute) was switched on to deposit the GaN main layer (ML) (Figure 9.1-D). The average growth rate of the main GaN layer was calculated to be about 1.6 µm/h from the in situ reflectance measurements. All growth parameters are summarized in Table 9.1. All samples (except the polycrystalline) grown with the ATS method had a mirror-like surface with characteristic brown/yellow color.

The samples grown using the GTS method were annealed in a TMG (120 *µmol* of TMG per minute) atmosphere for 40 min at a temperature of 1060, 1170 and 1200 °C (Table 9.2). Next, the temperature was set to 1130 °C and the 2 µm thick of GaN layer was deposited. In opposite to the samples grown using the ATS method, the samples

Table 9.1: Details of the GaN growth procedure for the samples grown using the Al treatment step method (ATS).

Sample id	TMA flow $\mu mol/min$(B)	TMA annealing time [min] (B)	NH_3 annealing time [min] (C)	TMGa+NH_3 main layer growth time [min](D)
#1	32	35	-	30 (polycrystal)
#2	32	15	-	160
#3	32	7	-	30
#4	32	15	10	70
#5	16	30	10	70
#6	16	33	10	70
#7e, a, b, c, d	16	36	10	70,1,7,12,22

Table 9.2: Details of the GaN growth procedure for the samples grown using the Ga treatment step method (GTS).

Sample id	TMG flow $\mu mol/min$(B)	TMG annealing time [min] (B)	TMG annealing Temp. [°C] (B)	TMGa+NH_3 main layer growth time [min](D)
#8	120	38	1130	45
#9	120	38	1200	45
#10	120	38	1060	45 (polycrystal)

grown based on the GTS method were colorless with smooth surface (except sample #10 where the GaN material was polycrystalline). As a convention, the letters A, B, C, D are used to describe the epitaxial process in Figure 9.1 and are also used in next tables and figures to refer to appropriate process steps.

9.3 Results and discussion

The in situ reflectance measurements for the GaN samples grown using the ATS method are presented in Figure 9.2. For sample #1, annealed in TMA for 40 minutes, the in situ reflectance oscillations from the deposited layer are clearly visible. The estimated growth rate for it is about 2 μm/h (calculated using the total thickness of the nucleation layer and the GaN epitaxial layer). Based on the observed reflectance oscillations (Figure 9.2-B) and the measured thickness the refractive index for this layer is about 1.2 (for comparison, the refractive index for pure Al [17] is 2.7). The oscillations decreased rapidly over time indicative of a deposition of polycrystalline material.

As it will be proved in the next part of this article, the layer contains besides aluminum a high concentration of carbon. Rocha-Rangel et al. [18] showed that carbon can improve the wetting behavior of Al on the sapphire substrate. The authors demonstrated that for a carbon-coated sapphire substrate the contact angle was reduced to 40^o at 1300 °C, while in absence of carbon the final angle was 82^o at the same conditions. This is probably the reason why during ATS, as opposed to GTS method, the in situ reflectance oscillations are clearly observed. In case of sample #2, the ATS time was 15 minutes resulting in a stable growth of the GaN layer (Figure 9.2-D). An interesting characteristic of the reflectance signal is observed at the point where the ATS layer is finished and GaN layer starts to be deposited. The reflectance intensity increases at the beginning of the GaN growth deposition process and after few minutes it decreases suddenly and then slowly increases again (Figure 9.2-D1). The slow increase of reflectance amplitude during the growth process indicates that the surface of the GaN epilayer starts smoothening. Similar behavior of in situ reflectance is measured during the transition from 3D to 2D growth

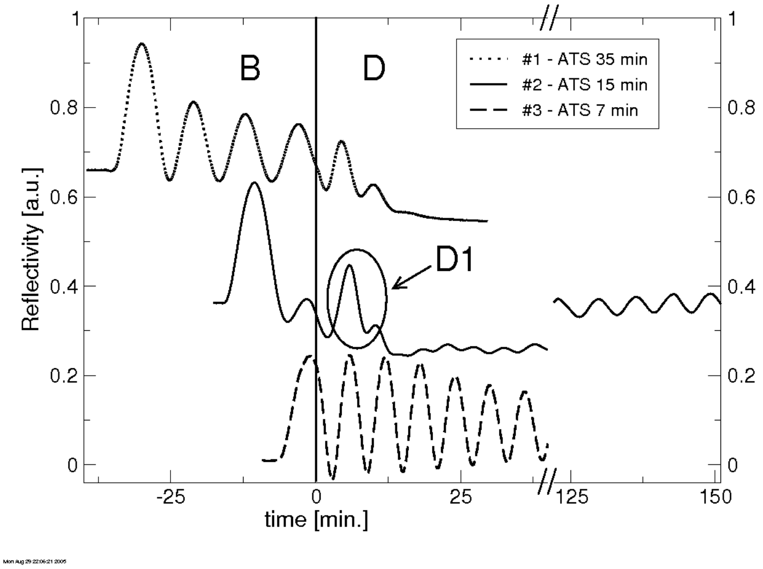

Figure 9.2: in situ reflectance measurements for sample #1-#3. The deposition of an Al containing layer (B) is clearly observed. During deposition of the main GaN layer (D) a characteristic of reflectance is observed (D1). The data are arbitrarily shifted along the vertical axis.

mode [19–21].

The transient observed for sample #3 differ significantly from sample #1 and #2. The film deposition process for sample #3 starts directly from 2D growth mode. The Al based layer does not cover the sapphire substrate completely so the GaN layer is deposited partly on a clean sapphire substrate resulting in partly growth of N-polar material [3]. It should be point out that as opposed to the GTS method, deposition of a layer during the annealing process in TMA is evidently observed (even at 1200 °C). Because the temperature range when deposition of the layer is observed is very broad, the experiments with ATS method were prepared at 1170 °C (at this temperature the surface morphology of samples was the most satisfactory). To illustrate this point more clearly it is useful to compare the in situ reflectance for data samples prepared using the GTS method at different temperatures (Figure 9.3). The main GaN layer was deposited at the similar conditions as for ATS method (Figure 9.3-D) but annealing in TMG was carried out at different temperatures - 1060, 1130, and 1200 °C (Figure 9.3-B). For samples annealed at a temperature of 1130 and 1170 °C the reflectance signal does not change during the GTS process. Moreover the reflectance signals are for both samples during the GaN layer deposition very similar. For the sample prepared at 1060 °C the reflectance signal decreases over time suggesting Ga metal deposition. Because the oscillations of reflectance are not clearly visible during GTS, it suggests that the Ga metal forms not a uniform layer but

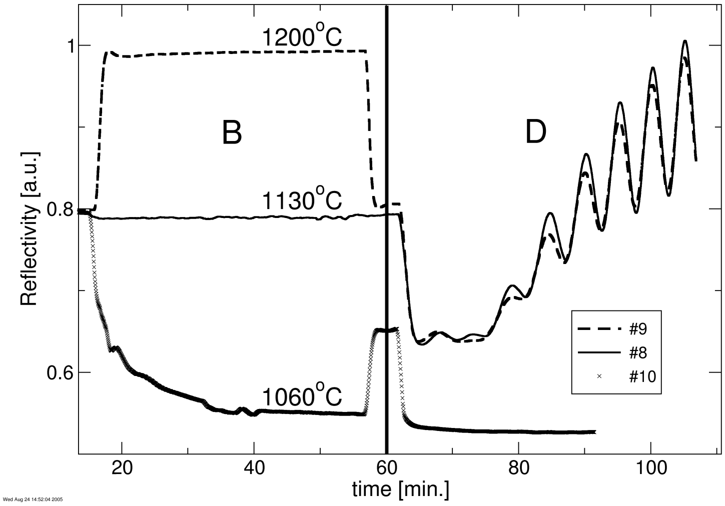

Figure 9.3: in situ reflectance measurements for samples grown using the GTS method. Annealing in TMG (B) was performed at 1060, 1130, and 1200 °C. As opposed to the ATS method, characteristic oscillations of the reflectance are not observed during the annealing period.

droplets on the sapphire surface. The final GaN layer deposited using such process results in polycrystalline material (sample #10).

The influence of annealing in an ammonia atmosphere after ATS on the growth of the GaN epilayer is illustrated in Figure 9.4. For sample #4, which is annealed in ammonia, the amplitude of reflectance oscillations increases much faster then the amplitude for sample #2 (Figure 9.4-D), which has not been annealed in ammonia. The additional annealing in ammonia decreases the transition time from the 3D to the 2D growth mode. If the oscillation amplitude remains constant, it is assumed that the growth is 2D. The same effect is observed for the GTS method - in extreme cases the 3D growth mode can be completely suppressed, as was demonstrated in the previous publication [6]. Figure 9.5 demonstrates the influence of the Al deposition time for samples grown using the ATS method and which have been additionally annealed for 10 minutes in ammonia atmosphere. For sample #5 and #6 annealed in TMA for 30 and 33 minutes respectively, the amplitude of the reflectance oscillations decreases over time and thus the roughness of the samples increases. The opposite effect is observed for sample #7, which has been treated for 36 minutes with TMA in the ATS process. For all these samples a differences in the oscillations amplitude are observed. Based on experiments that were prepared, it is not possible to give precise explanation of these phenomena.

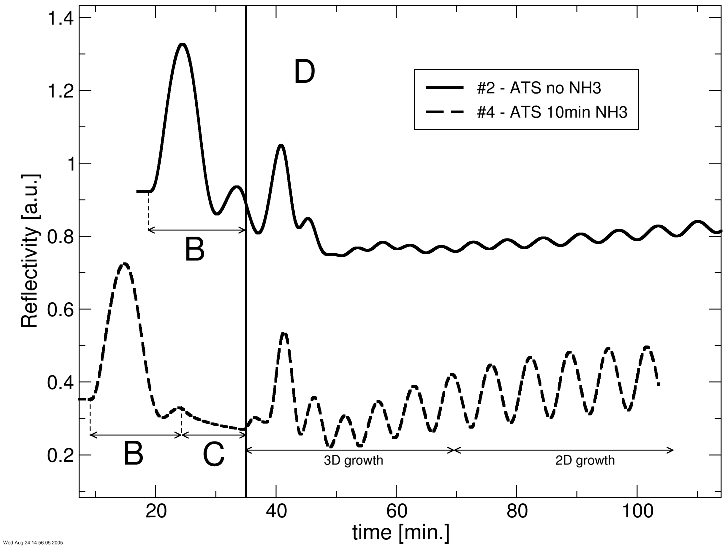

Figure 9.4: in situ reflectance spectra for samples grown using ATS with and without an ammonia treatment. For sample #4 (grown with the ammonia treatment) the amplitude of in situ reflectance oscillation saturates much faster then the amplitude of the oscillations of sample #2. The data are arbitrarily shifted along the vertical axis.

Since the observed behavior of the in situ reflectance for the ATS method is not typical for GaN growth [20], ex-situ evaluation of the film coalescence was performed (Figure 9.6). A series of samples similar to #7 but with different thickness of the GaN layer was examined by SEM and EDX. Figure 9.6a and 9.6b present SEM images of a GaN layer deposited for 1 and 7 minutes respectively. The growth starts from depositions of small crystallites that were sometimes 60^o misoriented to each other. The crystallites are not separate islands as observed after the standard two-step growth method [22] or after Si_3N_4 treatment method [23] but are somehow connected to each other. These crystallites act as nucleation sites for following epitaxial layer growth.

In the next step of the epitaxial process, the full coalescence or overgrowth of crystallites was observed (Figure 9.6c, d). For the 1.8μm thick GaN sample (Figure 9.6e) a complete coalescence of the epitaxial layer is observed. However, for samples with a more than 300 nm thick GaN layer on the top (Figure 9.6c, d, e - circled areas) characteristic dark inclusions are present. These dark inclusions are observed only by SEM what suggests that the electrical properties of the material differ locally. The EDX analysis did not reveal a difference in composition between the dark inclusions and the clean surface. For a 1.8μm thick GaN layer Ga, N, and small amounts of carbon atoms are detected. Traces of Al from the sapphire substrate

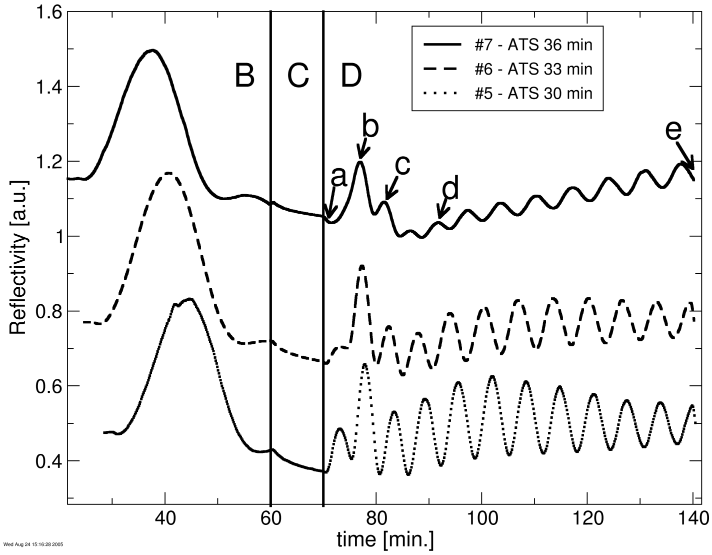

Figure 9.5: in situ reflectance data for samples grown with different ATS time. All samples were annealed in ammonia after ATS. Letter a, b, c, d, and e refers to the SEM images presented on Figure 9.6.

or the aluminum layer deposited during ATS are not observed (Figure 9.7). To determine the polarity of the inclusions, the samples were etched in a KOH solution [24]. Inspection with SEM of the etched surface revealed that the dark inclusions were removed by etching process. This suggests that the dark inclusions are inversion domains and that these N-polar inclusions result from the locally non optimized nucleation layer for GaN growth. Figure 9.8 shows the EDX spectra for a sample with GaN layer deposited for 1 minute (see also Figure 9.6a). The peaks from Al and O atoms that are related to the sapphire substrate and ATS layer are clearly visible in Figure 9.8. Surprisingly, the peak from carbon atoms is clearly observed as well. The carbon atoms are probably incorporated into the Al layer from the methyl group of the mono-methyl aluminum growth species according to the stoichiometric relation [25]:

$$[Al(CH_3)_3]_4 \rightarrow Al_4C_3 + 9CH_4. \tag{9.1}$$

The increased carbon incorporation in Al based nucleation layer can be attributed to the greater strength of the Al-C (Al-CH_3, $65\,kcal \cdot mol^{-1}$) bond as compared with Ga-C (Ga-CH_3, $59\,kcal \cdot mol^{-1}$) [26]. It is possible that during ATS the Al_4C_3 compound is formed on the sapphire surface [27–29]. Kim et al. [29] used chemical vapor deposition technique to produce ultra-fine aluminum nitride powder. The authors, similarly to our setup, used TMA and ammonia as precursors of Al and

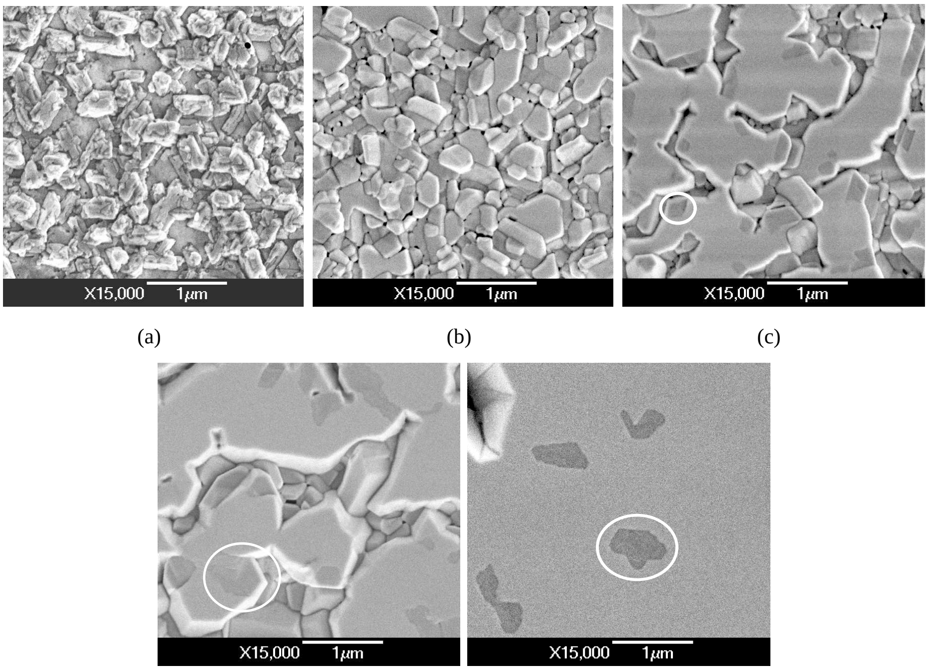

(a) (b) (c)

(d) (e)

Figure 9.6: SEM images for a sample similar to #7 with different thickness of the top GaN layer. The growth process was stopped after (see Figure 9.5) a) 1 min, b) 7 min, c) 12 min, d) 22 min, and e) 70 min. The circle indicates an area with a misoriented crystallite or a cubic inclusion.

N, respectively. They observed that a higher TMAl/NH_3 ratio results in a higher percentage of the Al_4C_3 phase in the powder. To check if samples grown using ATS method contains Al_4C_3, X-ray measurements were performed (only symmetric peaks are visible). Figure 9.9 presents X-ray diffraction pattern for sample #8, #3, and #1. For sample #8, which was grown using the GTS method, only diffraction peaks from the sapphire substrate and the GaN layer are visible. For sample #3, which was grown using the ATS method, the same peaks are visible but also the peaks from Al_4C_3 are evident [30]. For sample #1 with a polycrystalline GaN layer on top (see Figure 9.2) only peaks from sapphire and Al_4C_3 are present. To reveal more diffraction peaks additional powder diffraction measurements were carried out on epitaxial material mechanically removed from sample #1. This measurement revealed additional peaks from GaN as well as from Al_4C_3. It should be pointed out that it was not possible to identify explicitly the diffractions peaks from pure Al. The reason for this is that amount of pure Al is to small to detect it by the X-ray diffraction method, as it was also the case for [29] in which no pure Al in the layer was observed although a similar

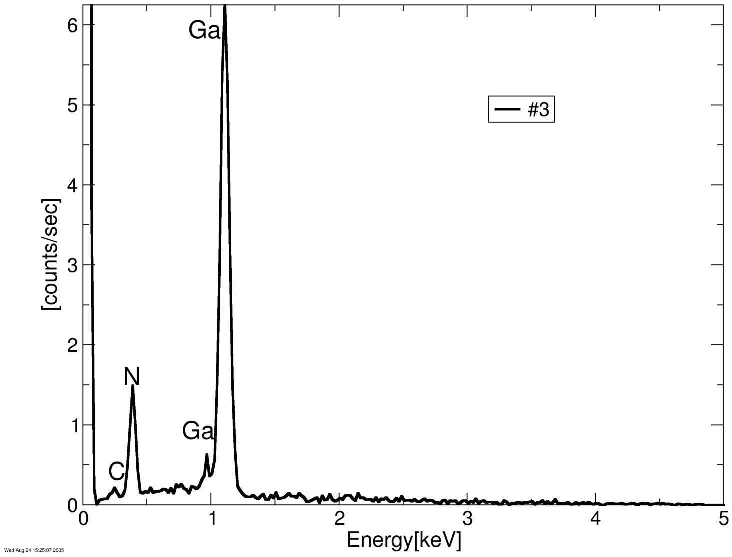

Figure 9.7: Typical EDX spectra for a 1.8μm thick GaN sample grown using the ATS method. No differences in EDX spectra between the circled area presented on Figure 9.6 and the "clean" areas were observed.

experimental technique was used.

In the MOCVD growth of GaN there is always a certain level of oxygen impurities present which can be incorporated into the deposited layer [31]. Not identified X-ray diffraction peaks, that were not observed in publication [29], can be related to the compounds containing oxygen e.g. AlOC or Al_2O_3. Because of the high temperature deposition process (where Al is very reactive), also compounds like AlO_xN_y [32] can be formed. For the GTS method the deposited [6] Ga layer is only few atomic layers thick so it was not possible to verify the presence of C or O atoms in the nucleation layer.

9.4 Conclusions

In summary, the ATS is a new and simple method of GaN growth on sapphire. It was demonstrated that Ga-polar GaN material with a smooth surface morphology can be grown by the deposition of a thin layer containing Al_4C_3 on sapphire. The results obtained from the in situ reflectance measurements and ex-situ SEM images clearly indicate that the growth process dynamics for ATS method is different than that observed for both the two-step growth method and the GTS method. The main advantage of the ATS method is the simplification of the growth procedure

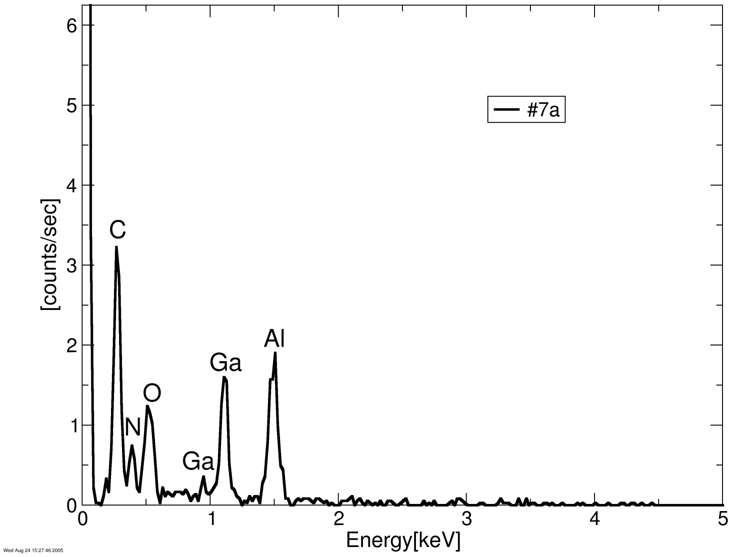

Figure 9.8: The EDX spectra for the sample presented in Figure 9.6a grown using the ATS method. During deposition of the Al layer, carbon is incorporated into the layer.

and through this, an improvement of the epitaxial process reproducibility. In order to assess the quality of GaN layers grown using the new method, it is necessary to optimize the growth procedure. Moreover, to identify the crystal structure of the inclusions found in GaN layers, additional examination of the samples by transmission electron microscopy should be conducted.

9.5 Acknowledgements

The authors would like to thank G. Kamler and A. Presz for EDX and SEM measurements. This work was performed as a part of the research program of the Dutch Technology Foundation (STW).

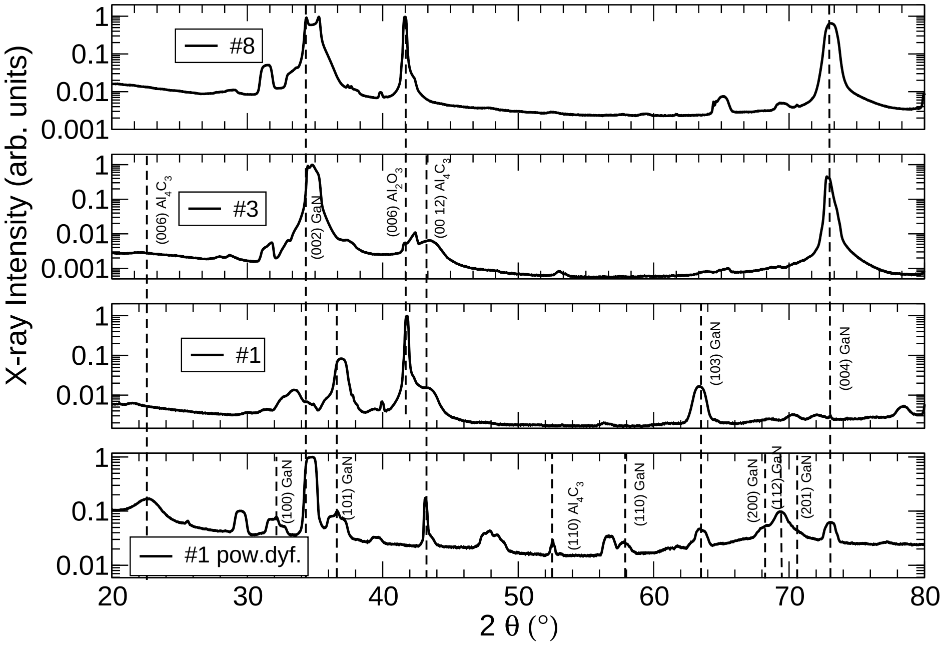

Wed Sep 28 02:17:23 2005

Figure 9.9: X-ray diffraction spectra ($\theta - 2\theta$ curves) for sample #8 (grown using GTS method), #3 (grown using ATS method - 15 min), and #1 (grown using ATS method, 35 min, polycrystalline epilayer) and powder diffraction spectra for epilayer #1 mechanically removed from sapphire substrate.

Bibliography

[1] H. Manasevi, F. M. Erdmann, W. I. Simpson, J Electrochem Soc 118 (11) (1971) 1864.

[2] H. Amano, N. Sawaki, I. Akasaki, Y. Toyoda, APL 48 (5) (1986) 353–355.

[3] S. Nakamura, Jpn J Appl Phys 2 30 (10A) (1991) L1705–L1707.

[4] T. Kachi, K. Tomita, K. Itoh, H. Tadano, APL 72 (6) (1998) 704–706.

[5] S. Sakai, T. Wang, Y. Morishima, Y. Naoi, J Cryst Growth 221 (1-4) (2000) 334.

[6] A. P. Grzegorczyk, P. R. Hageman, J. L. Weyher, P. K. Larsen, J Cryst Growth 283 (1-2) (2005) 72–80.

[7] P. D. Brown, M. Fay, N. Bock, S. Marlafeka, T. S. Cheng, S. V. Novikov, C. S. Davis, R. P. Campion, C. T. Foxon, J Cryst Growth 234 (2-3) (2002) 384–390.

[8] M. Vermeersch, F. Malengreau, R. Sporken, R. Caudano, Surf Sci 323 (1-2) (1995) 175–187.

[9] J. A. Champion, B. J. Keene, J. M. Sillwood, J Mater Sci 4 (12) (1969) 1111.

[10] G. Levi, W. D. Kaplan, Acta Mater 51 (10) (2003) 2793–2802.

[11] G. Levi, W. D. Kaplan, Acta Mater 50 (1) (2002) 75–88.

[12] K. Naniwae, S. Itoh, H. Amano, K. Itoh, K. Hiramatsu, I. Akasaki, J Cryst Growth 99 (1-4) (1990) 381–384.

[13] D. Gogova, H. Larsson, R. Yakimova, Z. Zolnai, I. Ivanov, B. Monemar, Phys Status Solidi A 200 (1) (2003) 13–17.

[14] R. J. Molnar, W. Gotz, L. T. Romano, N. M. Johnson, J Cryst Growth 178 (1-2) (1997) 147–156.

[15] K. H. Ploog, O. Brandt, R. Muralidharan, A. Thamm, P. Waltereit, Journal of Vacuum Science & Technology B 18 (4) (2000) 2290–2294.

[16] W. G. Breiland, K. P. Killeen, Journal of Applied Physics 78 (11) (1995) 6726–6736.

[17] E. D. Palik, Handbook of optical constants of solids, Academic Press, Orlando, 1998.

[18] E. Rocha-Rangel, P. F. Becher, E. Lara-Curzio, Surface and Interface Analysis 35 (2) (2003) 151–155.

[19] P. Vennegues, B. Beaumont, S. Haffouz, M. Vaille, P. Gibart, J Cryst Growth 187 (2) (1998) 167.

[20] S. Figge, T. Bottcher, S. Einfeldt, D. Hommel, J Cryst Growth 221 (2000) 262–266.

[21] R. S. Balmer, C. Pickering, A. J. Pidduck, T. Martin, J Cryst Growth 245 (3-4) (2002) 198–206.

[22] J.-H. Lee, M.-B. Lee, S.-H. Hahm, Y.-H. Lee, J.-H. Lee, Y.-H. Bae, H. K. Cho, MRS Internet J. Nitride Semicond. Res. . 8, (5).

[23] H. P. D. Schenk, P. Vennegues, O. Tottereau, T. Riemann, J. Christen, J Cryst

Growth 258 (3-4) (2003) 232–250.
[24] D. S. Li, M. Sumiya, S. Fuke, D. R. Yang, D. L. Que, Y. Suzuki, Y. Fukuda, J Appl Phys 90 (8) (2001) 4219–4223.
[25] L. M. Yeddanapalli, C. C. Schubert, Journal of Chemical Physics 14 (1) (1946) 1–7.
[26] A. C. Jones, J Cryst Growth 129 (3-4) (1993) 728–773.
[27] J. Leitner, J. Stejskal, P. Vonka, J Cryst Growth 267 (1-2) (2004) 8–16.
[28] G. A. Jefrey, V. Y. Wu, Acta Crystallographica 20 (1966) 538.
[29] K. H. Kim, C. H. Ho, H. Doerr, C. Deshpandey, R. F. Bunshah, J Mater Sci 27 (10) (1992) 2580–2588.
[30] Y. Ozcatalbas, Composites Science and Technology 63 (1) (2003) 53–61.
[31] L. Macht, J. L. Weyher, P. R. Hageman, M. Zielinski, P. K. Larsen, J Phys-Condens Mat 14 (48) (2002) 13345–13350.
[32] Y. Watanabe, Y. Hara, T. Tokuda, N. Kitazawa, Y. Nakamura, Surface Engineering 16 (3) (2000) 211–214.

Chapter 10

GaN/AlGaN based HEMTs - development of the product

In this chapter part of the results of the optimization process of the GaN based HEMT structure will be presented. The results are compared with GaN epitaxial material produced in the other laboratories and from commercial companies. It should be mentioned that some of the presented data is the result of a collaboration with Eindhoven University of Technology in the Netherlands and Chalmers University of Technology in Sweden.

10.1 How good are we?

The development of the HEMT structures based on GaN/AlGaN material started on the University in Nijmegen in year 2000. Before that time research was focused on GaN epitaxy for opto-electronic applications including the first experiments with Mg and Si doping of GaN. The growth process developed at that time allows to deposit state of the art unintentionally doped GaN material on sapphire with a free carrier concentration between 5×10^{16} and 2×10^{17} cm^{-3}, a mobility in the range 300-500 $\mathrm{cm}^2\mathrm{V}^{-1}\mathrm{s}^{-1}$, and an electrical resistivity typically about 0.5-100 $\Omega\,\mathrm{cm}$. This material forms the base for light emitting diodes and laser production. Unfortunately, the first experiments showed that this material is completely useless for HEMT structures. A reasonable value for the pinch-off voltage, necessary to process a HEMT, could not be obtained due to the high conductivity of the GaN layer. The final and most important goal of the experiments was to find a method for growth of high resistivity GaN. The first idea was to dope and compensate the GaN using Mg. The results of these experiments pointed to the right direction. For the first time it was possible to measure a pinch-off voltage. It was -6.7 V but it was still too

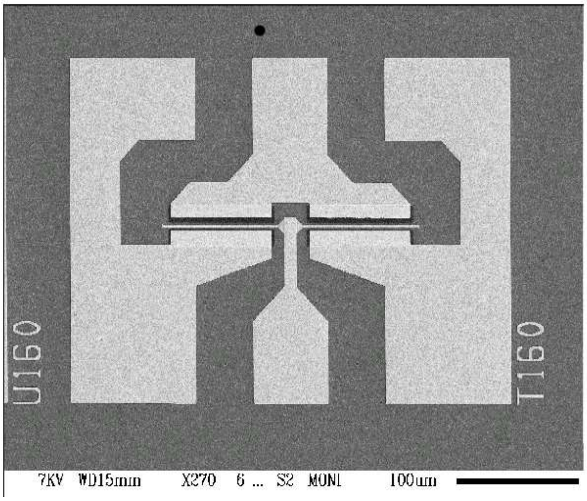

Figure 10.1: SEM image of the first Dutch HEMT prepared at Eindhoven University of Technology on material grown at the Radboud University Nijmegen. The gate width was 200 μm and length 1 μm. (B. Jacobs/TUE)

large (the maximum value of this parameter should be -6V). In contrast the very high value of the 2DEG density, being $1{\times}10^{13}$ cm^{-2}, was very satisfactory. Doping with Mg seemed to be a very promising method for the development of highly resistive GaN. Unluckily, the next experiments revealed a serious memory effect (traces of Mg were observed in the samples even after a couple of days since the last use of Mg), which appears after the growth of Mg doped samples, forces one to find a new method of GaN resistivity control. In addition, uncontrolled Mg compensation of the $Al_xGa_{1-x}N$ top layer decreases the 2DEG density in the HEMT structure. In Chapter 6 and 7 a method for the control of the GaN resistivity based on the use of different types of carrier gas (H_2 or N_2) was presented. By applying this method it was possible to produce GaN epilayers with a electrical resistivity exceeding 10^{11} Ω cm , which reduces the pinch-off voltage to -3.6 – -5.5 V. Figure 10.2 presents the leakage current characterization for GaN/AlGaN HEMT structures. This method measures the current between two mesas 100 μm apart through the GaN buffer layer and gives in this way an indication of the resistivity of the layer. The samples produced using the method demonstrated in chapter 6 show at least 2 orders of magnitude lower leakage currents compared to the commercial samples (produced by the company QinetiQ[*] and RFMD[†]).

After solving the problem of the resistivity, the next iteration step in optimization process for producing HEMTs was the inserting of an additional AlN interlayer as

---

[*] http://www.qinetiq.com/

[†] http://www.rfmd.com/

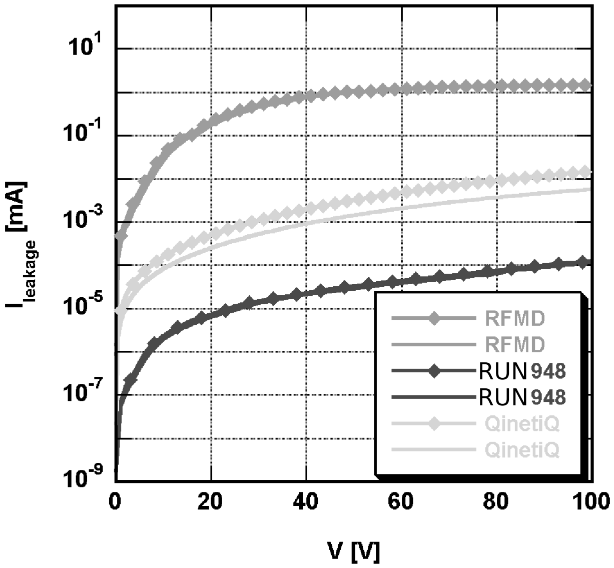

Figure 10.2: GaN buffer electrical characterization. Leakage current between two isolated mesa 100 microns apart is measured for samples from RFMD, QinetiQ, and Radboud University (RUN948). It is clear that the sample RUN948 is much more resistive.

it was already explained in Chapter 1. This interlayer should be able to increase the mobility considerably. Figure 10.3 shows the dependence of the mobility of the 2DEG carriers on the AlN layer deposition time (= AlN thickness). For all presented HEMT structures the 2DEG was about $1.1\times10^{13}\,\mathrm{cm}^{-2}$. Introducing a AlN layer with a thickness between 1-2 nm improves the mobility of the 2DEG. For a HEMT structure without an AlN interlayer the mobility of the 2DEG is about $1200\,\mathrm{cm}^2\mathrm{V}^{-1}\mathrm{s}^{-1}$ whereas for a structure with a thin AlN layer the mobility exceeds $1400\,\mathrm{cm}^2\mathrm{V}^{-1}\mathrm{s}^{-1}$. From Fig. 10.3 it follows that it is crucial to precisely control the AlN layer thickness to obtain the desired mobility enhancement. According to Wallis et al. [1], longer growth times result in a transition from 2D to 3D growth mode associated with an increased sheet resistivity relative to the optimum structure. Also, the thicker AlN layer results in cracking of the $\mathrm{Al}_x\mathrm{Ga}_{1-x}\mathrm{N}$ top layer and through this degeneration of mobility.

Figure 10.4 shows a comparison of samples grown in our laboratory with material obtained by other scientific groups and companies. The mobility of the HEMT deposited on sapphire at RUN is higher compared to the commercial products

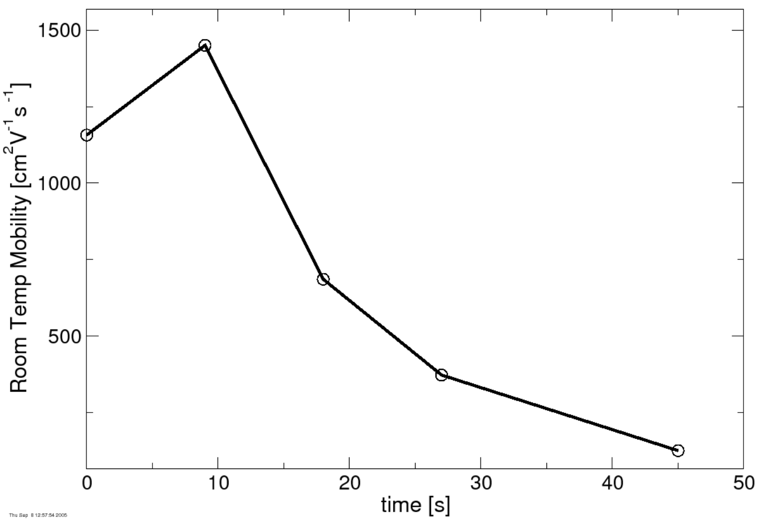

Figure 10.3: Mobility of the 2DEG measured for GaN/AlN/AlGaN HEMT structure as a function of the deposition time of AlN layer. For all presented samples the 2DEG density was about 1.1×10^{13} cm^{-2}.

(ATMI [‡], THALES[§]) available on the market. These results are close to the theoretical values calculated by Ridlely et al. [2]. Additionally, it to be reminded that HEMT structures grown on SiC show also very good parameters. Details of the processing of the HEMT structures grown at the Radboud University Nijmegen will be presented in the PhD thesis written by Mark Kramer from Technical University in Eindhoven. Because the final transistor performance is a function of good epitaxial material, optimized processing, and design of the transistor the comparison of the devices with other groups is very difficult (see Tabel 10.1). The evaluation of the quality of epitaxial material used for HEMT application can be done based on three parameters: mobility of 2DEG, density of 2DEG, and resistivity of the buffer layer. If these parameters not exceed critical values the material will be useless for HEMT applications. The good example of this fact is the publication [3] where epitaxial material with extremely high 2DEG mobility exceeding 2500[cm^{2}V^{-1}s^{-1}] but with a 2DEG density too low to process high power devices (they also do not show the value of resistivity of GaN buffer layer).

Since the first demonstration of a GaN/AlGaN HFET by Khan et al.[4], enormous progress has been observed in the field of GaN/AlGaN transistors operating in C-X band and above. The fastest transistors, based on GaN, that were grown on SiC, can work with a maximum oscillation frequency exceeding 170 GHz [5]. Similar

---

[‡] http://www.atmi.com/

[§] http://www.thales-nederland.nl/

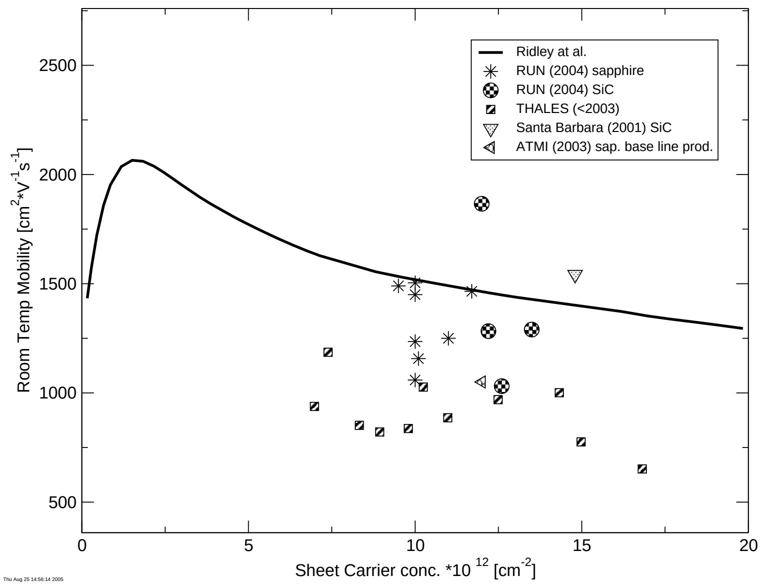

Figure 10.4: Comparison of the HEMT structures prepared on Radboud University Nijmegen with the material obtained in other laboratories.

results were obtained for sapphire substrates [6]. The AlGaN/GaN HEMT structures grown on very expensive free standing GaN substrates have already demonstrated continuous-wave (CW) output power density of 9.4 W/mm at 10 GHz [7]. State of the art GaN based transistors grown on SiC exhibit a CW output power density of 16.5 W/mm in X band [8]. Moreover, in 2005, Toshiba presented impressive results of 174W total output power at a frequency of 6 GHz. These very encouraging results forces one to start focusing on the reliability of the devices as well as on power issues [9, 10]. It was already presented that GaN/AlGaN based devices can demonstrate stable operation under RF stress for 1000 h at a drain bias voltage of 60V [11]. In table 10.1 the performance of the best HEMT based on RUN material is compared with results from other laboratories. All these results show that GaN has a great perspective toward applications for high power, high frequency devices. The processing of AlGaN/GaN HEMT structures starts to be the dominant factor defining the reliability, reproducibility, and technical parameters of the HEMTs [12]. Device processing improvements regarding surface passivation pushes the GaN technology close to theoretical limits of the HEMT. Passivation of the surface reduces current slump but also it decreases the breakdown voltage of the devices. The use of a field plate design increases the breakdown voltage, reduces the electrons trapping effect and reduces frequency dispersion [13]. By reduction of the gate length it is possible to achieve a better microwave performance and an increasing of the cut-off frequencies but it also can reduce the breakdown voltage. So there is always trade-off between different parameters of the HEMTs. Moreover, a new trend is observed to use sapphire substrates as a low cost, development platform for new devices, whereas, SiC and free standing GaN are used as a substrate for the ultimate product. The best produced HEMT based on material from the Radboud University Nijmegen demonstrates a maximum output power exceeding 9.5 W/mm[¶] at 3 GHz with a maximum oscillation frequency exceeding 60 GHz. The epitaxial layer was deposited on SiC and the initial 2DEG density exceeded 1×10^{13} cm^{-2} and electron mobility 1150 $\mathrm{cm}^2\mathrm{V}^{-1}\mathrm{s}^{-1}$.

Sample /ref.	Year	Power density [W/mm]	Gate length [μm]	Freq. [GHz]	F_{max}	Subs.	Field plate	Passivation
RUN	2005	9.5	0.1	3	60	SiC	-	-
[14]	2003	6.7	0.25	18	115	6H-SiC		
[13]	2004	30	0.5	8		SiC	+	+
[15]	2004	12	0.7	2	31	Si(111)		+
[16]	2005	9.5	0.1	10		SiC		
[17]	2005	5.7		30		SiC	+	
[7]	2004	9.4	0.15	10		GaN		+
[18]	2003	8.2	0.2	2		6HSiC		-

Table 10.1: Comparison of the best HEMT's prepared on epitaxial material from Radboud University Nijmegen with the material obtained in other laboratories.

10.2 Suggestions for future research

Development of a technology towards reduction of dislocations in GaN material still leaves a broad field to be explored in a further research. The methods for reduction of the dislocation density presented in Chapter 1 can be slightly modified in order to improve GaN epitaxial material. In Chapter 5 the method of dislocation reduction by using ELO of GaN epilayers using hole openings in Si(111) (Figure 5.1) was presented.

Moreover, Figure 6.4 presents pits created after selective etching of GaN material. Dislocations in this case are etched (so material is theoretically dislocation free) and only holes are present. Then material can be used as a substrate for a next GaN epitaxial process and similar process of reduction of dislocations as presented in Figure 5.2 should be observed. Future research should examine the mechanism of dislocations reduction in such a material.

The GTS method demonstrated in Chapter 8 offering interesting possibility for future research. The model presented on Figure 8.9 shows that after the GTS step, the sapphire surface is covered by randomly placed Ga clusters. Two significant questions arise from these experiments. First, is it possible to apply this method for other substrates like Si or SiC? The second question is: what is the influence of a possible misorientation of the substrate on the deposition of Ga clusters and are this clusters still randomly oriented? Future experimental work should address both questions.

[¶] the sample was grown by M. Rudzinski

The last subject, that seems to be very interesting not only from a scientific but also from technological point of view, is a deposition of thick (above $1\,\mu$m) AlN layers. Recent publications [19, 20] concerning the use of AlN/sapphire templates for the deposition of HEMT structures show that the mobility of 2DEG can be increased up to $2100\,\mathrm{cm}^2\mathrm{V}^{-1}\mathrm{s}^{-1}$ with a 2DEG density equal $1{\times}10^{13}\,\mathrm{cm}^{-2}$, already above the theoretical limits predicted by [2, 21]. Understanding of this problem should be the main goal of a future research in the field of III-V nitrides.

Bibliography

[1] D. J. Wallis, R. S. Balmer, A. M. Keir, T. Martin, Appl Phys Lett 87 (4).

[2] B. K. Ridley, B. E. Foutz, L. F. Eastman, Phys Rev B 61 (24) (2000) 16862–16869.

[3] C. Skierbiszewski, K. Dybko, W. Knap, M. Siekacz, W. Krupczynski, G. Nowak, M. Bockowski, J. Lusakowski, Z. R. Wasilewski, D. Maude, T. Suski, S. Porowski, Appl Phys Lett 86 (10) (2005) –.

[4] M. A. Khan, A. Bhattarai, J. N. Kuznia, D. T. Olson, Appl Phys Lett 63 (9) (1993) 1214–1215.

[5] J. A. Bardwell, Y. Liu, H. Tang, J. B. Webb, S. J. Rolfe, J. Lapointe, Electron Lett 39 (6) (2003) 564–566.

[6] M. Higashiwaki, T. Matsui, Japanese Journal of Applied Physics Part 2-Letters Express Letters 44 (16-19) (2005) L475–L478.

[7] K. K. Chu, P. C. Chao, M. T. Pizzella, R. Actis, D. E. Meharry, K. B. Nichols, R. P. Vaudo, X. Xu, J. S. Flynn, J. Dion, G. R. Brandes, Ieee Electron Device Letters 25 (9) (2004) 596–598.

[8] R. Thompson, T. Prunty, V. Kaper, J. R. Shealy, Ieee T Electron Dev 51 (2) (2004) 292–295.

[9] C. Lee, L. Witkowski, H. Q. Tserng, P. Saunier, R. Birkhahn, D. Olson, D. Olson, G. Munns, S. Guo, B. A. C. Lee, L. Witkowski, H. Q. Tserng, P. Saunier, D. Olson, D. Olson, D. Olson, G. Munns, S. Guo, B. Albert, Electron Lett 41 (3) (2005) 155–157.

[10] J. Kuzmik, D. Pogany, E. Gornik, P. Javorka, P. Kordos, Solid State Electron 48 (2) (2004) 271–276.

[11] T. Kikkawa, Compound Semiconductors 2004, Proceedings 184 (2005) 51–58.
[12] V. Desmaris, Processing and Characterization of AlGaN/GaN HEMTs on Sapphire, 2004.
[13] Y. F. Wu, A. Saxler, M. Moore, R. P. Smith, S. Sheppard, P. M. Chavarkar, T. Wisleder, U. K. Mishra, P. Parikh, Ieee Electron Device Letters 25 (3) (2004) 117–119.
[14] V. Kumar, J. W. Lee, A. Kuliev, O. Aktas, R. Schwindt, R. Birkhahn, D. Gotthold, S. Guo, B. Albert, I. Adesida, Electron Lett 39 (22) (2003) 1609–1611.
[15] J. W. Johnson, E. L. Piner, R. Therrien, P. Rajagopal, J. C. Roberts, J. D. Brown, S. Singhal, K. J. Linthicum, Ieee Electron Device Letters 25 (7) (2004) 459–461.
[16] Y. J. Sun, L. F. Eastman, Ieee T Electron Dev 52 (8) (2005) 1689–1692.
[17] J. S. Moon, S. Wu, D. Wong, I. Milosavljevic, A. Conway, P. Hashimoto, M. Hu, M. Antcliffe, M. Micovic, Ieee Electron Device Letters 26 (6) (2005) 348–350.
[18] M. J. Manfra, N. G. Weimann, O. Mitrofanov, T. Waechtler, D. M. Tennant, Phys Status Solidi A 200 (1) (2003) 175–178.
[19] M. Makoto, E. Takashi, I. Hiroyasu, A. Kei-Ichiro, S. Tomohiko, T. Mitsuhiro, O. Osamu, J Appl Phys 98 (6) (2005) 063713.
[20] M. Miyoshi, H. Ishikawa, T. Egawa, K. Asai, M. Mouri, T. Shibata, M. Tanaka, O. Oda, Appl Phys Lett 85 (10) (2004) 1710–1712.
[21] R. Oberhuber, G. Zandler, P. Vogl, Appl Phys Lett 73 (6) (1998) 818–820.

Summary

GaN is a very promising material for high power and high-frequency electronics due to its wide, direct bandgap (3.4 eV), high thermal stability, and high breakdown voltage. The valuable electrical and optical properties of GaN and its ternary and quaternary alloys with indium and aluminum make this material the key semiconductor material for future technologies and the new generation of electronic devices. Due to the outstanding material properties, III-V nitrides have the potential to fulfill the commercial and military needs for optical storage application, UV photodetectors, and devices operating at extremely hostile environments and elevated temperatures (up to 500 °C). Lack of properly matched substrates for GaN epitaxy implies large dislocation densities in the epilayers. Because of the diminishing effect on the device performance, a reduction of the dislocation density was and still is the key issue in the GaN material development.

This thesis focuses on growth and basic characterization of AlGaN/GaN based high electron mobility structures. In order to provide theoretical background for the presented research, presented in this thesis, the basic physical properties of III-V nitrides and the characteristics of the HEMT structures are discussed first. Additionally, properties of substrates used for GaN epitaxy are described.

In Chapter 3 the standard techniques used for the characterization of the samples are described. The research presented here concerns mostly the epitaxial growth of the semiconductor, and therefore fast and non-destructive methods such as AFM, SEM, XRD and XRR are discussed.

Chapter 4 deals with the growth of high quality GaN films on Si (111) substrates by Metal Organic Chemical Vapor Deposition technique. In order to improve the quality of the epitaxial films different nucleation or buffer layers and combinations of them are introduced. The results obtained on an optimized AlN nucleation layer serve as a reference point. In order to improve the quality of the epitaxial films different combinations of nucleation and intermediate layers are applied. The first combination consists of an optimized AlN nucleation layer followed by a 1 μm thick GaN film, on which Si_xN_y/GaN intermediate layers was deposited. Based on the optimized AlN nucleation layer, AlGaN/GaN superlattices or AlN intermediate buffer layers

are introduced. Additionally, results on the modification of the Si(111) surface with NH_3 to promote nucleation from selective GaN islands are presented.

The maskless epitaxial lateral overgrowth of GaN on structured Si (111) substrates and its structural properties received by transmission electron microscopy and photo-electrochemical etching techniques are presented in Chapter 5. Photolithography and dry etching were used to obtain the silicon substrates structured by $4\,\mu$m deep holes of $1.5\,\mu$m in diameter, separated by $2.5\,\mu$m from each other. During the process of GaN epitaxy deposition takes first place on the Si (111) surface covered with AlN in between the holes. The GaN layer extends vertically and laterally over the holes until complete coalescence. Transmission electron microscopy shows that regions over the holes only contain dislocations in the basal plane resulting from the bending of dislocations nucleated at the Si/AlN interface and at the coalescence boundary between the two laterally overgrown layers. A drastic decrease of dislocation density in these areas of the films was obtained. The revelation of dislocations is also achieved by PEC etching technique.

The influence of hydrogen and nitrogen carrier gases used during the deposition of the nucleation layer on the structural and electrical properties of GaN layers has been investigated in Chapter 6 and 7. In this chapter the solution for one of the main problems of HEMT structure deposition, i.e. control of the resistivity of the GaN buffer layer, was provided. The nucleation layer morphology strongly depends on the carrier gas affecting the electrical properties of GaN epitaxial films through changes of the ratio of edge to mixed and screw-type threading dislocations. The morphology of the individual NLs strongly depends on the carrier gas used during the growth and recrystallization and this is the key factor for control of the resistivity of the GaN layer grown on it. The GaN nucleation layer grown in presence of N_2 has a higher density of islands with a statistically smaller diameter than the samples grown in H_2 atmosphere. It has been found that the density of edge-type dislocations determines the resistivity of GaN epilayers and that one key factor for varying the density of these dislocations is the morphology of the nucleation layer. This morphology of the GaN nucleation layer can be controlled by the type of carrier gas used during the deposition of it. In this way the electrical resistivity of GaN epilayers can be varied from as low as $0.5\,\Omega\,\mathrm{cm}$ to higher than $1\times10^{11}\,\Omega\,\mathrm{cm}$.

The microscopic evolution of GaN layers grown by metal organic chemical vapor deposition was investigated in Chapter 8 and Chapter 8 using a new Ga and Al treatment method respectively. With the help of in situ reflectance measurements the coalescence and overgrowth of GaN epilayers was observed. The sample morphology was ex situ characterized by atomic force microscopy, scanning electron microscopy, and optical microscopy. By using orthodox etching in molten KOH-NaOH eutectic the dislocation and N-polar inclusion density were revealed. Photoluminescence measurements were performed in order to determine the optical properties of the GaN layers. The experimental results demonstrated that by annealing the c-plane sapphire in trimethylgallium it is possible to control the GaN epitaxial layer polarity. The ratio between N and Ga polarity in the deposited GaN layers can be adjusted by means of changing the annealing time in TMG atmosphere of the sapphire substrate. The experimental results demonstrated that it is possible to control the GaN epitaxial layer polarity and to induce a stable growth mode by depositing a thin Al based nucleation layer on the c-plane sapphire instead of using the classical two-step growth method. It was found, that during the annealing in trimethylaluminum at 1170 °C some amount of carbon is incorporated into the layer. The X-ray diffraction measurement revealed traces of Al_4C_3 in the nucleation layer. In GaN epilayers with thickness exceeding 300 nm, inclusions of probably misoriented crystallites or of cubic GaN were observed.

Finally general conclusions regarding GaN/AlGaN based HEMT structures as well as the direction for further research are presented in the concluding part of this thesis. Additionally the attempt has been made to compare the results obtained at Radboud University Nijmegen with other laboratories.

Samenvatting

GaN is een veelbelovend materiaal voor hoog-vermogen en hoge frequentie elektronica vanwege de grote, directe bandafstand (3.4 eV), de hoge thermische stabiliteit en de hoge doorslag spanning. De combinatie van deze waardevolle eigenschappen met de mogelijkheid van GaN om met indium en aluminium ternaire en quarternaire legeringen te vormen en daarmee ”bandgap engeneering” te realiseren, maken deze familie van materialen tot een belangrijke bouwsteen voor toekomstige technologien en nieuwe generaties van elektronische devices. De familie van de III-V nitriden heeft de potentie om te voldoen aan de commercile en militaire vraag naar optische data-opslag mogelijkheden, UV-fotodetectoren, en devices die moeten opereren in extreem agressieve (chemische) omgevingen en/of bij hoge temperaturen (tot 500 °C).

Het gebrek aan substraten met de juiste roosterafstand voor GaN depositie impliceert dat de hierdoor noodgedwongen GaN heteroepitaxie grote dislocatie dichtheden in de epilagen veroorzaakt. Deze defecten verminderen de kwaliteit van de devices sterk waardoor reductie van de dislocatie dichtheid tot het sleutelgebied in de ontwikkeling van het GaN materiaal is geworden. Het gebruik van deze substraten met een niet passende roosterafstand forceert het gebruik van zogenaamde nucleatielagen om op deze wijze toch epitaxiaal GaN van device kwaliteit te kunnen deponeren. Dit proefschrift concentreert zich op het groeien en karakteriseren van GaN lagen op Si (111) als substraat en van HEMT structuren gebaseerd op AlGaN/GaN op saffier als substraat . In de eerste twee hoofdstukken wordt een theoretische achtergrond gegeven van het te presenten onderzoek waarin allereerst wat algemene fysische eigenschappen van de familie van III-V nitriden en de karakteristieken van HEMT structuren besproken worden. Hierna worden de eigenschappen van de in dit proefschrift meest gebruikte, niet rooster passende substraat voor de GaN depositie (saffier) beschreven.

In hoofdstuk 3 worden een aantal standaard technieken voor de karakerisatie van AlGaN/GaN gebaseerde HEMT structuren geprenteerd welke voor dit proefschrift gebruikt zijn. Het moet opgemerkt worden dat het hier gepresenteerde onderzoek voornamelijk de epitaxiale groei van de halfgeleider betreft en daarom zijn vooral snelle en niet-destructieve analyse methoden, zoals AFM, SEM, XRD en XRR gebruikt. Hoofdstuk 4 heeft betrekking op de groei van hoge kwaliteit GaN lagen op Si (111) substraten met de Metal-Organic Chemical Vapor Deposition (MOCVD) techniek. Om de kwaliteit van de gedeponeerde lagen verder te verbeteren worden verschillende nucleatielagen, soms ook aangeduid als bufferlagen maar in dit proefschrift wordt alleen over nucleatielagen gesproken, en combinaties hiervan gentroduceerd. De resultaten behaald op een geoptimaliseerde AlN nucleatie laag dienen als referentiepunt. De eerste geteste nieuwe combinatie bestaat uit een geoptimaliseerde AlN nucleatie laag gevolgd door een 1 mm dikke GaN laag, waarop vervolgens een Si_xN_y/GaN intermediaire laag werd gedeponeerd. Daarnaast werden in lagen GaN gegroeid op de geoptimaliseerde AlN nucleatielaag, AlGaN/GaN superroosters of AlN intermediaire buffer lagen ingebouwd. Resulaten van deze experimenten werden vergeleken met het referentiepunt.

Het lateraal overgroeien zonder masker van GaN op gestructureerde Si (111) substraten en de structurele eigenschappen zoals bepaald met transmissie elektronen microscopie en foto-elektrochemische ets technieken worden beschreven in hoofdstuk 5. De gestructureerde silicium substraten bestonden uit $4\,\mu$m diepe gaten met een doorsnede van elk $1.5\,\mu$m gepositioneerd met een onderlinge tussenliggende afstand van $2.5\,\mu$m. Na depositie van de AlN nucleatielaag vindt gedurende de daar op volgende GaN groei eerst depositie plaats op het met AlN bedekte oppervlak van het gedeelte van het Si (111) substraat tussen de gaten. Vervolgens groeit de GaN laag vertikaal en lateraal over de gaten tot dat er een compleet gesloten laag ontstaat en er vindt geen depostie plaats in de gaten. Zowel transmissie elektronen microscopie als de PEC etstechniek geeft aan dat in de overgroeide regio's, dat wil zeggen de overgroeide gaten in het Si (111), slechts dislocaties voorkomen die parallel aan het substraatvlak liggen. Er komen geen dislocaties voor die loodrecht op dit vlak staan, de zogenaamde ”threading” dislocaties. Dit is het resultaat van het ombuigen van dislocaties die ontstaan zijn aan het Si/AlN grensvlak en bij het grensvlak van samensmelting tussen de twee lateraal overgroeide lagen. Hierdoor is een drastische verlaging van dislocatiedichtheid bereikt in de overgroeide gedeeltes.

De invloed van verschillende soorten dragergassen (waterstof of stikstof), gedurende de groei van de nucleatielaag, op de structurele en elektrische eigenschappen van de daarop gedeponeerde GaN lagen is onderzocht in hoofdstuk 6 en 7. In deze hoofdstukken wordt de oplossing gegeven voor een van de grootste problemen van de depositie van HEMT structuren, namelijk de controle over de (elektrische) weerstand van de GaN buffer laag. Deze weerstand moet zo hoog mogelijk zijn om geleiding door de bufferlaag te voorkomen. De morfologie van de nucleatielaag hangt sterk af van het gebruikte dragergas tijdens de depositie van deze laag. Op zijn beurt beïnvloedt de morfologie van de nucleatielaag weer de elektrische eigenschappen van de daarop gedeponeerde GaN lagen door de verhouding tussen enerzijds de rand dislocaties en anderzijds de gemengde- en schroef type dislocaties te veranderen. Zoals hierboven al vermeld hangt de morfologie van de individuele nucleatielagen sterk af van het dragergas dat wordt gebruikt tijdens de groei en rekristallisatie van de nucleatielaag en dit is de belangrijkste factor voor controle van de weerstand van de GaN laag die er bovenop wordt gegroeid. De GaN nucleatie laag die wordt gegroeid in aanwezigheid van N_2 heeft een morfologie die gekenmerkt wordt door een hoge dichtheid van eilandjes met een statistisch kleinere diameter dan de morfologie kenmerkend voor de structuren die zijn gegroeid met H_2 als dragergas. Er werd gevonden dat de dichtheid van de rand-type dislocaties de weerstand van het GaN bepaalt en dat de morfologie van de nucleatie laag de belangrijkste parameter is voor variatie van de dichtheid van dit type dislocatie. Zo kan de elektrische weerstand van de GaN epilagen worden gevarieerd tussen $0.5\,\Omega\,\mathrm{cm}$ en meer dan $1\times10^{11}\,\Omega\,\mathrm{cm}$. Deze laatste waarde is te preferen voor de bufferlaag in een HEMT structuur.

In de hoofdstukken 8 en 9 worden twee nieuwe methoden gepresenteerd om GaN op saffier te groeien. De klassieke nucleatielaag (2 stapsgroeimethode) is vervangen door het saffier te behandelen met TMGa (trimethylgallium, hoofdstuk 8) of met TMAl (trimethylaluminium, hoofdstuk 9). Met behulp van in-situ reflectie metingen werd de samensmelting en overgroei van de GaN epilagen geobserveerd versus verschillende groeiparameters van de nieuwe methode. De morfologie werd ex-situ bepaald met atomic force microscopy (AFM), scanning electron microscopy (SEM) en optische microscopie. Door te etsen in een gesmolten KOH-NaOH eutecticum werden de dislocaties en N-gepolariseerde insluitsels zichtbaar gemaakt. Met behulp van fotoluminescentie metingen zijn de optische eigenschappen van de GaN lagen bepaald. De experimentele resultaten demonstreren dat door sterke verhitting van het c-vlak van saffier in trimethylgallium het mogelijk is om de polariteit van de daar op te groeien GaN laag te sturen. De ratio tussen materiaal met de N en met de Ga polariteit in de gedeponeerde GaN laag kan worden aangepast door de tijd van verhitting van het saffier substraat in de TMG atmosfeer te veranderen. Met deze methode bleek het mogelijk om volledige Ga-polaire GaN lagen te groeien. De behandeling met TMAl maakt het ook mogelijk om de polariteit van de GaN epitaxiale laag te bepalen en een stabiele groei-mode te induceren door een dunne Al bevattende nucleatielaag op het c-vlak van saffier te deponeren. Er werd gevonden dat gedurende de verhitting in trimethylaluminium bij 1170 °C een gedeelte van de koolstof afkomstig van het TMAl wordt ingebouwd. Met Rntgen diffractie werden in de nucleatielaag sporen van Al_4C_3 gevonden. In GaN epilagen met een dikte van meer dan 300 nm werden insluitingen van waarschijnlijk misgeorinteerde kristalletjes GaN of kubische GaN insluitingen waargenomen. In het laatste hoofdstuk worden algemene conclusies betreffende GaN/AlGaN gebaseerde HEMT structuren en een mogelijke richting voor verder onderzoek gepresenteerd. De resultaten behaald aan de Radboud Universiteit Nijmegen worden vergeleken met resultaten van andere laboratoria.

Publication list

[1] A. Grzegorczyk, L. Macht, P. Hageman, J. Weyher, P. Larsen, J Cryst Growth 273 (3-4) (2005) 424–430.

[2] A. P. Grzegorczyk, P. R. Hageman, J. L. Weyher, P. K. Larsen, J Cryst Growth 283 (1-2) (2005) 72–80.

[3] A. Grzegorczyk, L. Macht, P. Hageman, M. Rudzinski, P. Larsen, phys. stat. sol.(c) (1-4).

[4] A. P. Grzegorczyk, P. R. Hageman, J. L. Weyher, P. K. Larsen, Submitted to J Cryst Growth.

[5] L. Macht, J. Kelly, J. Weyher, A. Grzegorczyk, P. Larsen, J Cryst Growth 273 (3-4) (2005) 347–356.

[6] C. Dam, A. Grzegorczyk, P. Hageman, R. Dorsman, C. Kleijn, P. Larsen, J Cryst Growth 271 (1-2) (2004) 192–199.

[7] T. J. Ochalski, A. P. Grzegorczyk, M. Rudzinski, P. Larsen, E. Kowalczyk, P. Holtz, P. Bergman, P. Paskov, phys.stat.sol. (c) (1-5).

[8] S. Haffouz, A. Grzegorczyk, P. Hageman, P. Vennegues, E. van der Drift, P. Larsen, J Cryst Growth 248 (2003) 568–572.

[9] A. Wojcik, T. Piwonski, T. Ochalski, E. Kowalczyk, A. Bugajski, M. Grzegorczyk, L. Macht, P. Larsen, phys.stat.sol. (c) 0 (1) (2002) 491.

[10] P. R. Hageman, S. Haffouz, V. Kirilyuk, A. Grzegorczyk, P. K. Larsen, Phys Status Solidi A 188 (2) (2001) 523–526.

[11] P. R. Hageman, S. Haffouz, V. Kirilyuk, L. Macht, J. L. Weyher, A. Grzegorczyk, P. K. Larsen, Phys Status Solidi A 188 (2) (2001) 659–662.

[12] M. Rudzinski, P. R. Hageman, A. Grzegorczyk, L. Macht, J. Pernot, T. Rodle, H. Jos, P. Larsen, Phys Status Solidi (C).

Curriculum Vitae

Andrzej Paweł Grzegorczyk was born on the 21st January, 1976 in Warsaw, Poland. He finished secondary school in 1995. In the same year he started studying physics at the Technical University in Warsaw at the department of the Technical Physics and Applied Mathematics. He specialized in the field of solid state physics. In 1998 he joined a research program on mechanical and thermal properties in novel nanodiamond composites in the High Pressure Research Center (Unipress) of the Polish Academy of Sciences and continued to work at Unipress as a graduate student. During his cooperation with Unipress, he participated in several research projects at Deutches Elektronen Synchrotron Institute (DESY) in Hamburg and at the Institute of High Pressure of the Russian Academy of Science in Troick near Moscow.

He received his Master of Science degree in 2000. His master thesis dealt with “Crystallographic and micro-crystallographic structure of AlN in high pressure and temperature conditions”.

His interest in science encouraged him to start his PhD study in the field of ÌIIV semiconductors at the University in Nijmegen, the Netherlands. His research at the department of Experimental Solid State Physics 3 focused on the epitaxy of the semiconductors by Metalorganic Chemical Vapor Deposition. During his doctoral studies he was also involved in research concerned with Hydride Vapor Phase Epitaxy of GaN. In 2005 he accomplished his research on “GaN grown on sapphire by MOCVD - application for HEMT structures” under supervision of Prof. P.K. Larsen and P.R. Hageman. The results of this research are presented in this thesis.